

PB97135826



U.S. Department
of Transportation
Federal Highway
Administration

Publication No. FHWA-RD-96-108
February 1997

Characterizing Roadside Hardware Materials for LS-DYNA3D Simulations

Research and Development
Turner-Fairbank Highway Research Center
6300 Georgetown Pike
McLean, Virginia 22101-2296

REPRODUCED BY: **NTIS**
U.S. Department of Commerce
National Technical Information Service
Springfield, Virginia 22161

FOREWORD

This report documents a study to investigate the material parameters for a variety of steel materials used in modeling roadside safety hardware using the LS-DYNA3D finite element program. A method for simulating standard American Association of State Highway and Transportation Officials (AASHTO) tensile tests using LS-DYNA3D is presented along with comparisons between simulated tests and actual physical tests.

LS-DYNA3D is an explicit, nonlinear 3-dimensional, finite element code that is being used by the Federal Highway Administration (FHWA) to simulate vehicle collisions into roadside structures like guardrails, bridge rails and luminaire supports. The LS-DYNA3D input parameters were derived from material properties determined in standard AASHTO tensile tests. Material model parameters are recommended for AASHTO M-180 guardrail steel, AASHTO M-183M guardrail-post steel, ASTM A-499 Grade 60 flanged channel sign-support steel, and the sheet steel from an automobile fender are documented.

The report will be of interest to researchers and engineers using LS-DYNA3D to model roadside safety structure collisions. The information in this report will help analysts to use consistent and reasonable values for material properties in their simulations of vehicle impacts with roadside safety hardware.




A. George Ostensen
Director, Office of Safety and Traffic
Operations Research and Development

NOTICE

This document is disseminated under the sponsorship of the Department of Transportation in the interest of information exchange. The United States Government assumes no liability for its contents or use thereof. This report does not constitute a standard, specification, or regulation.

The United States Government does not endorse products or manufacturers. Trade and manufacturers' names appear in this report only because they are considered essential to the objective of the document.

1. Report No. FHWA-RD-96-108		P897-135826 		3. Recipient's Catalog No.	
4. Title and Subtitle CHARACTERIZING ROADSIDE HARDWARE MATERIALS FOR LS-DYNA3D SIMULATIONS		5. Report Date February 1997		6. Performing Organization Code	
7. Author(s) Amy E. Wright and Malcolm H. Ray		8. Performing Organization Report No.		10. Work Unit No. (TRAIS) 1A5I	
9. Performing Organization Name and Address Turner-Fairbank Highway Research Center 6300 Georgetown Pike McLean, Virginia 22101-2296		11. Contract or Grant No. NHI GRF Project #DDE94-X-00425		13. Type of Report and Period Covered Final Report December 1994-April 1996	
12. Sponsoring Agency Name and Address Office of Safety and Traffic Operations R&D Federal Highway Administration 6300 Georgetown Pike McLean, Virginia 22101-2296		14. Sponsoring Agency Code		15. Supplementary Notes	
16. Abstract Finite element models have three parts: geometry, connections and material properties. Being the visible parts of a model, geometry and connections are generally carefully considered. Material properties are often not chosen with the same degree of care although they are every bit as important to obtaining good results. Accurate simulations of vehicles impacting roadside hardware require an understanding of both the material behavior and the mathematical material models in LS-DYNA3D. A method for comparing LS-DYNA3D simulations to typical ASTM materials tests is described. Material input properties for w-beam guardrail steel, guardrail posts, flanged-channel sign posts and Ford Festiva fenders are found for LS-DYNA3D based upon experimental quasi-static tests. Strain-rate sensitive material models in LS-DYNA3D are explored.					
17. Key Words Materials, simulation, finite element modeling, guardrail, flanged-channel post, post, fender, quasi-static, dynamic, strain-rate, AASHTO, ASTM, material testing, DYNA3D, LS-DYNA3D, LS-INGRID, TRUGRID, LS-TAURUS, crashworthiness.		18. Distribution Statement No restrictions. This document is available to the public through the National Technical Information Service, Springfield, Virginia 22161.			
19. Security Classif. (of this report) Unclassified	20. Security Classif. (of this page) Unclassified	21. No. of pages 120	22. Price		

SI* (MODERN METRIC) CONVERSION FACTORS

APPROXIMATE CONVERSIONS TO SI UNITS

APPROXIMATE CONVERSIONS FROM SI UNITS

Symbol	When You Know	Multiply By	To Find	Symbol	Symbol	When You Know	Multiply By	To Find	Symbol
LENGTH					LENGTH				
in	inches	25.4	millimeters	mm	mm	millimeters	0.039	inches	in
ft	feet	0.305	meters	m	m	meters	3.28	feet	ft
yd	yards	0.914	meters	m	m	meters	1.09	yards	yd
mi	miles	1.61	kilometers	km	km	kilometers	0.621	miles	mi
AREA					AREA				
in ²	square inches	645.2	square millimeters	mm ²	mm ²	square millimeters	0.0016	square inches	in ²
ft ²	square feet	0.093	square meters	m ²	m ²	square meters	10.764	square feet	ft ²
yd ²	square yards	0.836	square meters	m ²	m ²	square meters	1.195	square yards	yd ²
ac	acres	0.405	hectares	ha	ha	hectares	2.47	acres	ac
mi ²	square miles	2.59	square kilometers	km ²	km ²	square kilometers	0.386	square miles	mi ²
VOLUME					VOLUME				
fl oz	fluid ounces	29.57	milliliters	mL	mL	milliliters	0.034	fluid ounces	fl oz
gal	gallons	3.785	liters	L	L	liters	0.264	gallons	gal
ft ³	cubic feet	0.028	cubic meters	m ³	m ³	cubic meters	35.71	cubic feet	ft ³
yd ³	cubic yards	0.765	cubic meters	m ³	m ³	cubic meters	1.307	cubic yards	yd ³
MASS					MASS				
oz	ounces	28.35	grams	g	g	grams	0.035	ounces	oz
lb	pounds	0.454	kilograms	kg	kg	kilograms	2.202	pounds	lb
T	short tons (2000 lb)	0.907	megagrams (or "metric ton")	Mg (or "t")	Mg (or "t")	megagrams (or "metric ton")	1.103	short tons (2000 lb)	T
TEMPERATURE (exact)					TEMPERATURE (exact)				
°F	Fahrenheit temperature	5(F-32)/9 or (F-32)/1.8	Celcius temperature	°C	°C	Celcius temperature	1.8C + 32	Fahrenheit temperature	°F
ILLUMINATION					ILLUMINATION				
fc	foot-candles	10.76	lux	lx	lx	lux	0.0929	foot-candles	fc
fl	foot-Lamberts	3.426	candela/m ²	cd/m ²	cd/m ²	candela/m ²	0.2919	foot-Lamberts	fl
FORCE and PRESSURE or STRESS					FORCE and PRESSURE or STRESS				
lbf	poundforce	4.45	newtons	N	N	newtons	0.225	poundforce	lbf
lbf/in ²	poundforce per square inch	6.89	kilopascals	kPa	kPa	kilopascals	0.145	poundforce per square inch	lbf/in ²

NOTE: Volumes greater than 1000 l shall be shown in m³.

* SI is the symbol for the International System of Units. Appropriate rounding should be made to comply with Section 4 of ASTM E380.

GENERAL DISCLAIMER

This document may be affected by one or more of the following statements

- **This document has been reproduced from the best copy furnished by the sponsoring agency. It is being released in the interest of making available as much information as possible.**
- **This document may contain data which exceeds the sheet parameters. It was furnished in this condition by the sponsoring agency and is the best copy available.**
- **This document may contain tone-on-tone or color graphs, charts and/or pictures which have been reproduced in black and white.**
- **This document is paginated as submitted by the original source.**
- **Portions of this document are not fully legible due to the historical nature of some of the material. However, it is the best reproduction available from the original submission.**

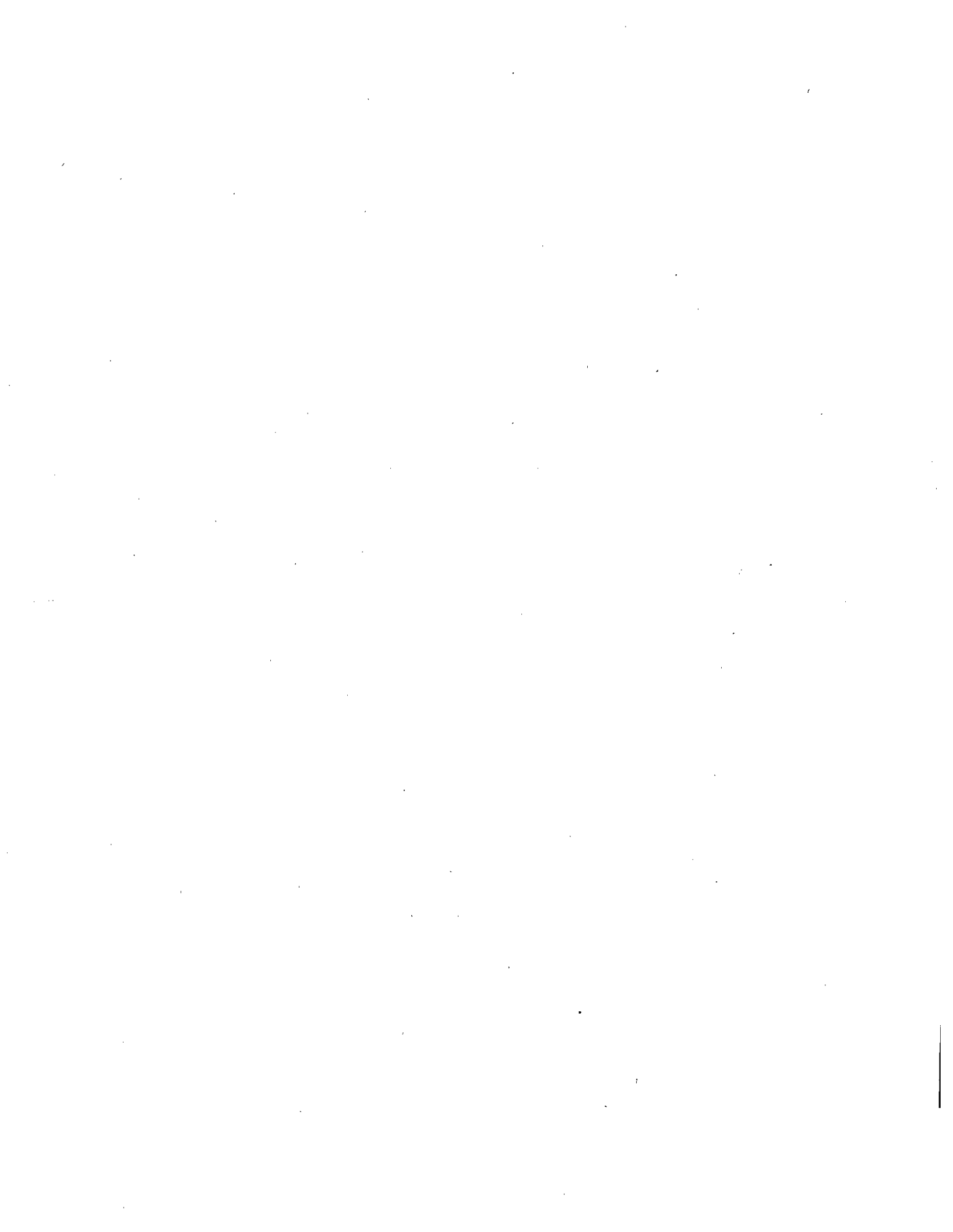


TABLE OF CONTENTS

CHAPTER 1. INTRODUCTION	1
CHAPTER 2. QUASI-STATIC COUPON TESTS	3
Standard Laboratory Tests	3
Finite Element Model	4
<i>Strain Rate</i>	5
<i>Elastic Wave Speed and Amplitude</i>	5
<i>Kinetic Energy</i>	8
<i>Mesh Density</i>	8
<i>Belytschko-Lin-Tsay Shell</i>	12
<i>Mathematical Material Models</i>	15
Analyzing Results	16
CHAPTER 3. GUARDRAIL STEEL	19
Experimental Test Results	19
Finite Element Analysis Results	27
<i>Material Type 3</i>	27
<i>Material Type 24</i>	31
<i>Material Type 19</i>	33
CHAPTER 4. STEEL GUARDRAIL POST	37
Experimental Results	37
Finite Element Analysis Results	41
<i>Material Type 3</i>	41
<i>Material Type 24</i>	45
CHAPTER 5. FLANGED CHANNEL SIGN-POST	47
Experimental Results	49
Finite Element Analysis Results	52
<i>Material Type 3</i>	52
<i>Material Type 24</i>	56
CHAPTER 6. FORD FESTIVA FENDER	59
Experimental Results	61
Finite Element Analysis Results	65
<i>Material Type 3</i>	65
<i>Material Type 24</i>	68

PROTECTED UNDER INTERNATIONAL COPYRIGHT
ALL RIGHTS RESERVED.
NATIONAL TECHNICAL INFORMATION SERVICE
U.S. DEPARTMENT OF COMMERCE

TABLE OF CONTENTS (continued)

CHAPTER 7. DYNAMIC TENSION COUPON TESTS	71
Standard Laboratory Tests	72
Finite Element Simulations	84
<i>Material Models</i>	85
<i>Instantaneous Strain Rates</i>	85
<i>Conclusions</i>	87
CHAPTER 8. CONCLUSION	99
APPENDIX A- TRUGRID INPUT FILE	103
REFERENCES	105
BIBLIOGRAPHY	109

LIST OF FIGURES

<u>Figure</u>	<u>Page</u>
1 AASHTO T-244 longitudinal flat test specimen. ⁽³⁾	3
2 Quarter model of a longitudinal flat tension test.	4
3 Load versus elongation curve for various loading rates.	7
4 Three quarter models with different mesh densities.	10
5 Load versus elongation curve for different mesh densities.	11
6 Load versus elongation curve with 3 and 5 through-the-thickness integration points for a Belytschko-Lin-Tsay shell element.	13
7 Load versus elongation curve of simulations with and without shell thickness updates. .	14
8 Material type 3 behavior.	15
9 Material Type 24 behavior as defined by the user.	16
10 Load versus elongation curve showing the 90th percentile envelope.	17
11 Typical guardrail system.	20
12 Typical local buckling of a guardrail.	21
13 Typical guardrail damage.	22
14 Guardrail that has been impacted at an end terminal.	23
15 Post-test photograph of AASHTO M-180 Class A Type II steel test specimens.	24
16 Force versus elongation curves for AASHTO M-180 Class A Type II guardrail steel. . .	26
17 Load versus elongation curve of a bilinear simulated response of AASHTO M-180 Class A Type II guardrail steel for material type 3.	29
18 Load versus elongation curve for the perfectly plastic simulated response of AASHTO M-180 Class A Type II guardrail steel for material type 3.	30
19 Load versus elongation for the simulated response of AASHTO M-180 Class A Type II guardrail steel for material type 24.	32

LIST OF FIGURES (continued)

<u>Figure</u>		<u>Page</u>
20	Load versus elongation curve for the simulated response of AASHTO M-180 Class A Type II guardrail steel without strain rate sensitivity	34
21	Photograph of AASHTO M-183M steel guardrail posts supporting W-beam guardrail.	38
22	Load versus elongation curves for AASHTO M-183M steel.	39
23	Post-test photograph of AASHTO M-183M steel test specimens.	40
24	Load versus elongation curve for the bilinear simulated response of AASHTO M-183M steel using material type 3.	43
25	Load versus elongation curve for the perfectly plastic simulated response of AASHTO M-183M steel using material type 3.	44
26	Load versus elongation curve of the simulated response of AASHTO M-183M steel using material type 24.	46
27	A flanged channel sign-support.	48
28	Load versus elongation curves for ASTM A-499 Grade 60 steel.	50
29	Post-test photograph of ASTM A-499 Grade 60 steel test specimens.	51
30	Load versus elongation curve of the bilinear simulated response of ASTM A-499 Grade 60 steel using material type 3.	54
31	Load versus elongation curve of the perfectly plastic simulated response for ASTM A-499 Grade 60 steel using material type 3.	55
32	Photographs of flanged channel sign support failure modes.	57
33	Load versus elongation curve of the simulated response of ASTM A-499 Grade 60 steel using material type 24.	58
34	Photograph of a 1988 Ford Festiva.	60
35	Finite element model of a 1989 Ford Festiva.	61
36	Load versus elongation curves for Festiva fender steel.	63

LIST OF FIGURES (continued)

<u>Figure</u>		<u>Page</u>
37	Post-test photograph of Festiva fender steel test specimens.	64
38	Load versus elongation curve of the bilinear simulated response of Festiva fender steel using material type 3.	66
39	Load versus elongation curve of perfectly plastic simulated response for Festiva fender steel using material type 3.	67
40	Typical impact damage to the sheet-metal of a small car after a guardrail test.	69
41	Load versus elongation curve of the simulated response of Festiva fender steel using material type 24.	70
42	Stress versus strain curves with the typical strain rate effects for mild steel.	71
43	Dynamic tension specimen	72
44	Engineering stress versus engineering strain for M-180 guardrail steel tested at a strain rate of 1 s^{-1}	75
45	Engineering stress versus engineering strain for M-180 guardrail steel tested at a strain rate of 5 s^{-1}	76
46	Engineering stress versus engineering strain for M-180 guardrail steel tested at a strain rate of 10 s^{-1}	77
47	Engineering stress versus engineering strain for M-180 guardrail steel tested at a strain rate of 50 s^{-1}	78
48	Engineering stress versus engineering strain for M-180 guardrail steel at various strain rates.	79
49	Percent elongation versus strain rate.	81
50	Strain energy versus strain rate.	82
51	Yield stress versus strain rate with Cowper-Symonds predicted yield stress using the constants $C=100.4 \text{ s}^{-1}$ and $p=4.9$	83
52	Quarter model of a longitudinal flat tension test.	84

LIST OF FIGURES (continued)

Figure		Page
53	Material type 24 load versus elongation curve with and without strain rate sensitivity.	88
54	Effective strain rate and the z-direction strain rate versus time for material type 24 with strain rate sensitivity.	89
55	Effective strain rate and z-direction strain rate versus time for material type 24 without strain rate sensitivity.	90
56	Y-direction strain rate versus time for material type 24 with strain rate sensitivity.	91
57	Y-direction strain rate versus time for material type 24 without strain rate sensitivity. ...	92
58	Engineering stress versus strain for material type 3 with and without strain rate sensitivity.	93
59	Effective strain rate and z-direction strain rate versus time for material type 3 with strain rate sensitivity.	94
60	Effective strain rate and z-direction strain rate versus time for material type 3 without strain rate sensitivity.	95
61	Engineering stress versus strain for material type 19 with and without strain rate sensitivity.	96
62	Effective strain rate and z-direction strain rate versus time for material type 19 with strain rate sensitivity.	97
63	Effective strain rate and z-direction strain rate versus time for material type 19 without strain rate sensitivity.	98

LIST OF TABLES

<u>Table</u>	<u>Page</u>
1 Amplitude of a stress wave in a circular bar at various loading rates.	5
2 Kinetic and total energy at different loading rates.	8
3 Longitudinal flat tension tests of AASHTO M-180 Class A Type II steel.	25
4 LS-DYNA3D material parameters for modeling AASHTO M-180 Class A Type II steel with material type 3.	28
5 LS-DYNA3D material parameters for modeling AASHTO M-180 Class A Type II steel for material type 24.	31
6 LS-DYNA3D material parameters for modeling AASHTO M-180 Class A Type II steel for material type 19 (quasi-static parameter values).	33
7 Longitudinal flat tension tests of AASHTO M-183M Grade 250 steel.	37
8 LS-DYNA3D material parameters for modeling AASHTO M-183M steel.	42
9 LS-DYNA3D material parameters for modeling AASHTO M-183M steel using material type 24.	45
10 Longitudinal flat tension tests of ASTM A-499 Grade 60 steels.	49
11 LS-DYNA3D material parameters for modeling ASTM A-499 Grade 60 steel for material type 3.	53
12 LS-DYNA3D material parameters for modeling ASTM A-499 Grade 60 steel using material type 24.	56
13 Longitudinal flat tension tests of a 1990 Ford Festiva fender.	62
14 LS-DYNA3D material parameters for modeling Festiva fender steel for material type 3.	65
15 LS-DYNA3D material parameters for modeling Festiva fender steel using material type 24.	68
16 Tensile test results for strain rate 1 ($\dot{\epsilon}^P \approx 1 \text{ s}^{-1}$).	73
17 Tensile test results for strain rate 2 ($\dot{\epsilon}^P \approx 5 \text{ s}^{-1}$).	73

LIST OF TABLES (continued)

<u>Table</u>		<u>Page</u>
18	Tensile test results for strain rate 3 ($\dot{\epsilon}^p \approx 10 \text{ s}^{-1}$).	74
19	Tensile test results for strain rate 4 ($\dot{\epsilon}^p \approx 50 \text{ s}^{-1}$).	74
20	Summary of material type 3 bilinear model material parameters.	100
21	Summary of material type 3 perfectly plastic model material parameters.	100
22	Summary of material type 24 material parameters.	101
23	Summary of material type 19 quasi-static material parameters.	102

CHAPTER 1. INTRODUCTION

Traditionally guardrails, bridge rail, guardrail terminals, crash cushions, and other road side safety hardware have been designed primarily using intuition and basic engineering principles with relatively little use of analytical methods. Many highly effective roadside hardware systems have been developed using this technique, but difficult issues remain. Certain types of impacts require a better understanding of the nonlinear dynamics of impacts. To address this issue, nonlinear finite element codes are being incorporated into the development and evaluation of roadside safety hardware. The development of DYNA3D, an explicit nonlinear finite element program, provided a new tool for investigating the complicated mechanics inherent in designing roadside safety hardware.⁽¹⁾

Materials are an important, though often neglected, aspect of finite element models. Accurate simulations of vehicles impacting roadside hardware require an understanding of both physical material behavior and the mathematical material models in LS-DYNA3D.⁽²⁾ Unfortunately, relating the material properties obtained in standard materials tests to the material parameters needed to characterize a material in a finite element program, such as LS-DYNA3D, is not necessarily straightforward. One approach to finding the appropriate material parameters for LS-DYNA3D is to compare physical tests with finite element simulations of those same tests. Using this approach, a methodology to relate roadside hardware material properties to the material input parameters for LS-DYNA3D is presented.

The roadside hardware materials that are investigated include:

- AASHTO M-180 guardrail steel.
- A36 steel from hot-rolled structural shapes.
- Automotive sheet steels used in body panels.
- ASTM A499 re-rolled rail steel used in sign posts.

Both physical material properties and the mathematical material models in LS-DYNA3D are examined for a better understanding of the role of materials and for the selection of the most appropriate mathematical material model.

Accurate material models require accurate material input parameters. Some physical material properties for steel may be found in material handbooks and in specifications. This information, however, is not sufficient to simulate the behavior of steel during impact events for the following reasons:

- The values in handbooks/specifications are conservative.
- There is no failure or post yield information.
- There is no strain rate information.
- The values do not include cold-working effects or residual stresses.

Since the values in material specifications are minimum values, they do not accurately reflect the strength of the typical sample of each type of steel. In addition, there is no information about post

yield stresses and strains. During impact the hardware generally yields and moves well into the plastic region. It is important to understand the magnitude of the stresses and strains that the material undergoes. Also important to consider when simulating impacts are strain rate effects. Strain rate affects the behavior of steel, but the magnitude of the effect varies with each type of steel. Cold-working and residual stresses also affect how steel behaves. The specifications given for each material are pre-cold-working, thus they do not reflect the material that is used in the field. For these reasons, experimental testing is necessary to properly model develop the input parameters for LS-DYNA3D.

First, the material properties must be found without considering the effects of impact. This is possible using standard testing procedures for quasi-static tension tests. This will give information about yield stress, ultimate stress for the materials used. The results may be used to find the input parameters for LS-DYNA3D.

During impact, materials are strained at rates above the quasi-static loading rate used in standardized tests. The yield stress, the ultimate stress and stress at failure are some of the properties that are affected by higher strain rates. There is a need to understand how strain rate affects roadside hardware materials so that these effects may be properly incorporated in modeling impact simulations. Strain rate effects are introduced and explored. The effect strain rate has upon W-beam guardrail is examined. The mathematical material models in LS-DYNA3D that have strain-rate sensitivity are also explored.

CHAPTER 2. QUASI-STATIC COUPON TEST

Standard Laboratory Tests

The American Association of State Highway and Transportation Officials (AASHTO) publishes a variety of material and testing specifications. Test T-244 contains laboratory test procedures for determining the material properties of steels.⁽³⁾ A quasi-static longitudinal flat tension test is generally the most appropriate test for characterizing the properties of sheet steel used to build many roadside safety hardware components.

In a longitudinal flat tension test, a specimen is cut from a plate or sheet and machined into the shape shown in figure 1. The test specimen retains the thickness of the original sample and the width is 12.5 mm in the gauge length. The gauge length of the specimen is the 50.8-mm segment in the center of the narrowed section. During a test, the tensile load supported by the specimen is recorded along with the amount of elongation in the 50.8-mm gauge length. The deformation rate for this quasi-static test must be less than 1.6 mm of elongation per millimeter of gauge length per minute (0.03 mm/s).

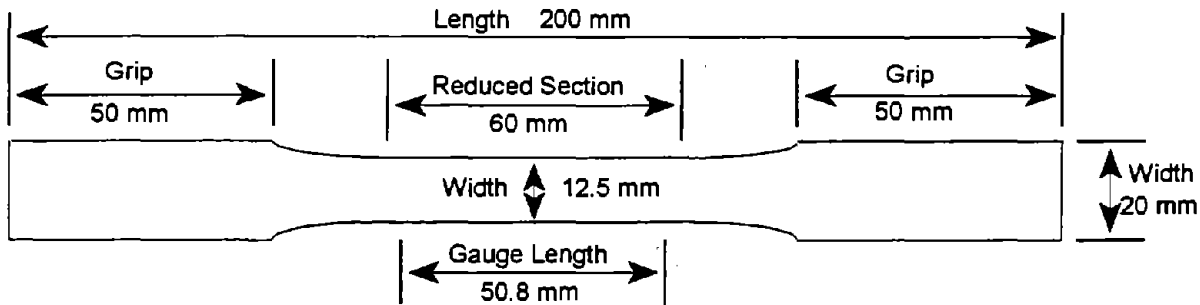


Figure 1 AASHTO T-244 longitudinal flat test specimen. ⁽³⁾

AASHTO and the American Society for Testing and Materials (ASTM) material specifications for steel generally specify the minimum allowable yield strength, ultimate strength and percent elongation at failure for a material. The stresses obtained in AASHTO T-244 tests are engineering stresses (i.e., the load divided by the initial area). The area where the necking and failure phenomena occur is very small in comparison to the total gauge length. The percent elongation in a longitudinal flat tension test is not equal to the infinitesimal strain. The infinitesimal strain is required by LS-DYNA3D. Thus, the "stress-strain" curves obtained in a test are not the "stress-strain" relationships required for an LS-DYNA3D material model. Although the data required for LS-DYNA3D is not directly provided by AASHTO T-244 (ASTM A-370) tests, their results may be used to derive the required material properties.

Finite Element Model

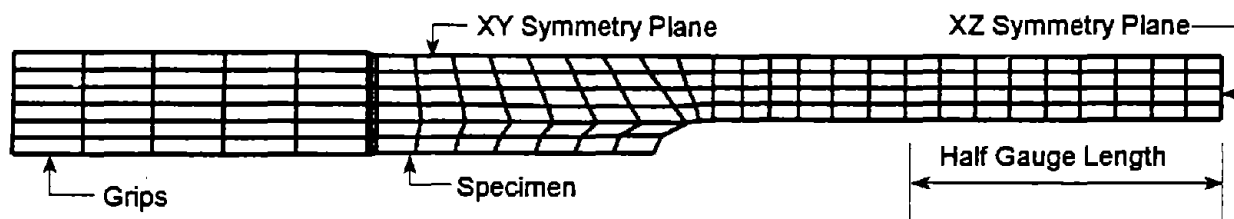


Figure 2 Quarter model of a longitudinal flat tension test.

The finite element mesh used to simulate an AASHTO T-244 longitudinal flat tension coupon test is shown in figure 2. Fortunately, there are two planes of symmetry in the tension test problem permitting the use of a quarter-section model. The problem is symmetrical about the XZ plane and about the XY plane when viewed from the center of the test specimen. The geometry of the quarter section model conforms to the geometry specified in AASHTO T-244 and shown in figure 1. The model consists of 260 nodes, 60 brick-elements and 140 shell-elements.

The longitudinal flat tension test is a quasi-static test with a maximum displacement rate of 1.33 mm/s for a 50.8-mm gauge length. Elongations required to produce failure in mild steels are usually on the order of 25 percent. The minimum time required to test a 50-mm long gauge-length model to failure would be:

$$\frac{1}{1.33 \text{ mm /s}} \cdot 50.8 \text{ mm} \cdot 0.25 = 9.549 \text{ s} \quad (1)$$

Even for a small model like the one shown in figure 2, performing a finite element analysis would take approximately 378 CPU hours using LS-DYNA3D on a Silicon Graphics Indigo workstation. LS-DYNA3D is an explicit dynamic code which is not usually suitable for quasi-static problems. To simulate the quasi-static flat longitudinal tension coupon test, the time-dependence effects must be eliminated or negated. Three issues must be addressed to determine a suitable loading rate that will allow the simulation to accurately predict the quasi-static results: (1) strain rate effects, (2) the speed and amplitude of an elastic wave through the material, and (3) the relative importance of kinetic versus strain energy.

In addition to finding the loading rate, there needs to be an understanding of how changing characteristics of the finite element model affect the results of the simulations. Each of the following characteristics may change not only the behavior of the model but the run time for that model: 1) mesh density, 2) the number of integration points through the shell thickness, and 3) updating the thickness of the shell.

Strain Rate

Strain rate effects can dramatically alter the yield and ultimate strength of mild steels.⁽⁴⁾ In fact incorporating strain rate effects should be an important feature for relevant roadside hardware simulations.⁽⁵⁾ In this case, however, the loading being simulated is quasi-static making the inclusion of strain rate effects counter productive. The simulation will be more like a quasi-static test if no strain-rate dependency is incorporated in the material model.

Elastic Wave Speed and Amplitude

The loading rate should be much slower than the speed of an elastic wave through the material. If the loading rate is similar to the wave speed, the time when the wave arrives at each part of the structure will be important. The speed of an elastic wave through a solid circular rod made of isotropic material with the conventional properties for steel is:⁽⁶⁾

$$c_L = \sqrt{\frac{E}{\rho}} = \sqrt{\frac{200E+03 \text{ MPa}}{7.89E-9 \text{ Mg/mm}^3}} = 5.03E+06 \text{ mm/s} \quad (2)$$

where E is the modulus of elasticity and ρ is the density of the material. The time required for the elastic wave to travel from one end of the model to the other is the 100-mm length of the model divided by the 5.03E+06-mm/s wave speed: 0.02 ms. A loading rate 5000 times slower than the elastic wave speed should "feel" like a static loading to the specimen in the absence of strain-rate and inertia effects.

The amplitude of the stress wave is also an important consideration in selecting the loading rate. The amplitude of an axial stress wave in a circular rod is given by:⁽⁶⁾

$$F_w = \sigma_w \cdot A = \rho \cdot c_L \cdot v \cdot A \quad (3)$$

where σ is the amplitude of the stress wave, F_w is the amplitude of the stress wave in force units, v is the velocity of a particle on the rod and A is the cross-sectional area of the rod. The loading rate is the upper bound for the particle velocity. Using values of 7.86E-09 Mg/mm³ for the material density, and 5.03E+06 mm/s for the stress wave speed through the material, the values in table 1 are obtained.

When the loading rate is 5000 mm/s (i.e., three orders of magnitude less than the wave speed) the elastic stress wave amplitude is 6.8

Table 1 Amplitude of a stress wave in a circular bar at various loading rates.

Loading Rate (mm/s)	Wave Amplitude (kN)	Percent Yield Force (%)
5000	6.80	47.9
1000	1.36	9.6
200	0.27	1.9
40	0.05	0.4

kN, almost half the value of the 14.2-kN yield force. These high-amplitude stress waves are clearly visible in figure 3 for the 5000-mm/s curve. The amplitude decreases to 10 percent of the yield force when the loading rate is decreased by a factor of 5 to 1000 mm/s. The stress wave amplitude is still clearly visible in figure 3 for the 1000 mm/s loading rate though much less pronounced than at 5000 mm/s. The amplitude of the stress wave is only 2 percent of the yield force at a loading rate of 200 mm/s. These small amplitude waves are not seen on the force-elongation plot (figure 3) resulting in a curve that has a more quasi-static appearance.

Figure 3 shows a comparison of the response of exactly the same material model parameters for four different loading rates. The highest rate is 5000 mm/s. Each loading rate is 5 times smaller than the next higher resulting in loading rates of 5000, 1000, 200 and 40 mm/s. The output rate is always selected such that the simulation produced 2,000 data points so that each of the four curves may be compared point-to-point. With the exception of the stress wave amplitude effects discussed above, all four curves have a very similar force-elongation history up to about 20 percent elongation. The most important feature of these curves is the failure point. The higher loading rate simulations result in a larger failure elongation. The loading rate is decreased until no change was observed in the failure point. A loading rate of 200 mm/s, for example, results in a failure elongation of 26 percent. The response for a loading rate of 40 mm/s, a loading rate 5 times slower, also results in a failure elongation of 26 percent. The loading rate required to produce an essentially quasi-static response is therefore judged to be 200 mm/s or less.

In addition, a non-reflecting boundary was created for a more quasi-static response. A non-reflecting boundary permits the elastic stress wave pass through the boundary without being reflected, further reducing the effect of stress waves. A surface can be defined as a non-reflecting boundary in LS-DYNA3D. Unfortunately, however, non-reflecting boundaries must be surfaces, but the upper boundary of the shell-element specimen shown in figure 2 is a simple line. Sixty small solid-elements are attached to the model of the specimen in the area where the test grips are attached to allow for the use of a non-reflecting boundary. These solid elements are connected to the shells with a tied contact surface and are only used so that the non-reflective boundary feature can be used.

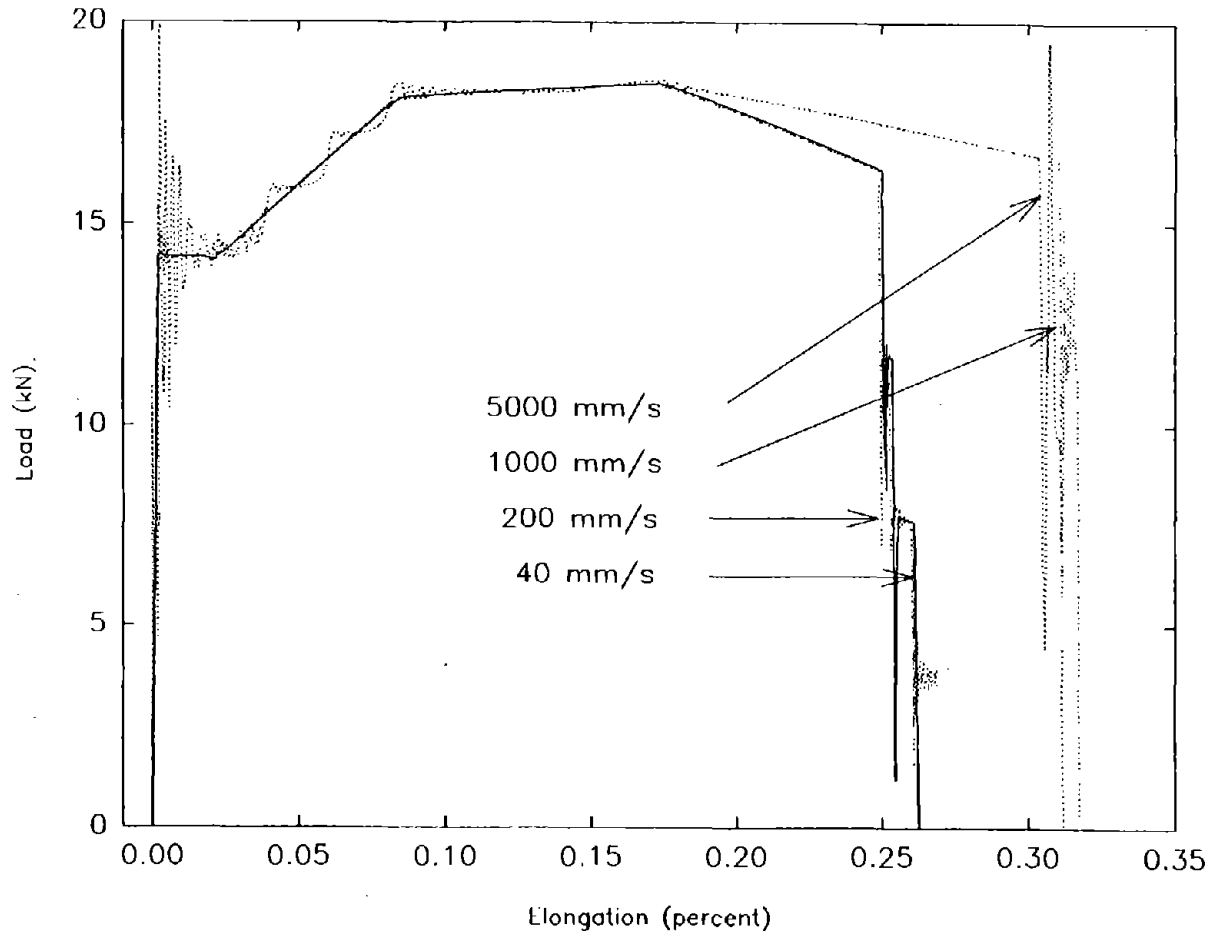


Figure 3 Load versus elongation curve for various loading rates.

Kinetic Energy

The kinetic energy of the system should be very small in comparison to the strain energy to minimize internal effects on the analysis. The specimen, whose total mass is a little less than 10 g, has a very small kinetic energy with respect to the strain energy required to cause failure. Table 2 shows a comparison of the internal strain energy and the kinetic energy in a mild steel simulation for several loading rates. As shown in the table, for the loading rates used, kinetic energy is always four orders of magnitude less than the internal strain energy needed to fail the mild-steel specimen. The kinetic energy in these simulations represents a trivial amount of the total energy for all loading rates. Using a dynamic load in the range of loading rates given in table 2, does not introduce an appreciable amount of extraneous energy into the problem.

Table 2 Kinetic and total energy at different loading rates.

Loading Rate (mm/s)	Kinetic Energy (J)	Strain Energy (J)
<i>At yield stress</i>		
40	4.8E-5	4.15
200	0.001	4.16
1000	0.032	4.08
5000	0.736	4.12
<i>At ultimate stress</i>		
40	5.8E-5	252.19
200	0.002	250.36
1000	0.037	265.60
5000	0.896	266.00

It is also interesting to note that, in the absence of strain rate effects, the amount of strain energy at both the yield point and the ultimate point is not a function of the loading rate. This suggests that simulation time is indeed a "pseudo time" when the following conditions are met:

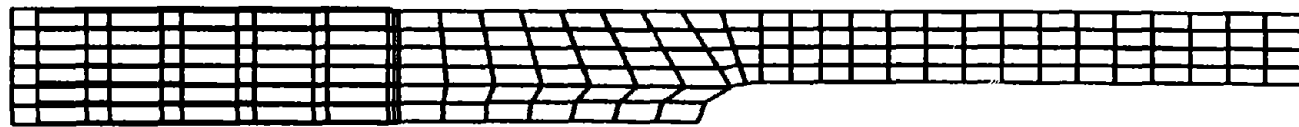
- Strain rate effects are not included.
- The amplitude of the stress wave is no more than 2 percent of the yield stress.
- Kinetic energy is small compared to the strain energy required for failure.

When these conditions are met, the simulation will respond in an essentially quasi-static manner that allows the simulation results to be compared directly with quasi-static laboratory tests. The loading rate of 200 mm/s meets the stated conditions and was therefore selected for the quasi-static finite element simulations using LS-DYNA3D.

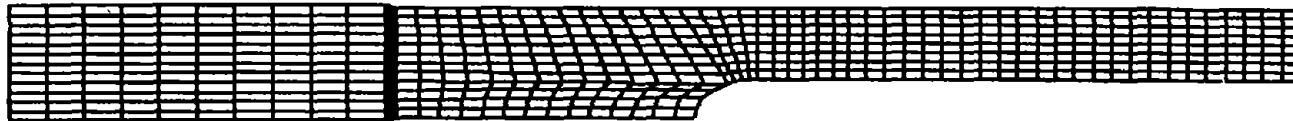
Mesh Density

The effect of different mesh densities upon the results was examined. The original mesh was compared to two denser meshes. Figure 4 shows these meshes which are two and three times as dense as the original mesh. Fortunately there does not appear to be any effect upon the response

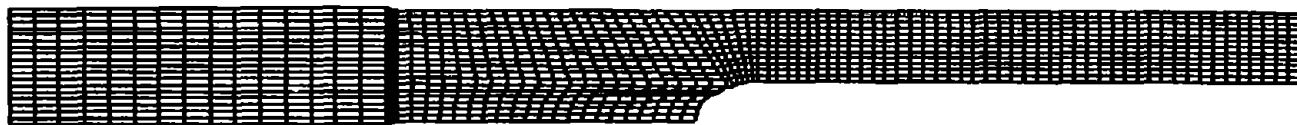
of the model as seen in figure 4. The computational time of the different meshes, however, did vary greatly. The computational time increased from 1.5 CPU hours for the coarsest mesh to 59.4 hours for the densest mesh. Since refining the mesh density did not change the results the original mesh was retained.



Original Mesh



Mesh Twice as Dense



Mesh Three Times as Dense

Figure 4 Three quarter models with different mesh densities.

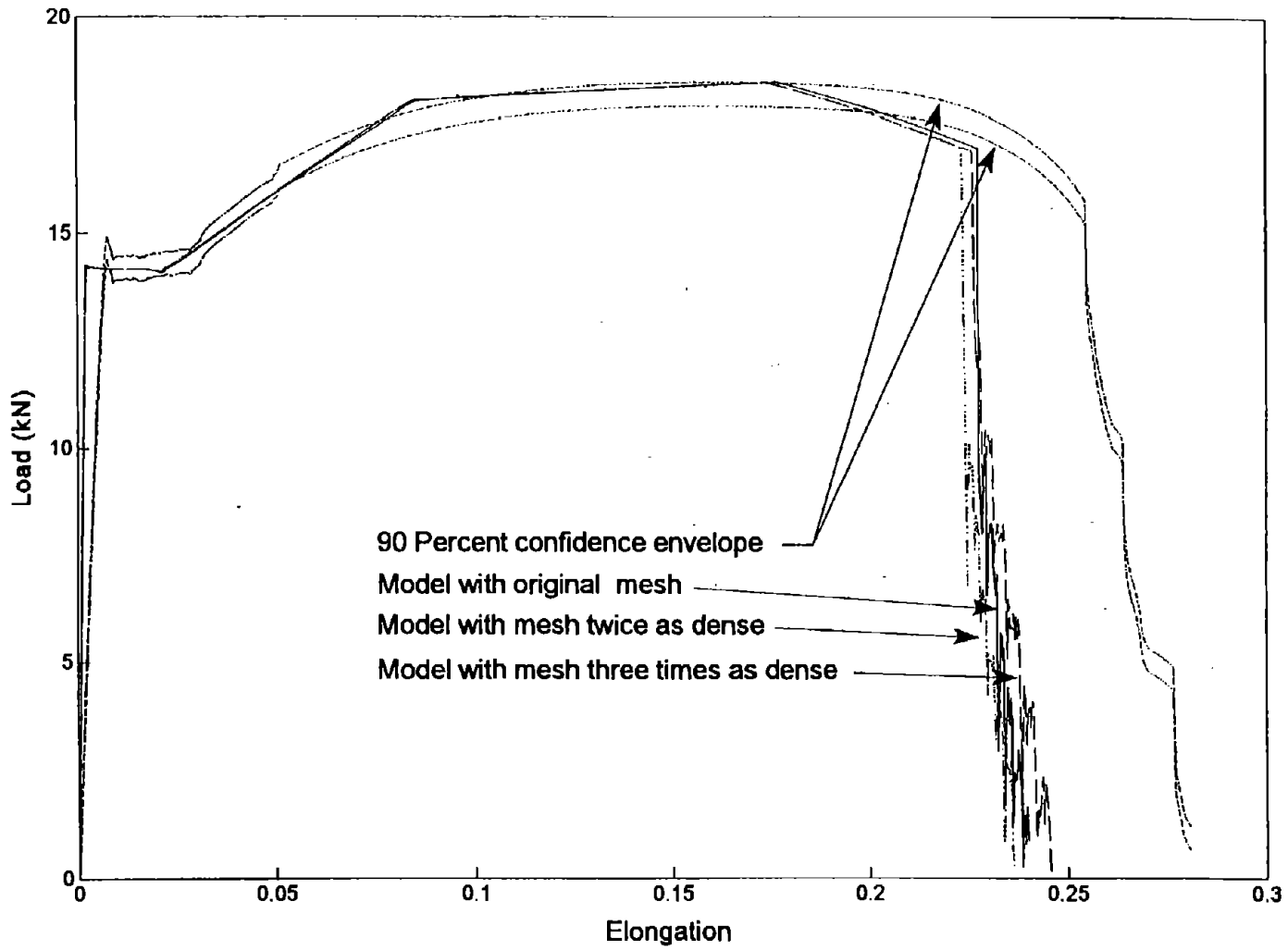


Figure 5 Load versus elongation curve for different mesh densities.

Belytschko-Lin-Tsay Shell

The Belytschko-Lin-Tsay shell formulation is used for modeling of the coupon. This type of shell is typically used for sheet steels in roadside safety hardware simulations. In addition, this shell is also the default shell element option in LS-DYNA3D. It is more computationally efficient than the Hughes-Lui shell element. The Belytschko-Lin-Tsay element requires only 17.8 percent of the mathematical operations required by the Hughes-Lui shell element with 5 through-the-thickness integration points.^(7, 8)

The number of through-the-thickness integration points can be varied in LS-DYNA3D. The greater number of integration points, the more accurate the shell behavior will be. The quarter model shown in figure 2 was simulated with 3 and 5 through-the-thickness integration points. Figure 6 shows that the simulation with 3 through-the-thickness integration points fails earlier than the one with 5. When 3 points through-the-thickness are used, the material plasticizes too early, thus the elongation of the coupon is too high too early.⁽⁹⁾ Both simulations have approximately the same computational time of 1.5 CPU hours. Five through-the-thickness integration points are used for all simulations.

LS-DYNA3D also has the option of updating the shell thickness due to large membrane stretching during the simulation. By updating the thickness, the normal strain is more accurately calculated.⁽⁷⁾ This provides a more accurate representation of the effective stress and effective strain. Figure 7 shows that the load-elongation behavior is quite different. The model with the option to update the thickness does not reach the same load for same effective strain that was used for the effective stress-strain curve input into the model. The effective strain is also reduced. While the behavior changes, both models have approximately the same computational time of 1.5 CPU hours. For crash simulations it is recommended that the thickness update option be ignored. All simulations documented in this report were conducted without shell thickness updates.

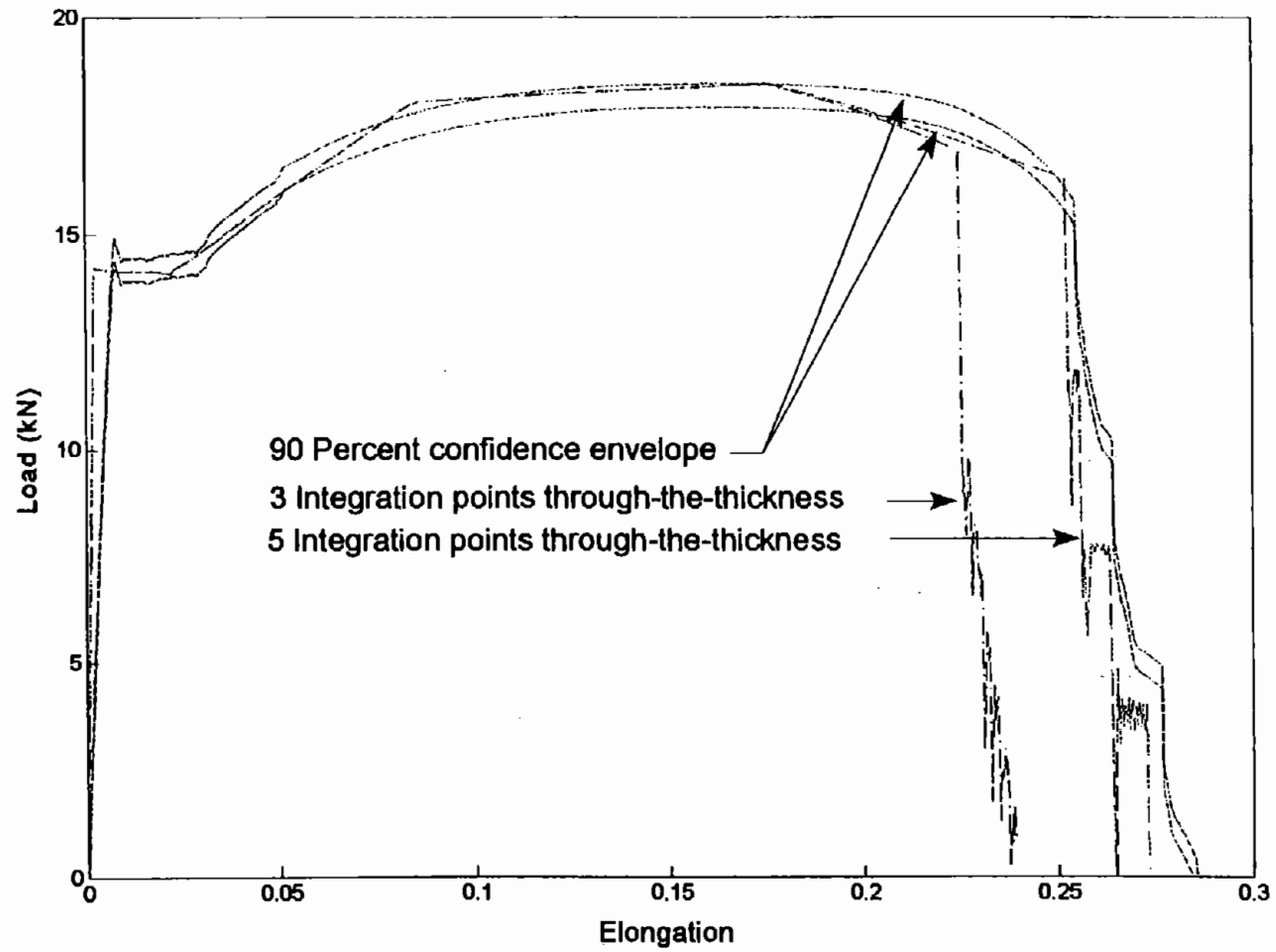


Figure 6 Load versus elongation curve with 3 and 5 through-the-thickness integration points for Belytschko-Lin-Tsay shell element.

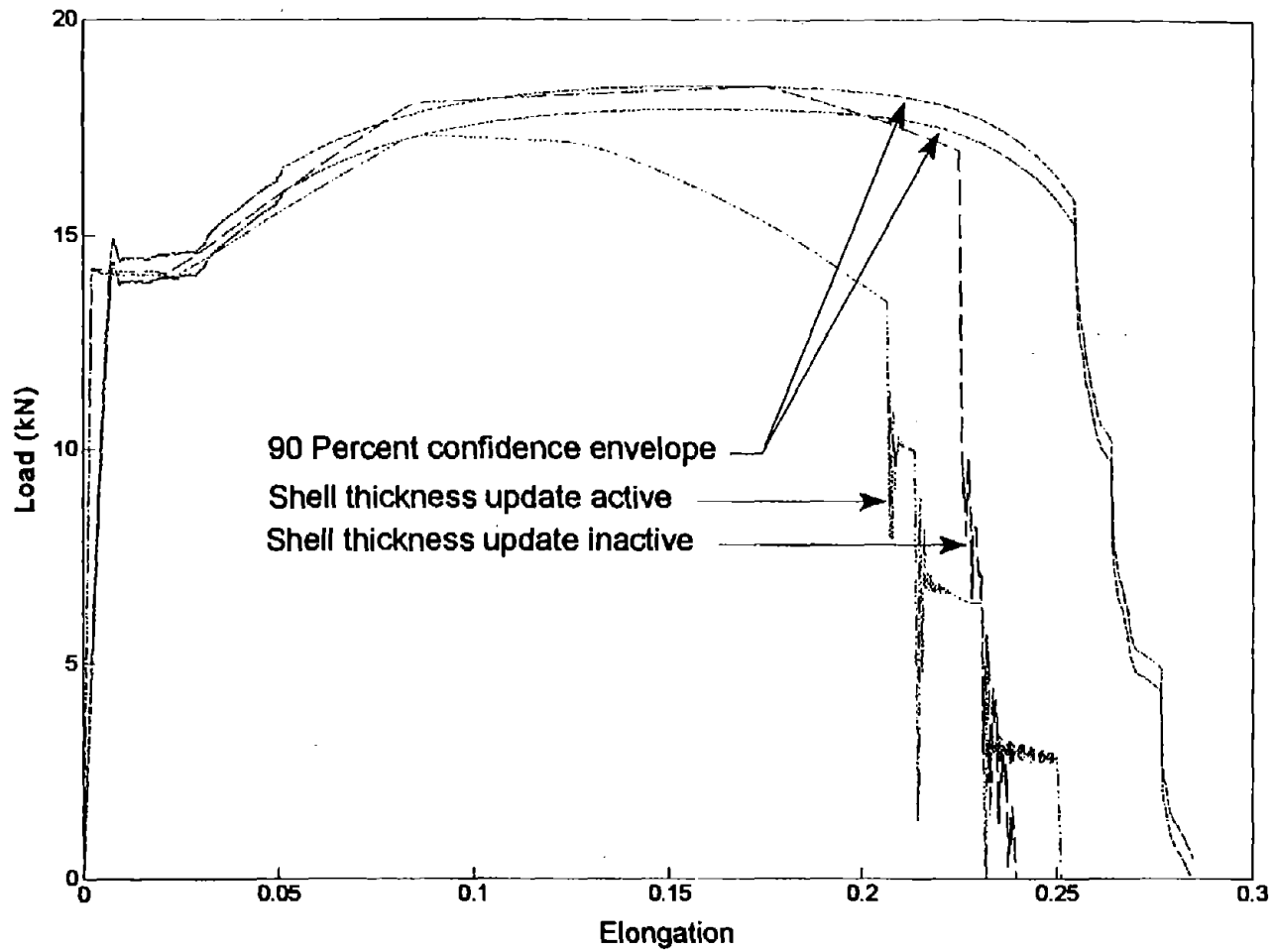


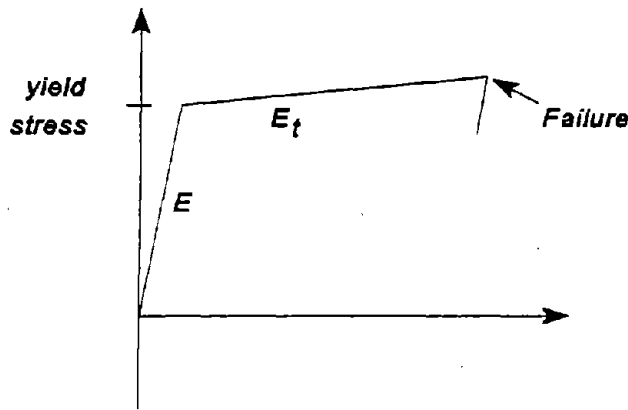
Figure 7 Load versus elongation curve of simulations with and without shell thickness updates.

Mathematical Material Models

LS-DYNA3D has more than 50 mathematical material models. Using a model that behaves in a manner similar to the material being modeled is important. Four mathematical material models were examined for simulating the quasi-static tests in this report. The behavior of all four models is suitable for simulating steel materials. These four mathematical material models are:

- Kinematic/isotropic plasticity (material type 3).
- Isotropic elastic-plastic with failure (material type 13).
- Strain rate dependent isotropic plasticity (material type 19).
- Piecewise linear isotropic plasticity (material type 24).

Material type 3 is a simple bilinear model. It follows the elastic modulus to the yield stress and then follows the hardening modulus (tangent modulus), E_t , to failure. Figure 8 shows the material model behavior.¹⁰ LS-DYNA3D material type 3 models failure using a specified plastic strain.



The Young's modulus, yield stress, hardening modulus, hardening parameter and the failure strain are all user defined.

Material type 13 is also a simple bilinear model with failure. The material follows a curve similar to the one shown for material type 3. The user defines the shear modulus, yield stress, hardening modulus, failure strain, failure pressure and bulk modulus. Material type 13, however, can only be used with solid elements.⁽⁸⁾ Shell elements are usually preferred for modeling the types of roadside hardware materials discussed. The finite element model of the coupon is composed of

Figure 8 Material type 3 behavior.

shells in the failing section, thus this material type was not used.

Material type 19 is a bilinear strain-rate sensitive model. It may be used without strain-rate sensitivity very easily. The user defines Young's modulus, Poisson's ratio, the hardening modulus, E_p , and the load curves for strain rate effects. The load curves are for the yield stress, Young's modulus, tangent modulus and von Mises stress at failure. All these curves must be defined for the model to work. In order to remove strain rate effects, the user defines each property to be the same for all strain rates given in the load curves, e.g., for an input with two strain rate entries of 0 s^{-1} and 3000 s^{-1} the yield stress would be 415 MPa for both entries. LS-DYNA3D has enough information for proper modeling with only two input values in each load curve.

Material type 24 is a more complicated mathematical model than the previous three material models. The user may input a tabular stress-versus-strain curve, which allows the material

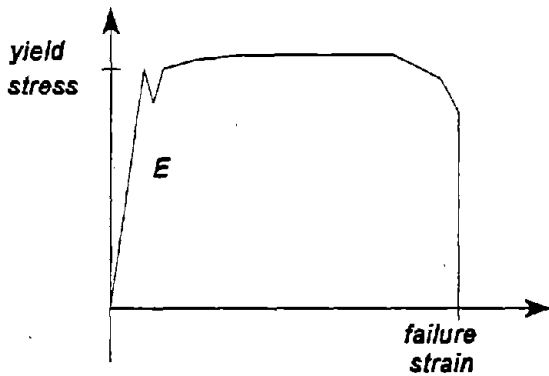


Figure 9 Material type 24 behavior as defined by the user.

behavior to be more accurately modeled. LS-DYNA3D interpolates between each point to define the material behavior at any state of stress resulting in a curve similar the one shown in figure 9. The user defines Young's modulus, Poisson's ratio, the yield stress, the plastic strain at failure and the tabular effective plastic strain versus stress values.⁽¹⁰⁾ This material model has an effective-plastic-strain based failure model. Material types 3, 19 and 24 are used to model the quasi-static tension test.

Analyzing Results

While the "stress-strain" curves are not the same for LS-DYNA3D and AASHTO T-244 (ASTM A-370) tests, their load-versus-elongation curves are equivalent providing a basis for comparison. Multiple laboratory tests are performed to find the average material properties. Using the results of these tests, a 90th percentile envelope is created as seen in figure 10, meaning 9 out of 10 test results should fall within this envelope. If the force values at each increment of elongation are averaged for all the tests, the average response curve is obtained. The standard deviation of the residuals is then calculated. The product of the standard deviation of the residual and 1.6449 is added and subtracted from the average response creating the 90th percentile envelope.^(11, 12)

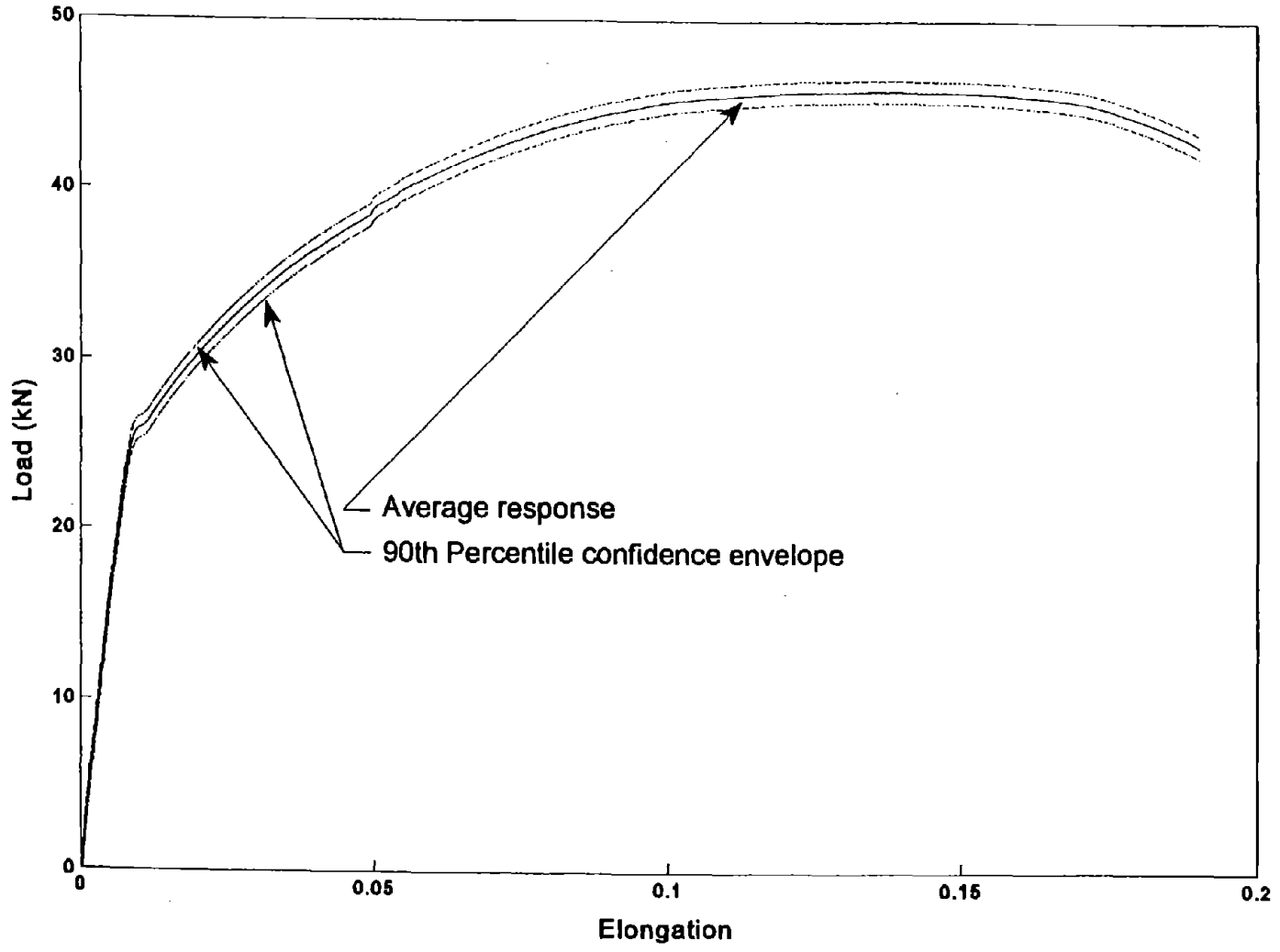
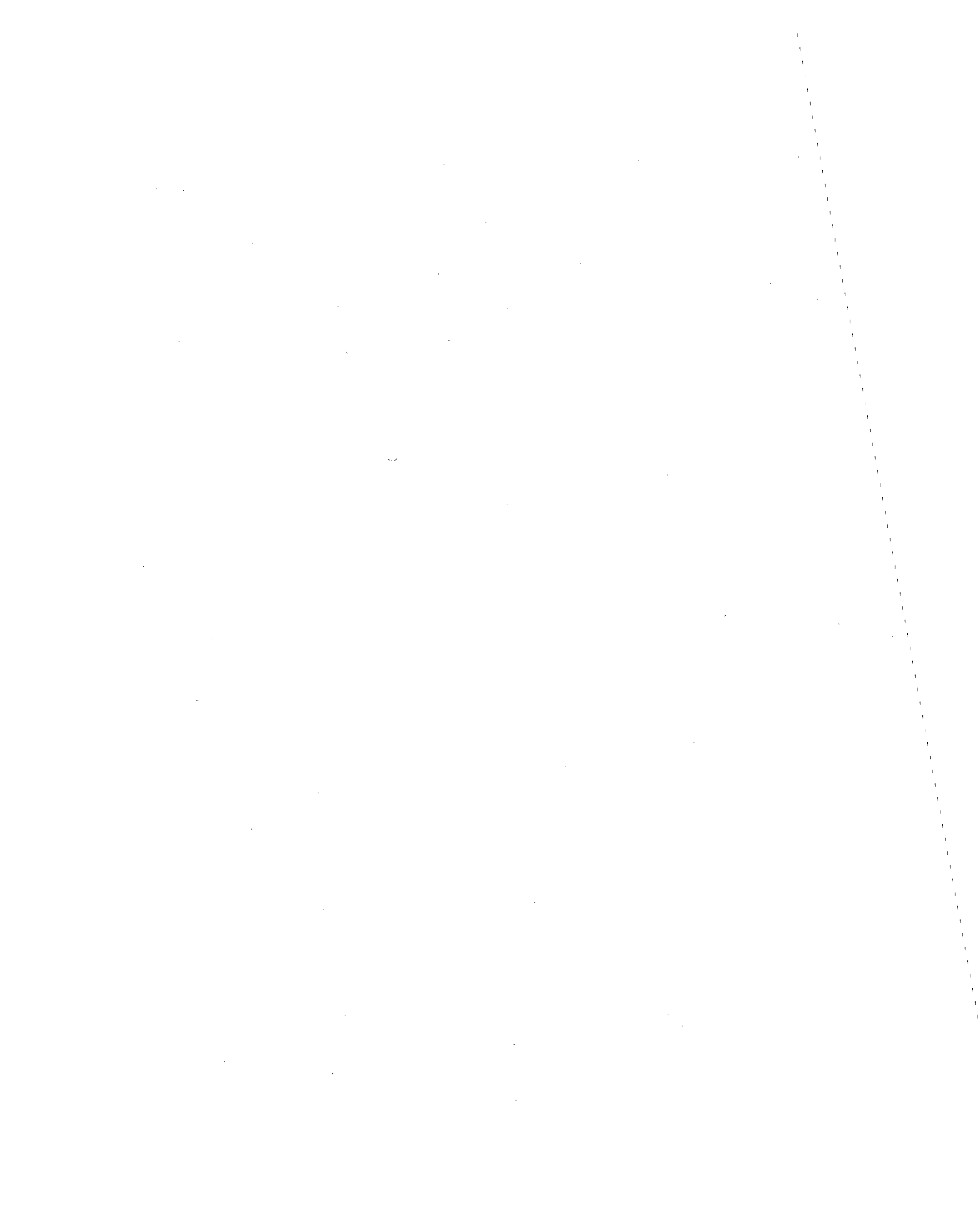


Figure 10 Load versus elongation curve showing the 90th percentile envelope.



CHAPTER 3. GUARDRAIL STEEL

Corrugated steel guardrails are one of the most common structural elements used in roadside hardware applications. Guardrail systems similar to the one in figure 11 are widely used throughout the United States. Because guardrail systems are used so widely, it is important that they are continually tested for the current vehicle fleet. When a vehicle impacts W-beam guardrail, the rail redirects the car and absorbs some of the energy from the impact by deforming. Guardrails may fail in tension or in bending/buckling which are shown in figure 12, figure 13, and figure 14. Specifications for manufacturing guardrails and the minimum required mechanical material properties are given in AASHTO M-180.^(13, 14) Minimum values are not very useful as a basis for the material parameters needed by LS-DYNA3D since actual properties may be significantly greater. Standard laboratory tests were performed to provide realistic data used to find the material properties needed for LS-DYNA3D.

Experimental Test Results

Four samples of Class A Type II (12 gauge zinc coated) W-beam guardrail were cut, machined and tested according to AASHTO T-244. The specimens were cut from the flattest part of the sloping edge of the beam and the longitudinal direction of the coupon was aligned with the longitudinal direction of the guardrail. This ensured that the tensile load applied in the test corresponded to the tension normally experienced in a guardrail impact. The total thickness given in AASHTO M-180 for Class A Type II steel is 2.82-mm consisting of a 2.67-mm base-metal thickness and a 0.075-mm thick coat of zinc galvanizing on each side. The actual failed test specimens are shown in figure 15. The load-versus-elongation curves for three of the specimens are shown in figure 16. The data from only three of the samples were used, the fourth specimen slipped during testing. The specimens exhibit behavior typical of mild steels.

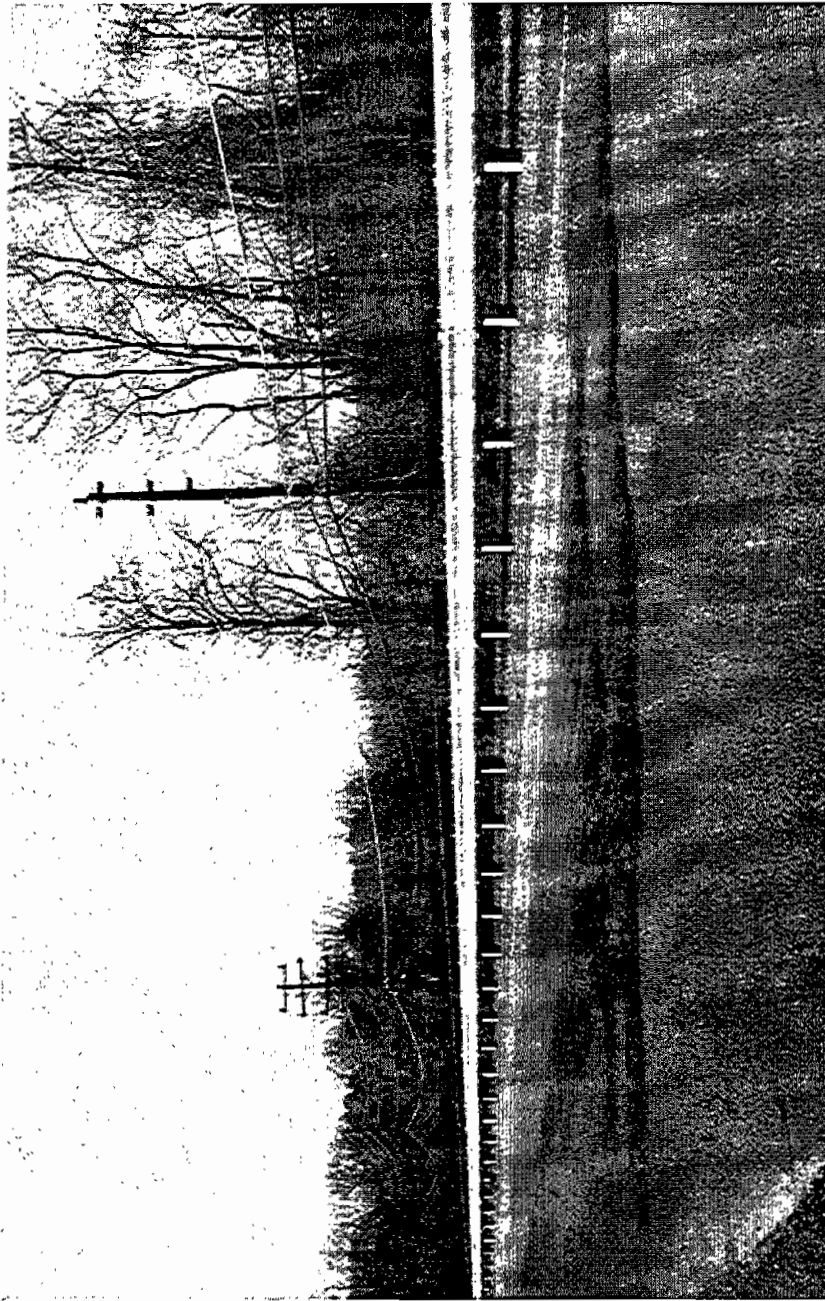


Figure 11 Typical guardrail system.



Figure 12 Typical local buckling of a guardrail.

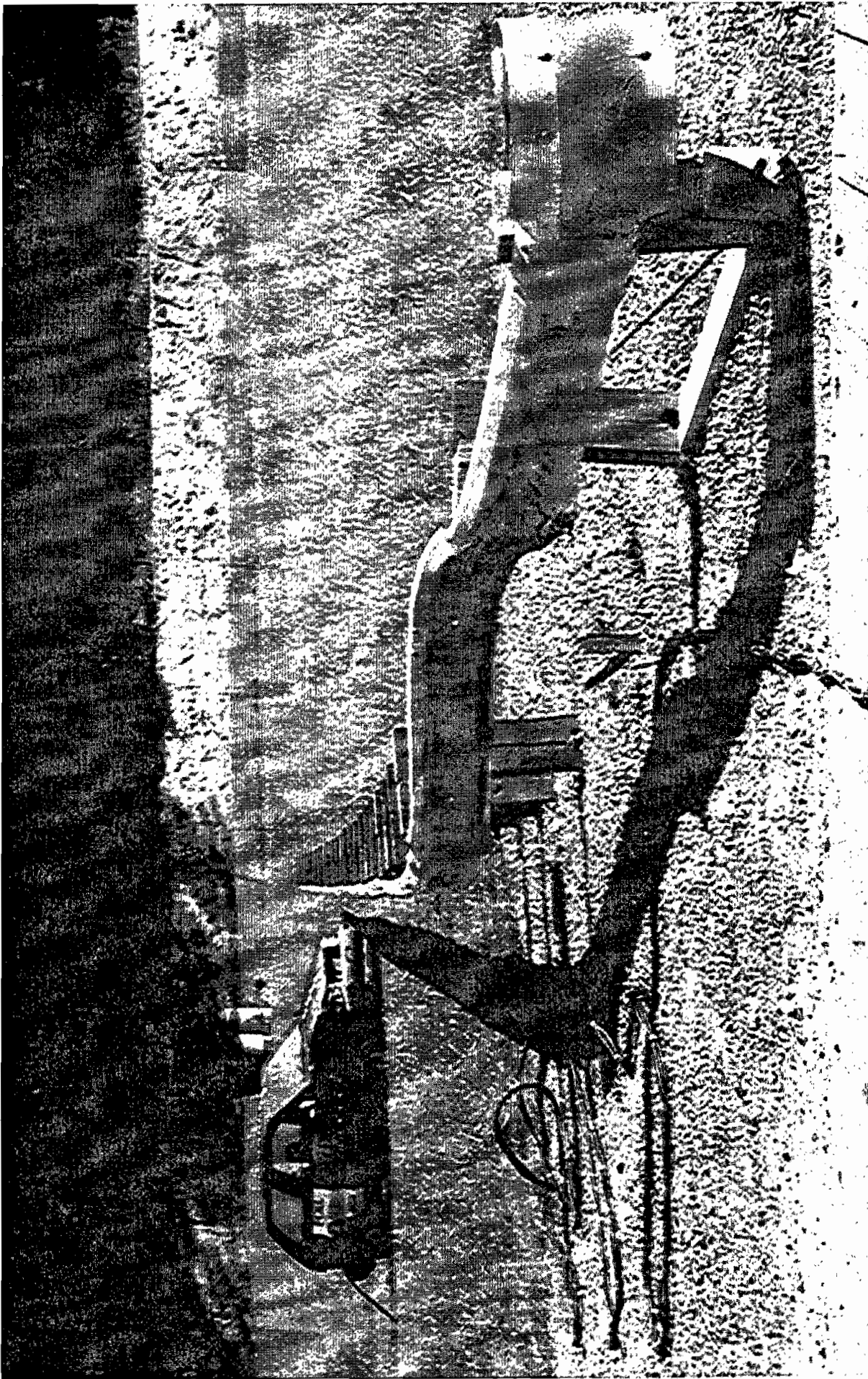


Figure 13 Typical guardrail damage.



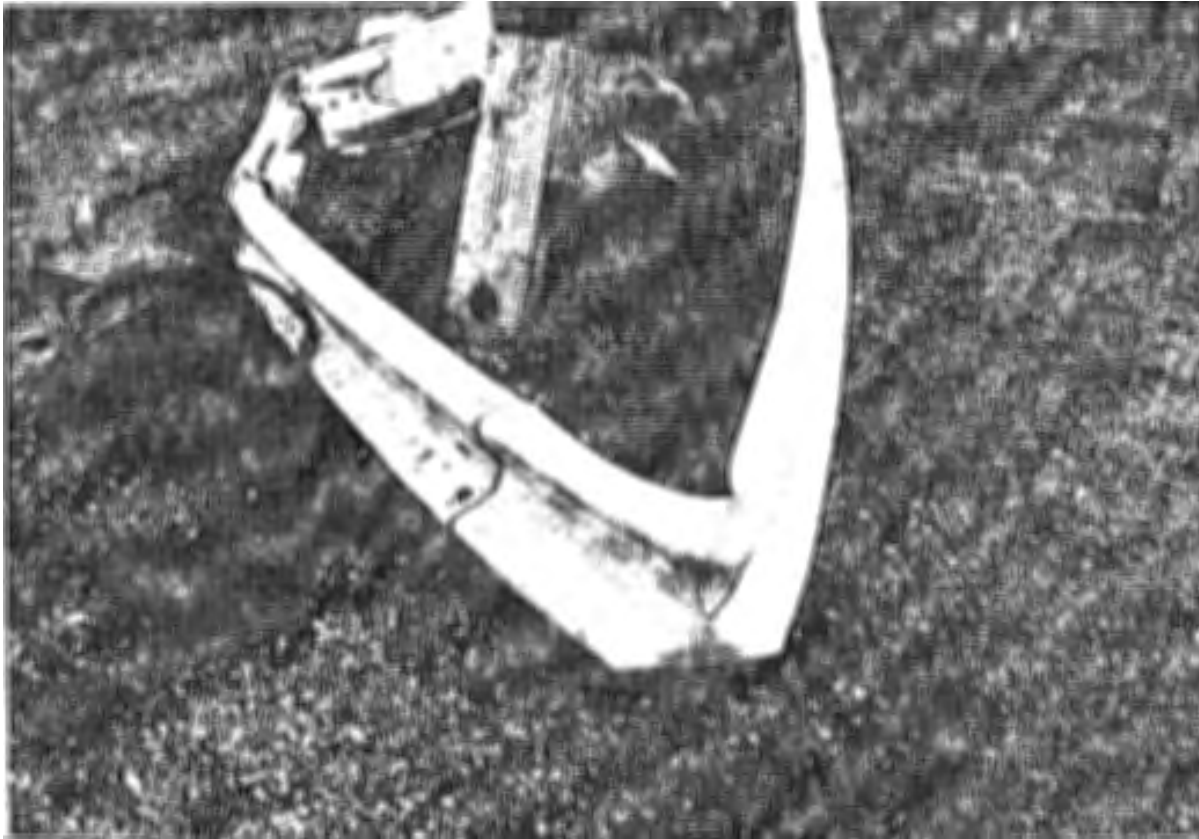


Figure 14 Guardrail that has been impacted at an end terminal.

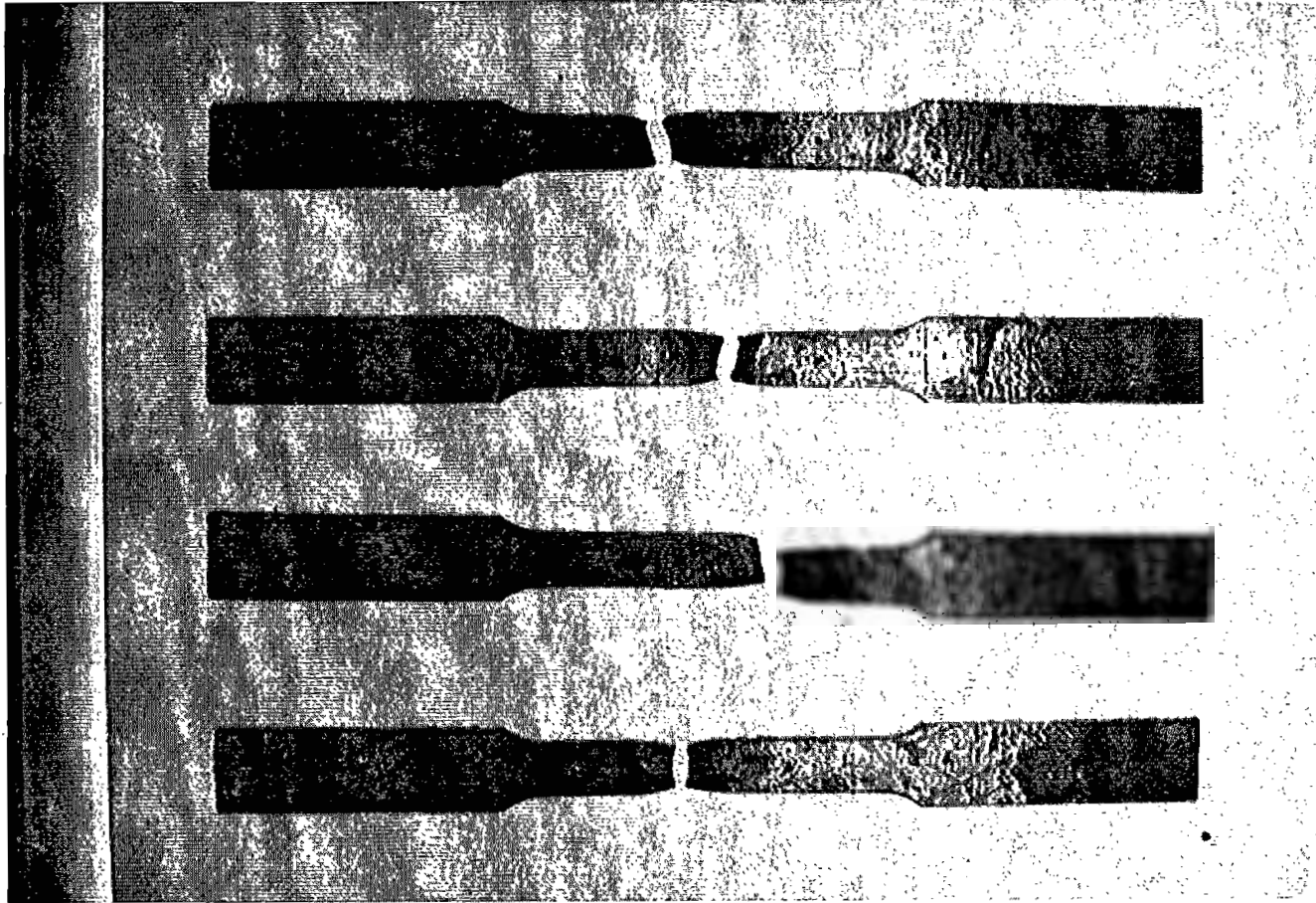


Figure 15 Post-test photograph of AASHTO M-180 Class A Type II steel test specimens.

Table 3 Longitudinal flat tension tests of AASHTO M-180 Class A Type II steel.

	M-180 (minimum)	(1)	(2)
<i>Test Observations</i>			
Number of tests	--	--	4
Average Yield Strength (MPa)	345	393	393
Average Tensile Strength (MPa)	483	558	510
Average Elongation in 50 mm (%)	12	26	26
Average Specimen thickness (mm)	2.82	--	2.82
<i>Base Metal Properties</i>			
Yield Strength (MPa)	345	--	415
Tensile Strength (MPa)	483	--	538
Specimen thickness (mm)	2.67	--	2.67

Sources:

1. Material test report for order C816166, SYRO Steel Inc., August 8, 1991.
2. Tests by Federal Highway Administration, Structures Laboratory, January 10, 1994.

Table 3 summarizes mechanical properties of M-180 guardrail material obtained from longitudinal flat tension tests by SYRO Steel Inc. in column (1) and by the Federal Highway Administration in column (2). Although the results vary, the values exceed the minimum values required by AASHTO M-180 and are typical of guardrail material. The yield and tensile strength in these tests exceeded the specifications by approximately 15 and 5 percent respectively. The percent elongation at failure was approximately twice the specified value. Elongations at failure of 25 are, however, representative of typical guardrail material.

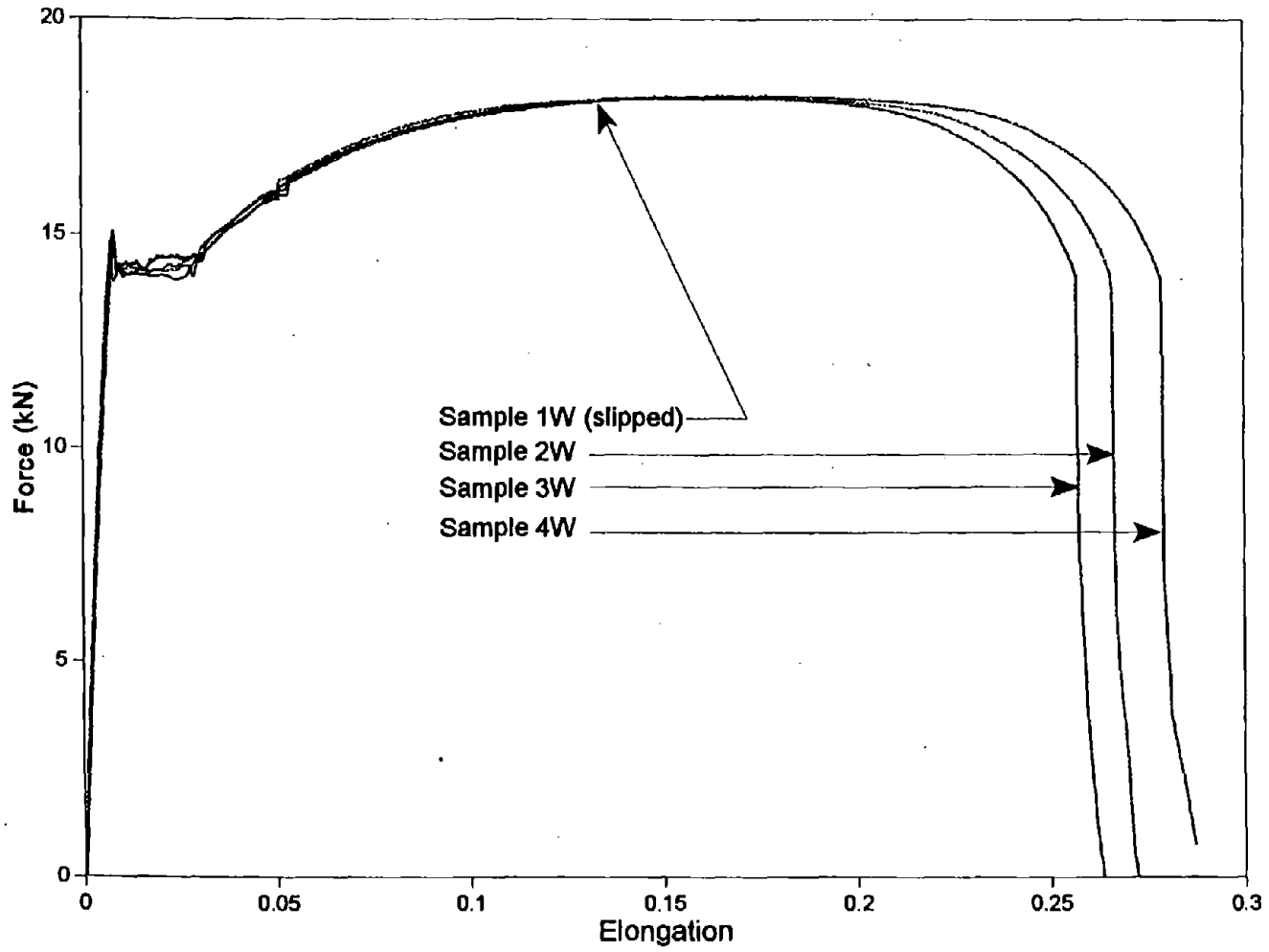


Figure 16 Force versus elongation for AASHTO M-180 Class A Type II guardrail steel.

Finite Element Analysis Results

Finite element analyses were conducted using LS-DYNA3D to determine the parameters that would result in behavior similar to longitudinal flat tension tests. The material was modeled using the Belytschko-Tsay shell formulation with five integration points through the thickness. This type of shell element is often used for modeling corrugated sheet steel in crashworthiness analyses. Two LS-DYNA3D material types were investigated for AASHTO M-180 steel: the Kinematic/Isotropic Elastic-Plastic material model (type 3) and the Rate-Dependent Tabular Isotropic Elastic-Plastic material model (type 24). The 90th percentile confidence envelope was created using the results of the experimental tests shown in figure 16 as discussed in chapter 2.

Material Type 3

When a simple material model is desired, LS-DYNA3D material type 3 is often a good choice for mild steels. Material type 3 is a bilinear model making it difficult to fit the response exactly within the 90th percentile confidence envelope. Material type 3 parameters were found for two different types of material behavior: bilinear (elongations up to 11 percent) and elastic-perfectly plastic (elongations up to and including failure). The parameters for these types of behavior are summarized in table 4.

The modulus of elasticity for the test specimens in figure 17 appears much lower than the commonly used value of 200E+03 MPa. Slipping of the grips during the physical testing causes this phenomena. The flat tension test is not a good method for measuring the small strains needed to determine the modulus of elasticity. For this reason, the simulated response appears much stiffer in the elastic phase than the physical tests. The commonly used value of the modulus of elasticity for steel was, therefore, used in the finite element simulations.

When elongations are expected to be relatively small (e.g., less than 11 percent), a simple bilinear model can be used. A tangent modulus of 1700 MPa yields the response shown in figure 17. This response remains as close to the tested response as is possible with a two-line segment model.

When elongations are expected to be very large (e.g., up to 22 percent) and may include failure, a perfectly plastic material model is appropriate. For this model, the yield stress is increased above the actual value and the true-stress true-strain tangent modulus is 300 MPa resulting in an essentially perfectly plastic force-elongation response as shown in figure 18. Since the yield stress is too high, this formulation requires more strain energy. The amount of strain energy that is inappropriately lost using this method is approximately 11 Joules, only about 5 percent of 230 Joules required to fail the specimen.

Table 4 LS-DYNA3D material parameters for modeling AASHTO M-180 Class A Type II steel with material type 3.

Bilinear model (elongations less than 11 percent)	
Density (Mg/mm ³)	7.86E-09
Young's Modulus (MPa)	200.E+03
Poisson's Ratio	0.33
Yield Stress (MPa)	400.0
Tangent Modulus (MPa)	1700.0
Hardening Parameter	1.0
Perfectly plastic model (elongations up 22 and including failure)	
Density (Mg/mm ³)	7.86E-09
Young's Modulus (MPa)	200.E+03
Poisson's Ratio	0.33
Yield Stress (MPa)	525.0
Tangent Modulus (MPa)	300.0
Hardening Parameter	1.0
Plastic Strain at Failure	0.24

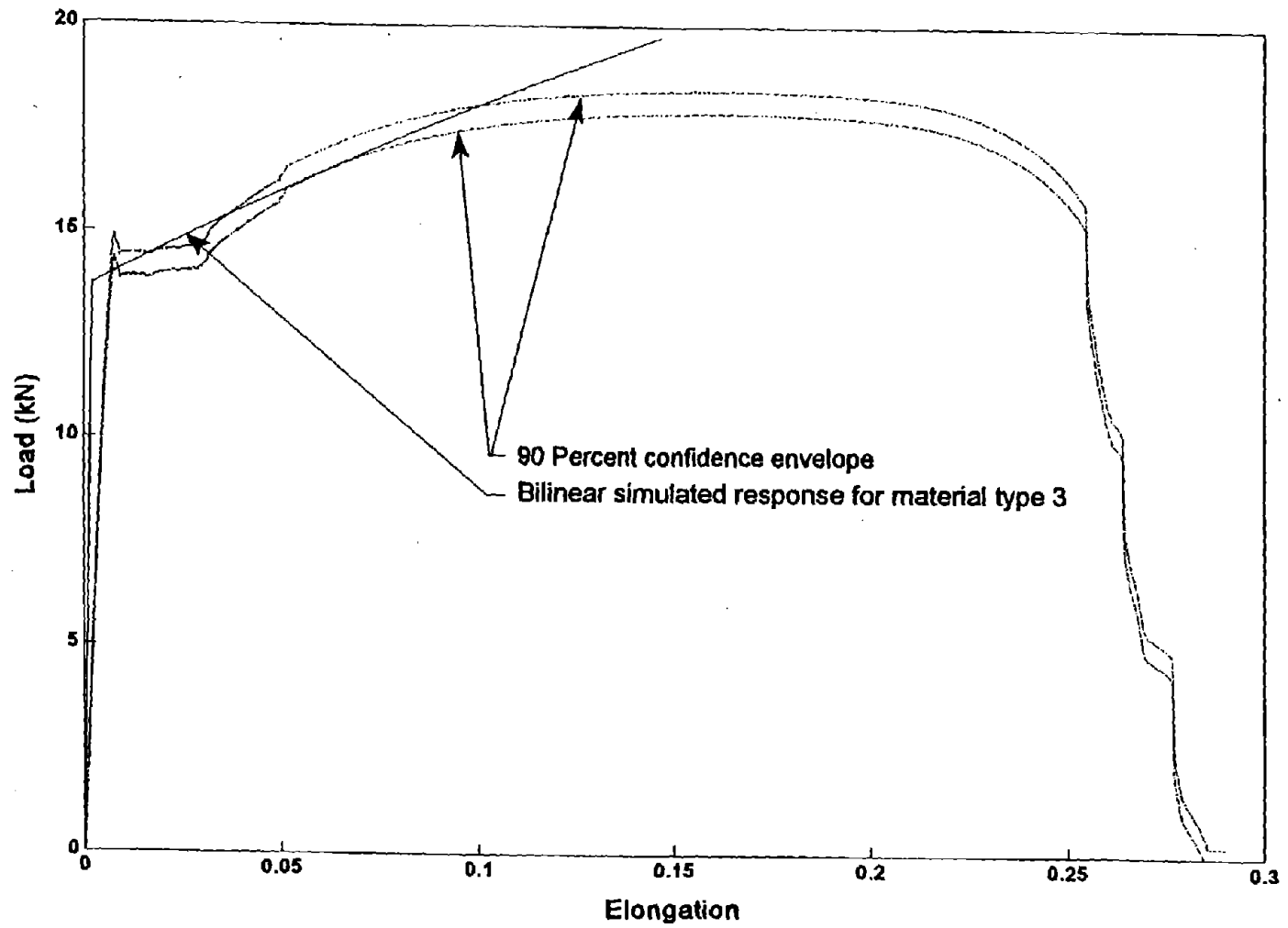


Figure 17 Load versus elongation curve of bilinear simulated response of AASHTO M-180 Class A Type II guardrail steel for material type 3.

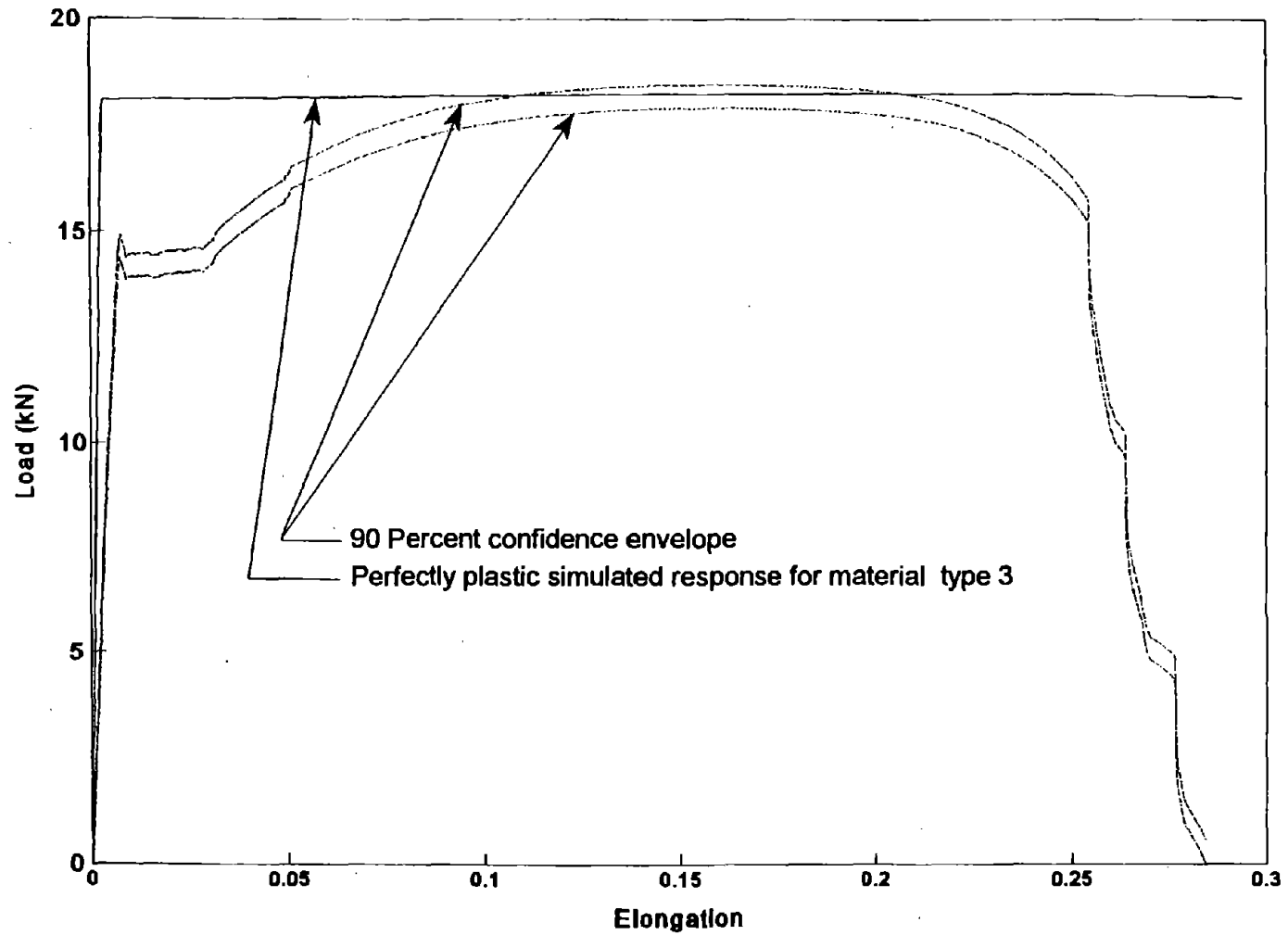


Figure 18 Load versus elongation curve for the perfectly plastic simulated response of AASHTO M-180 Class A Type II guardrail steel for material type 3.

Material Type 24

When the material is loaded to strains at or near failure, material type 24 is a good choice for steel. LS-DYNA3D parameters for material type 24 that yield good results are summarized in table 5. Material 24 allows the user to provide a tabular stress-strain curve and an effective plastic strain when the material fails. Basic properties like the modulus of elasticity, the density of steel and Poisson's ratio were taken from standard references on materials since these characteristics of steel do not vary appreciably among steels. The yield stress, the effective plastic strain at failure, and the effective-stress versus effective-plastic-strain curve are all determined using the experimental results. As shown in table 5, the parameters listed table 5 yield a force-elongation response that is almost completely within the 90 percent confidence envelope.

Table 5 LS-DYNA3D material parameters for modeling AASHTO M-180 Class A Type II steel for material type 24.

Density (Mg/mm ³)	7.86E-09
Young's Modulus (MPa)	200.E+03
Poisson's Ratio	0.33
Yield Stress (MPa)	415.0
Strain rate effects	none
Plastic Strain at Failure	0.66
Increments of strain	0.0 0.02 0.08 0.165 0.33 0.49 0.66 1.0
Increments of stress (MPa)	415 415 548 575 585 595 600 0

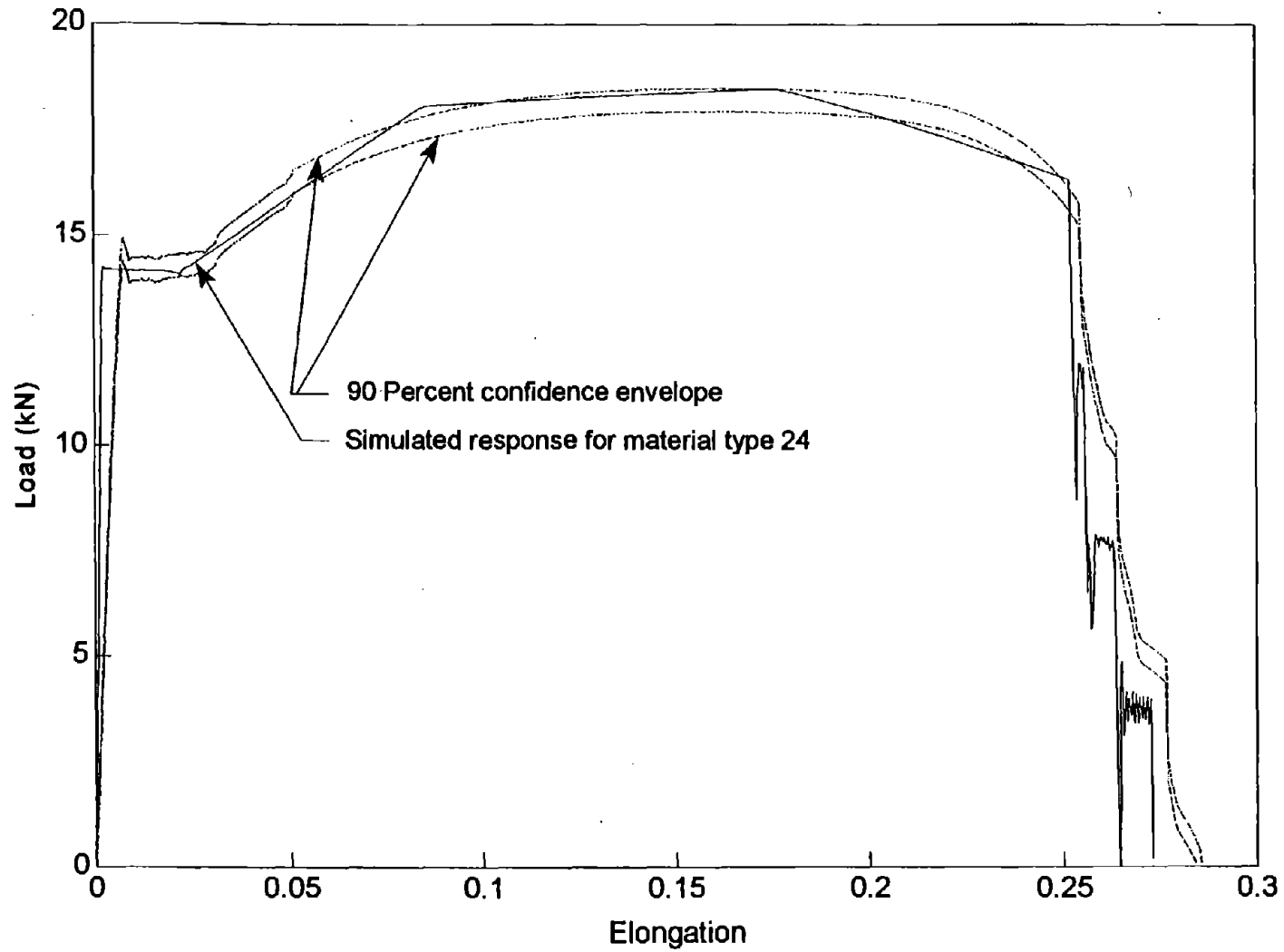


Figure 19 Load versus elongation curve for the simulated response of AASHTO M-180 Class A Type II guardrail steel for material type 24.

Material Type 19

Material type 19 is similar to material type 3 being a bilinear model, however, material type 19 was developed to be strain-rate sensitive. It is very easy to use without strain rate sensitivity. The LS-DYNA3D parameters are found for material type 19 with quasi-static loading for AASHTO M-180 guardrail steel. The quasi-static model is to be used to compare quasi-static results with strain-rate sensitive results in chapter 7. The parameters in table 6 provide good results as shown in figure 20. The effect of strain rate is not included in the input deck producing a quasi-static effect. There are four load curves for material type 19: yield stress, Young's modulus, tangent modulus, and failure stress. Although these load curves are marked optional in the LS-DYNA3D User's Manual, all load curves must be defined for LS-DYNA3D to run.⁽¹⁰⁾

Table 6 LS-DYNA3D material parameters for modeling AASHTO M-180 Class A Type II steel for material type 19 (quasi-static parameter values).

Density (Mg/mm ³)		7.86E-09
Young's Modulus (MPa)		200.E+03
Poisson's Ratio		0.33
Load curve 1		
Yield Stress (MPa)	440.0	440.0
Strain rate (s ⁻¹)	0.0	1.0E+05
Load curve 2		
Young's Modulus (MPa)	2.0E+05	2.0E+05
Strain rate (s ⁻¹)	0.0	1.0E+05
Load curve 3		
Tangent Modulus (MPa)	9.7E+02	9.7E+02
Strain rate (s ⁻¹)	0.0	1.0E+05
Load curve 4		
Failure Stress (MPa)	6.4E+02	6.4E+02
Strain rate (s ⁻¹)	0.0	1.0E+05

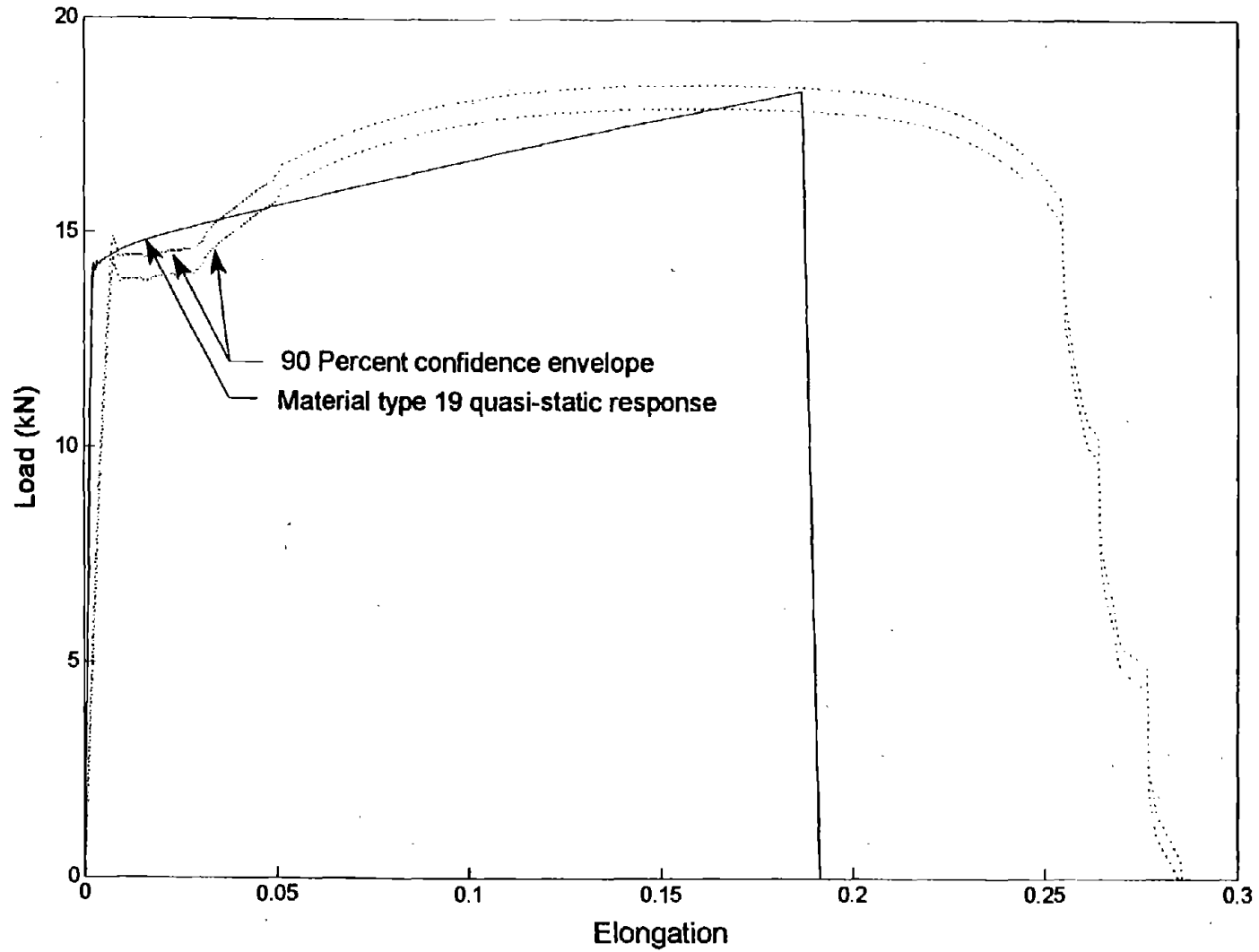


Figure 20 Load versus elongation curve for the simulated response of AASHTO M-180 Class A Type II guardrail steel without strain rate sensitivity.

Several cautionary points should be addressed before completing this discussion of modeling AASHTO M-180 Class A Type II steel. First, the properties shown in AASHTO M-180 are actually referring to the base metal characteristics of the sheet before it is cold worked into its final shape. The amount of cold working varies in different parts of the cross section. By its definition, the cold-rolling process introduces plastic strains and residual stresses into the section that change its properties somewhat. Although the effect of cold working on the guardrail is important to recognize, this effect is not examined in this report. The material properties probably vary somewhat with both the location and orientation of the cut from the specimen of guardrail. Specimens cut from the top of the corrugation will probably have slightly different properties than specimens cut from the flat sloping edge of the cross section. The samples discussed in this report were cut with the longitudinal axis of the specimen coinciding with the longitudinal axis of the guardrail. The tensile properties are, therefore, a good representation of the tensile strength of the guardrail beam since the orientation is the same. The specimens discussed in this paper were cut from the flattest part of the sloped surface of the guardrail. The properties given in the preceding paragraphs are thought to be representative of AASHTO M-180 Class A Type II guardrails but the user should be aware that details of a coupon test as well as the random nature of material properties can have an effect of the correlation between these tests and simulations and other tests.



CHAPTER 4. STEEL GUARDRAIL POST

Steel guardrail posts are used to support various w-beam and thrie-beam guardrail systems shown in figure 21. Guardrail posts are usually manufactured using AASHTO M-183M (ASTM A36M) steel commonly referred to as A36 steel.^(15, 16) This type of steel is used with many other roadside safety hardware systems including the weak steel post cable guardrail and the side-mounted rectangular bridge railing. While the material used in these systems is the same, the shape of the posts varies from one system to the other to meet the structural requirements of each system. The mechanical properties of M-183M steel, as given in the AASHTO specification, are summarized in table 7.

Experimental Results

Three samples of AASHTO M-183M steel guardrail posts were cut, machined and tested according to AASHTO T-244. The specimens were cut from the web of the post and the longitudinal direction of the coupon was aligned with the longitudinal direction of the post. The longitudinal direction corresponds to the direction of the tensile force for both the load applied in the test and the tension experienced during impact. The thickness of the specimens varied from 4.82 mm to 4.87 mm. The load-versus-elongation curves for the three specimens are shown in figure 22. The specimens exhibit behavior typical of mild steel.

Table 7. Longitudinal flat tension tests of AASHTO M-183M Grade 250 steel.

	AASHTO M-183M Grade 250	Tests
Number of tests	--	3
Min. Yield Strength (MPa)	250	314
Min. Tensile Strength (MPa)	400	460
Elongation in 50 mm (%)	23	30

Sources: Tests by Federal Highway Administration, Structures Division (HNR-10), September 8, 1995.

Table 7 summarizes mechanical properties of AASHTO M-183M steel obtained from the longitudinal flat tension tests. The yield and tensile strength in these tests exceed the required values specified in AASHTO M-183M by approximately 26 and 15 percent respectively and the percent elongation at failure was 13 percent greater than the specified value. The actual failed specimens are shown in figure 23.

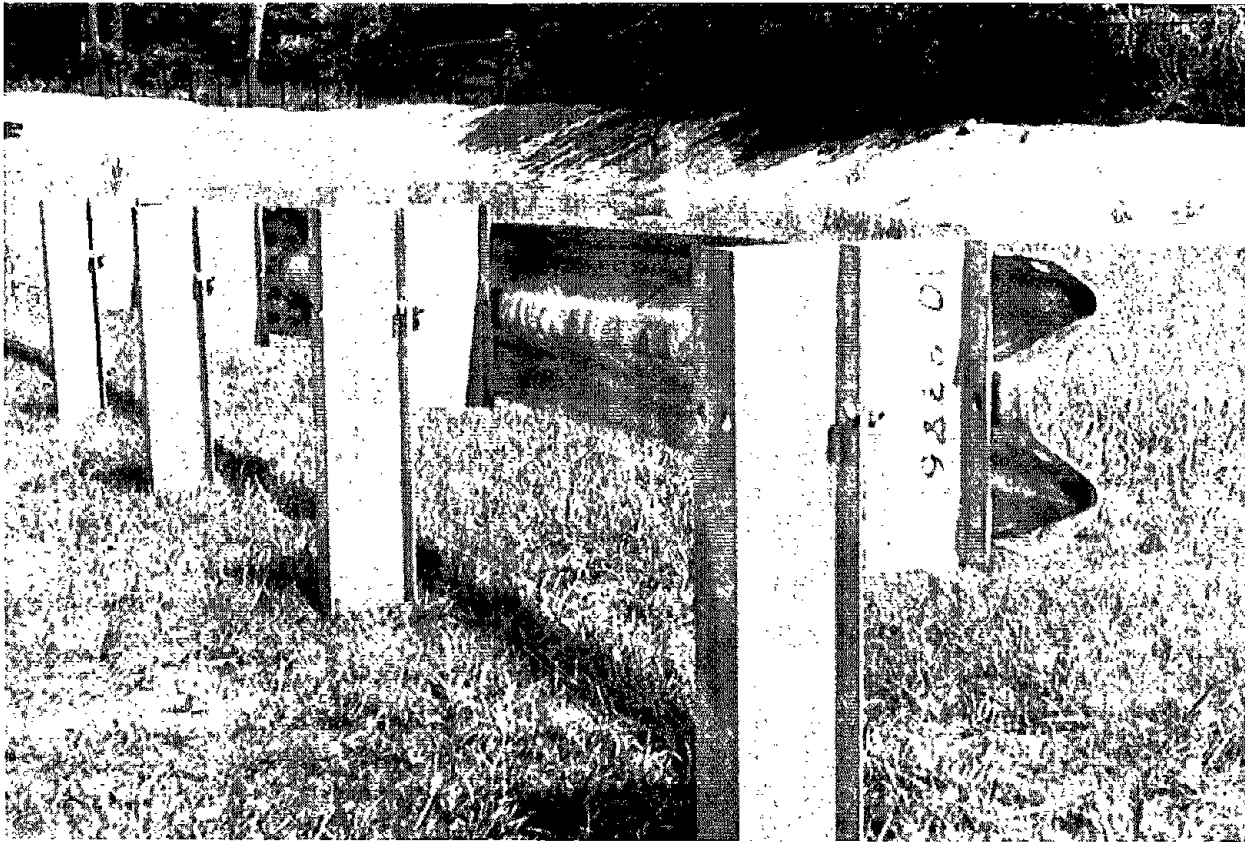


Figure 21 Photograph of AASHTO M-183M steel guardrail posts supporting W-beam guardrail.

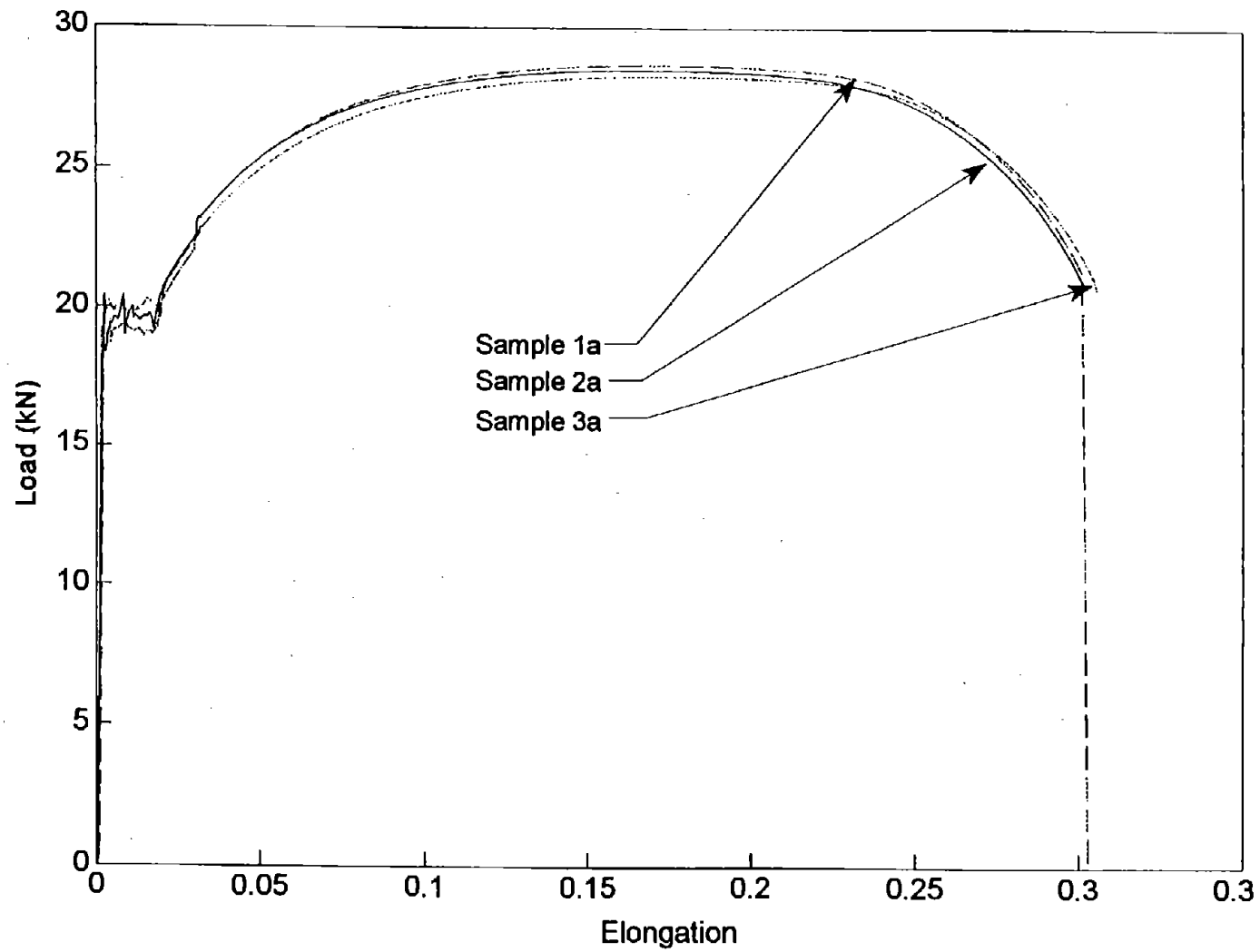


Figure 22 Load versus elongation curves for AASHTO M-183M steel.

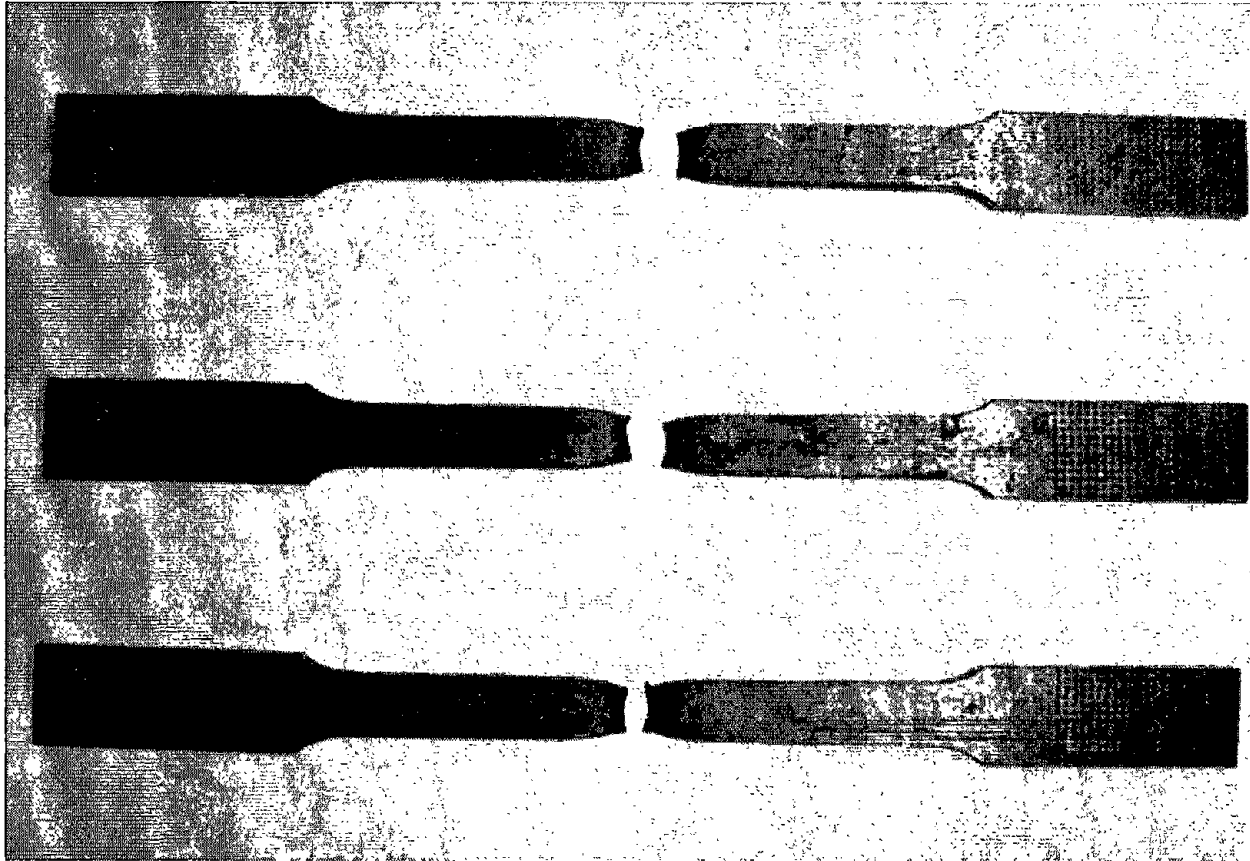


Figure 23 Post-test photograph of AASHTO M-183M steel test specimens.

Finite Element Analysis Results

The parameters that would result in behavior similar to longitudinal flat tension tests were found by conducting finite element analysis using LS-DYNA3D. The material was modeled using the Belytschko-Tsay shell formulation with five integration points through the thickness. Two LS-DYNA3D material types were investigated: the Kinematic/Isotropic Elastic-Plastic material model (type 3) and the Rate-Dependent Tabular Isotropic Elastic-Plastic material model (type 24). The 90th percentile envelope to compare the results of the simulations was created using the results from the experimental tests shown in figure 22.

Material Type 3

When a simple material model is desired, LS-DYNA3D material type 3 is a good choice for mild steels. Material type 3 is a bilinear model making it difficult to completely fit the response within the 90th percentile confidence envelope. Material type 3 parameters were found for two different types of material behavior: bilinear (elongations up to 7 percent) and elastic-perfectly plastic (elongations up to 25 percent). The parameters for these types of behavior are summarized in table 8. The load-elongation plots for these simulations are shown with the test results in figure 24 and figure 25 respectively. The modulus of elasticity for the test specimens in figure 24 appears much lower than the commonly used value of $200\text{E}+03$ MPa. The reason for this is that the flat tension test is not a good method for measuring the small strains needed to determine the modulus of elasticity. There is always some slipping in the grips which can cause this phenomena. For this reason, the simulated response appears much stiffer in the elastic phase than the tests. The commonly used value of the modulus of elasticity for steel was therefore used.

When elongations are expected to be very large (e.g., up to 25 percent), a perfectly plastic material model is a reasonable approximation. For this model, the yield stress is increased above the actual value and the true-stress true-strain tangent modulus is 300 MPa resulting in the perfectly plastic force-elongation response seen in figure 25. Since the yield stress is too high, this formulation requires more strain energy. The amount of strain energy that is inappropriately lost using this method is about 12 Joules, only about 3 percent of 380 Joules required to fail the specimen.

Table 8 LS-DYNA3D material parameters for modeling AASHTO M-183M steel.

Bilinear model (elongations less than 7 percent)

Density (Mg/mm ³)	7.86E-09
Young's Modulus (MPa)	200.E+03
Poisson's Ratio	0.33
Yield Stress (MPa)	315.0
Tangent Modulus (MPa)	2000.0
Hardening Parameter	1.0

Perfectly plastic model (elongations up to and including failure)

Density (Mg/mm ³)	7.86E-09
Young's Modulus (MPa)	200.E+03
Poisson's Ratio	0.33
Yield Stress (MPa)	440.0
Tangent Modulus (MPa)	300.0
Hardening Parameter	1.0
Plastic Strain at Failure	0.235

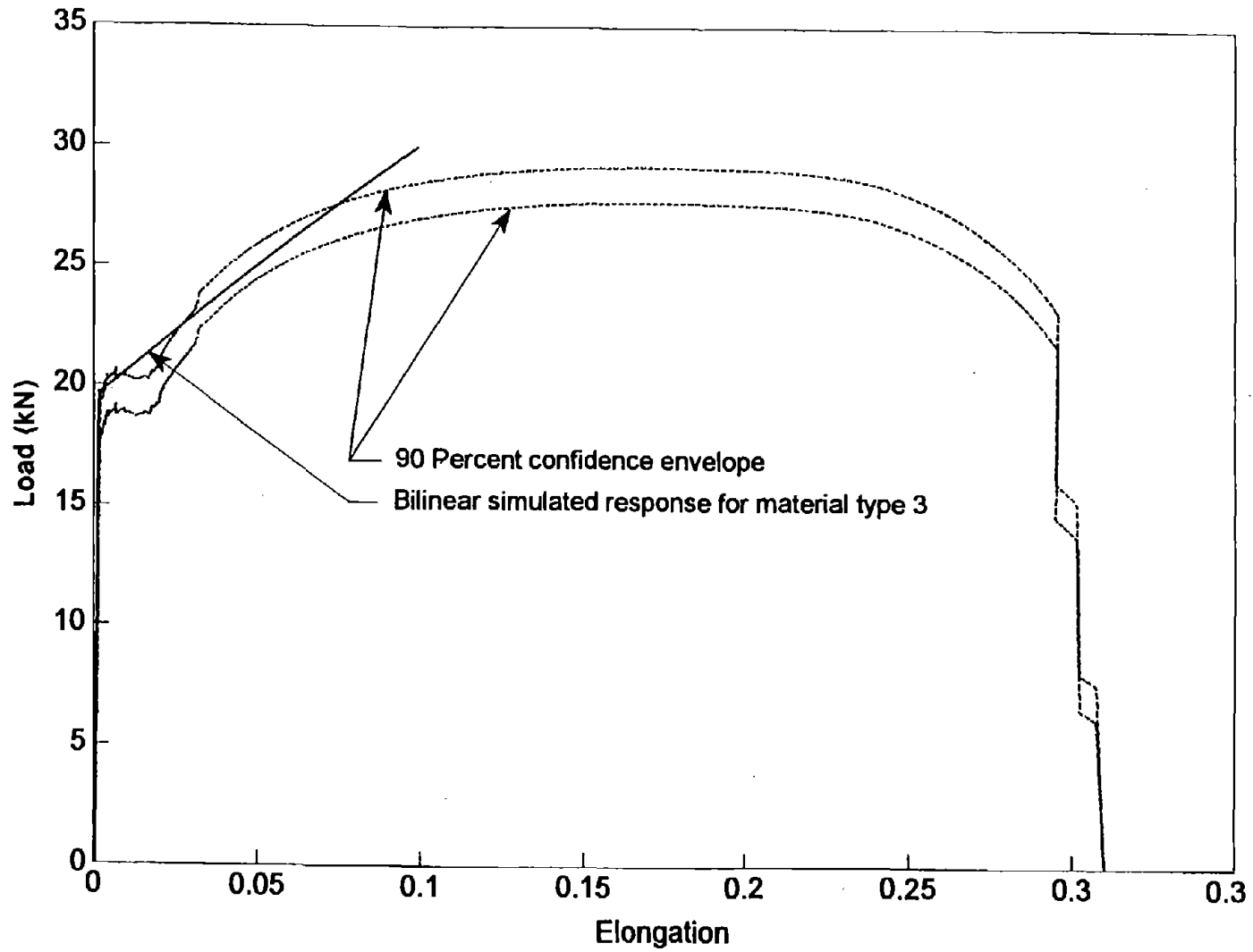


Figure 24 Load versus elongation curve for the bilinear simulated response of AASHTO M-183M steel for material type 3.

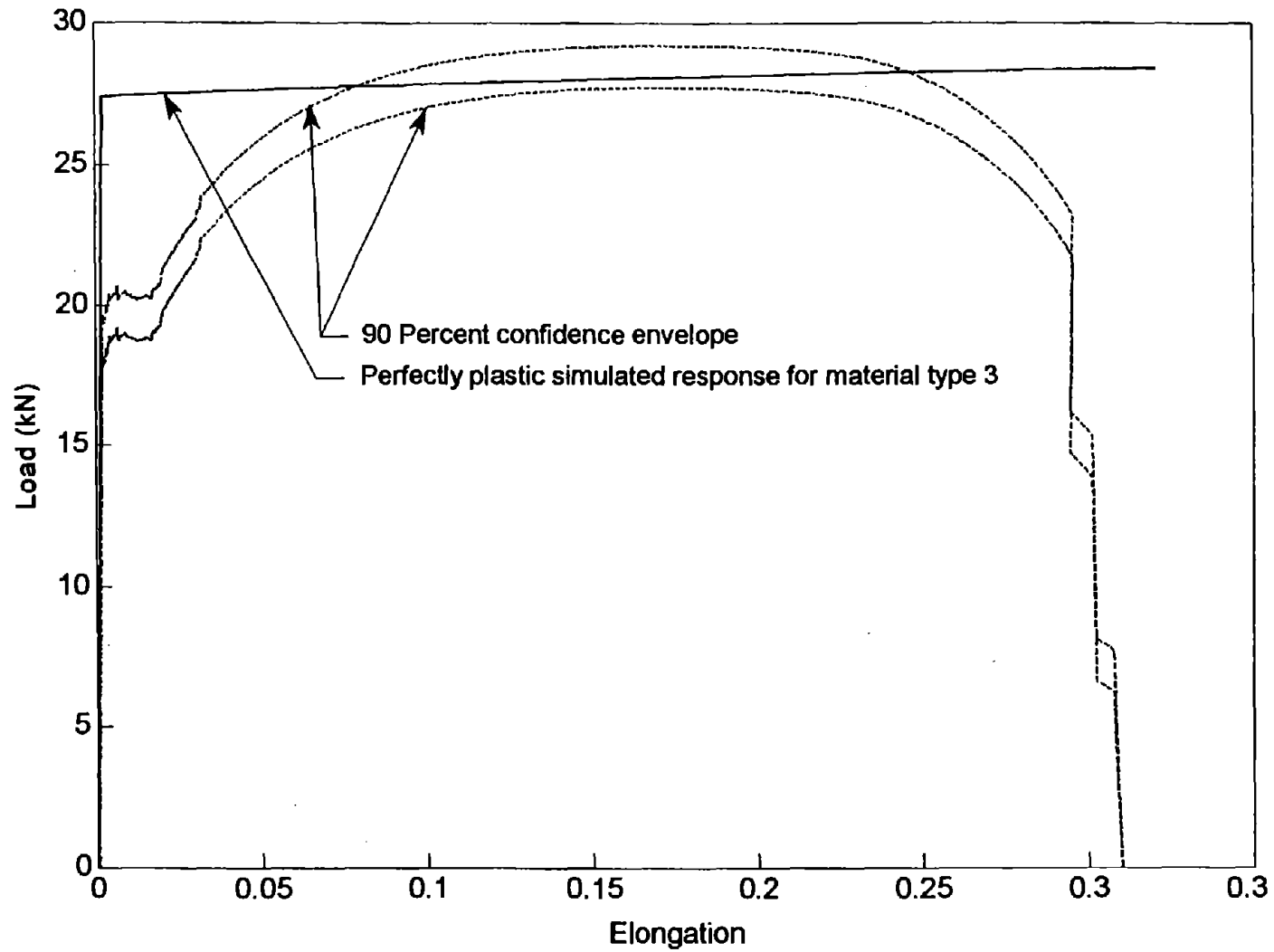


Figure 25 Load versus elongation curve for the perfectly plastic simulated response of AASHTO M-183M steel for material type 3.

Material Type 24

In an impact, M-183M posts generally fail either by twisting and bending to the ground if the foundation is relatively stiff. AASHTO M-183M steel posts should usually be modeled as shell elements since the thickness of the section is very small in comparison to its other dimensions. The rate-dependent tabular isotropic elastic-plastic material (type 24) is suitable for use with failing shell elements. The simulation response is shown in figure 26, and table 9 shows the parameters for DYNA3D material 24 that provide good correlation with the force-elongation tests performed on AASHTO M-183M steel.

Table 9 LS-DYNA3D material parameters for modeling AASHTO M-183M steel using material type 24.

Density (Mg/mm ³)	7.86E-09
Young's Modulus (MPa)	200.E+03
Poisson's Ratio	0.33
Yield Stress (MPa)	315.0
Strain Rate Effects	none
Plastic Strain at Failure	0.625
Increments of Strain	0.0 0.019 0.05 0.165 0.33 0.495 0.625 1.0
Increments of Stress (MPa)	315 315 427.8 500.8 504.3 506.5 400 0

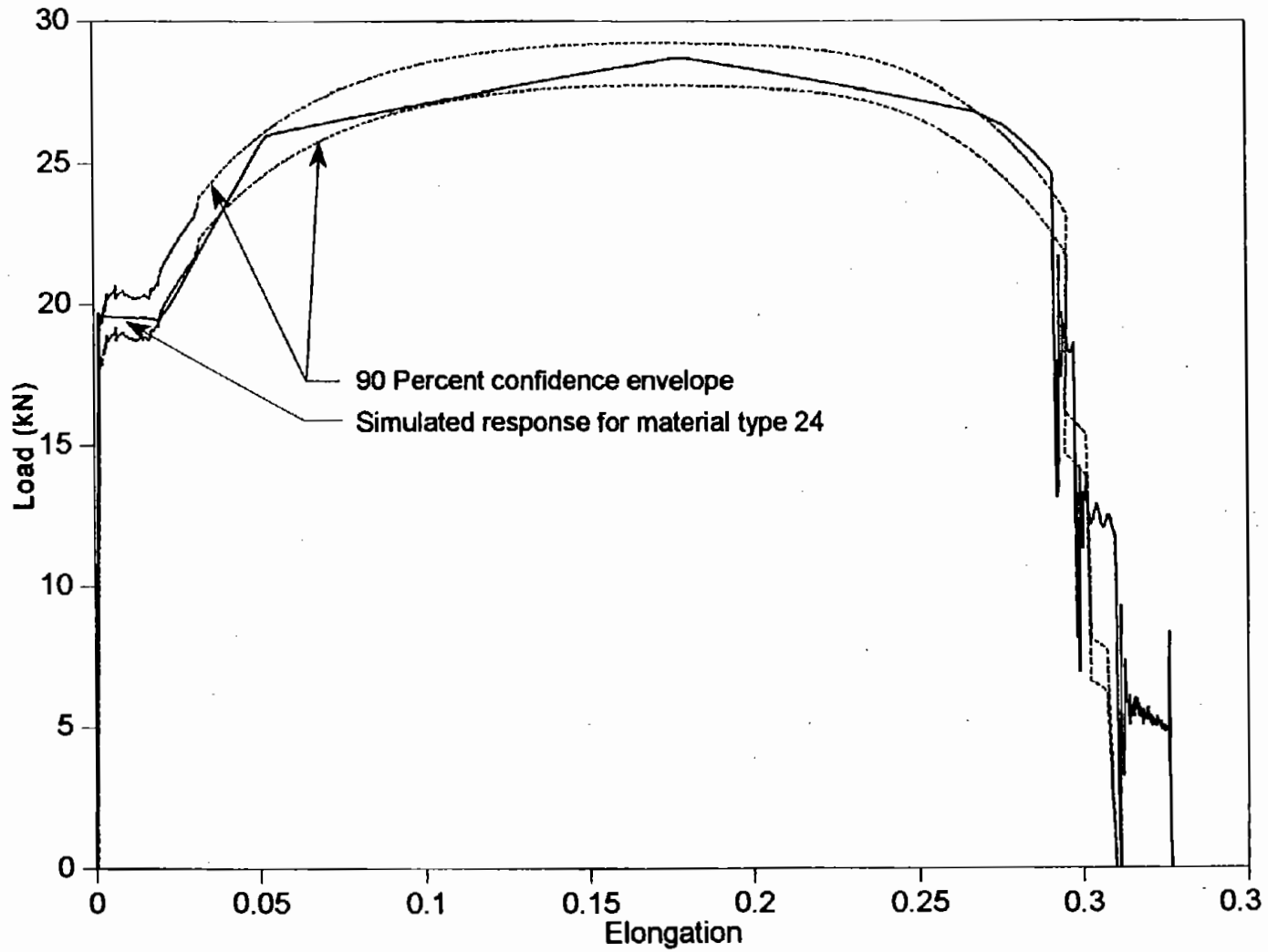


Figure 26 Load versus elongation of the simulated response of AASHTO M-183M steel using material type 24.

CHAPTER 5. FLANGED CHANNEL SIGN-POST

Flanged-channel posts are commonly used as roadside delineator posts as well as in several small sign support designs, shown in figure 27. They have also been used experimentally as weak-post W-beam guardrail and cable guide-rail posts. This type of post is usually manufactured using re-rolled rail steel conforming to ASTM A-499 Grade 60.^(17, 18) Delineator posts are often manufactured using 4.5 kg/m flanged-channel sections whereas sign posts and other structural applications usually use 6.0 kg/m flanged-channel sections. The mechanical properties of this material as given in the ASTM A-499 for Grade 60 steel specification are summarized in table 10.



Figure 27 A flanged channel sign-support.

Experimental Results

Four Samples of ASTM A-499 Grade 60 flanged-channel posts were cut, machined and tested according to AASHTO T-244. The specimens were cut from the flat sides of the post and the longitudinal direction of the coupon was aligned with the longitudinal direction of the post. The longitudinal direction corresponds to the direction of the tensile force for both the load applied in the test and the tension experienced during impact. The thickness of the specimens varied from 3.99 mm to 4.39 mm. The load-versus-elongation curves for the four specimens are shown in figure 28. The specimens exhibit behavior typical of brittle steels as expected since the steel is a cold-worked rail material.

Table 10 Longitudinal flat tension tests of ASTM A-499 Grade 60 steels.

	ASTM A-499 Grade 60	Tests
Number of tests	--	4
Min. Yield Strength (MPa)	415	495
Min. Tensile Strength (MPa)	620	903
Elongation in 50 mm (%)	7	17

Sources: Tests by Federal Highway Administration, Structures Division (HNR-10), January 10, 1994.

The values obtained from the longitudinal tension tests exceed the minimum values required by ASTM A-499 as shown in table 10. The yield and tensile strength in these tests exceed the specifications by approximately 16 and 46 percent respectively and the percent elongation at failure was more than twice the specified value. The actual failed specimens are shown in figure 29.

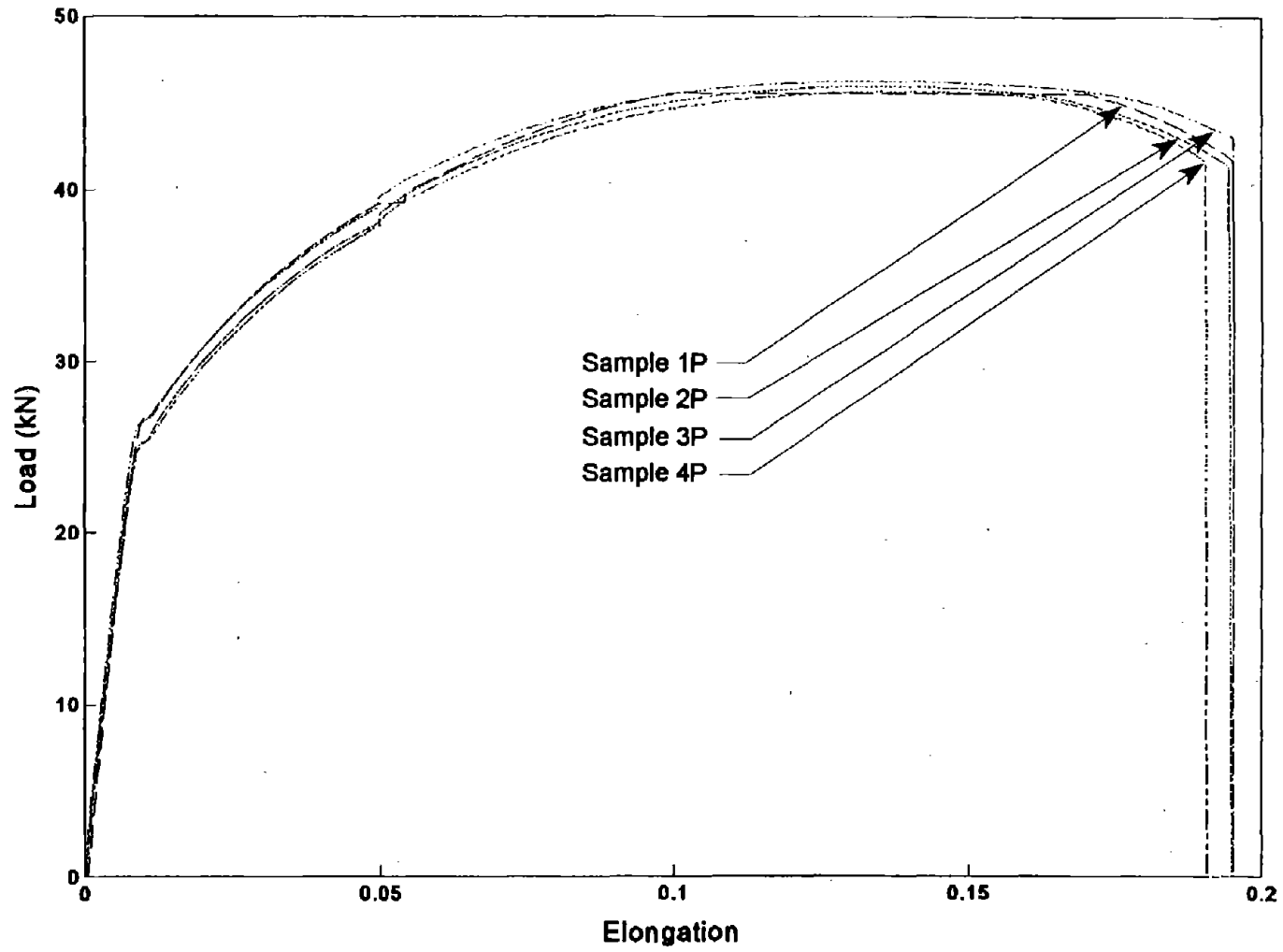


Figure 28 Load versus elongation curves for ASTM A-499 Grade 60 steel.

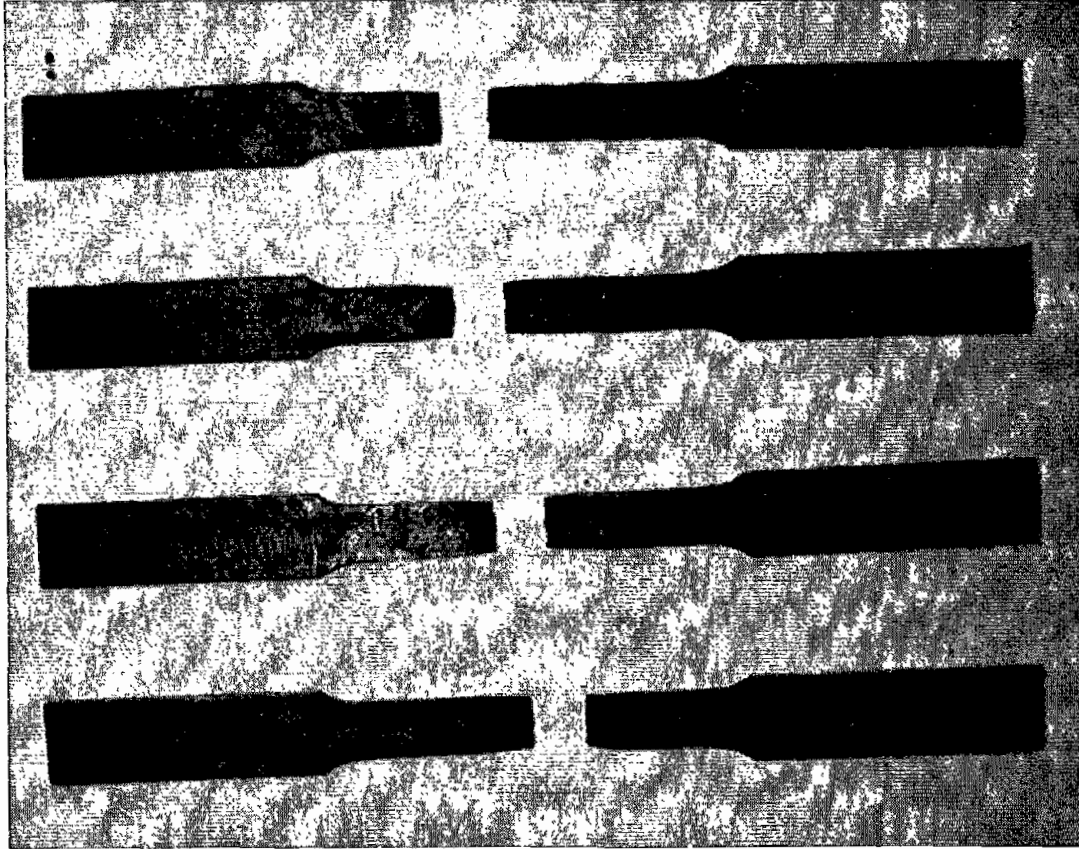


Figure 29 Post-test photograph of ASTM A-499 Grade 60 steel test specimens.

Finite Element Analysis Results

Finite element analyses were conducted using LS-DYNA3D to determine the parameters that would result in behavior similar to longitudinal flat tension tests. The material was modeled using the Belytschko-Tsay shell formulation with five integration points through the thickness. This type of shell element is often used for modeling corrugated sheet steel in crashworthiness applications. Two LS-DYNA3D material types were investigated: the Kinematic/Isotropic Elastic-Plastic material model (type 3) and the Rate-Dependent Tabular Isotropic Elastic-Plastic material model (type 24). The experimental results from the four tests were used to create the 90th percentile confidence envelope used to validate the simulated responses.

Material Type 3

When a simple material model is desired, LS-DYNA3D material type 3 is a good choice for mild steels. Material type 3 is a bilinear model making it difficult to fit the response completely within the 90th percentile confidence envelope. Material type 3 parameters were found for two different types of material behavior: bilinear (elongations up to 11 percent) and elastic-perfectly plastic (elongations up to failure). The parameters for these types of behavior are summarized in table 11. The load-elongation plots for these simulations are shown with the test results in figure 30 and figure 31. The modulus of elasticity for the test specimens in figure 30 appears much lower than the commonly used value of 200E+03 MPa since the flat tension test is not a good method for measuring the small strains needed to determine the modulus of elasticity. For this reason, the simulated response appears stiffer in the elastic phase than the tests. The conventional value for the modulus of elasticity is used in the finite element simulations.

When the elongations are expected to be relatively small (e.g., less than 6 percent), a simple bilinear model is sufficient. A tangent modulus of 6000 MPa yields the response shown in figure 30. This response remains as close to the tested response as is possible with a two-line model for relatively small elongations.

When elongations are expected to be very large (e.g., up to 19 percent), a perfectly plastic material model may be desirable. For this model, the yield stress is increased above the actual value and the true-stress true-strain tangent modulus is set equal to 700 MPa resulting in an essentially perfectly plastic force-elongation response as shown in figure 31. Since the yield stress is too high, this formulation requires more strain energy than the corresponding tests. The amount of strain energy that is inappropriately lost using these parameters is about 4 Joules, only about 1 percent of 416 Joules required to fail the specimen.

Table 11 LS-DYNA3D material parameters for modeling ASTM A-499 Grade 60 steel for material type 3.

Bilinear model (elongations less than 6 percent)	
Density (Mg/mm ³)	7.86E-09
Young's Modulus (MPa)	200.E+03
Poisson's Ratio	0.33
Yield Stress (MPa)	464.0
Tangent Modulus (MPa)	6000.0
Hardening Parameter	1.0
Perfectly plastic model (elongations up to and including failure)	
Density (Mg/mm ³)	7.86E-09
Young's Modulus (MPa)	200.E+03
Poisson's Ratio	0.33
Yield Stress (MPa)	810.0
Tangent Modulus (MPa)	750.0
Hardening Parameter	1.0
Plastic Strain at Failure	0.155

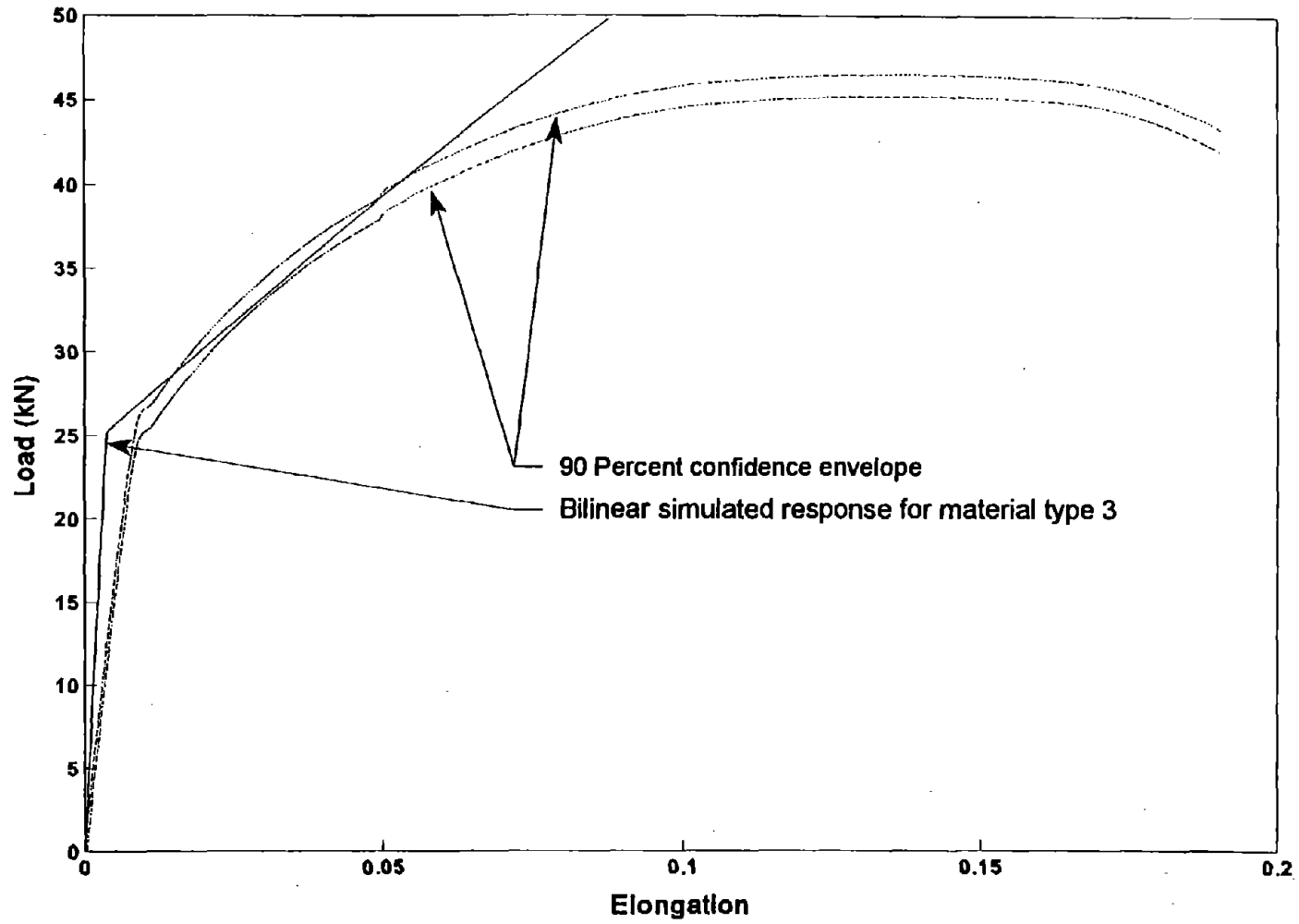


Figure 30 Load versus elongation curve of the bilinear simulated response of ASTM A-499 Grade 60 steel using material type 3.

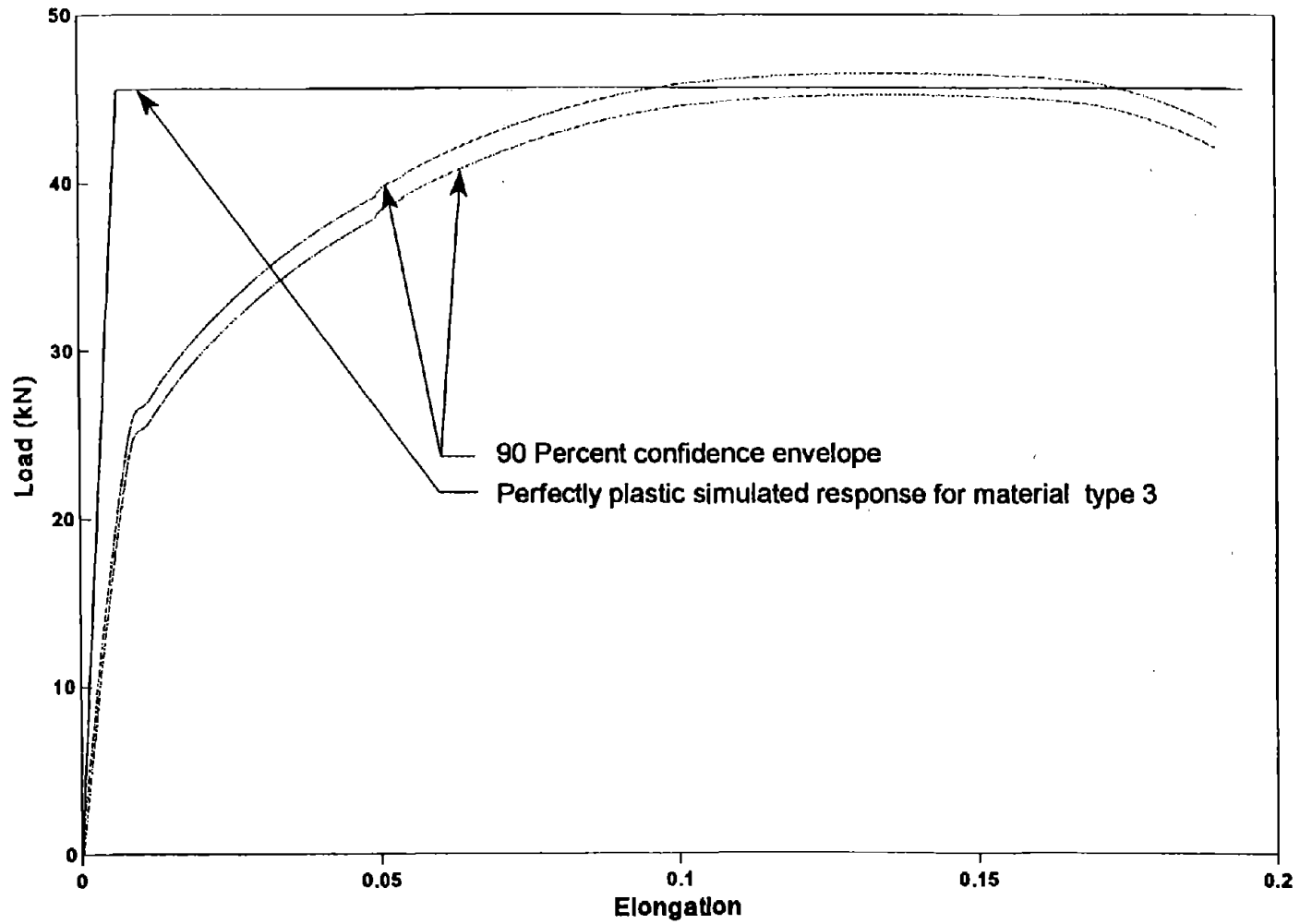


Figure 31 Load versus elongation of the perfectly plastic simulated response for ASTM A-499 Grade 60 steel using material type 3.

Material Type 24

In an impact, flanged-channel posts generally fail either by shearing at the base if the foundation is very stiff (i.e., a concrete footing) or cracking through the line of holes in the compression flange of the section as shown in figure 32. Since both failure modes involve tearing, material a material model that incorporates failure is desirable for many situations where ASTM A-499 Grade 60 steel is used. Flanged-channel posts are usually modeled as shell elements since the thickness of the section is very small in comparison to its other dimensions. The rate-dependent tabular isotropic elastic-plastic material (type 24) is suitable for use with failing shell elements. As shown in figure 33, table 12 shows the parameters for LS-DYNA3D material type 24 that provide good correlation with the force-elongation tests performed on ASTM A-499 Grade 60 steel.

Table 12 LS-DYNA3D material parameters for modeling ASTM A-499 Grade 60 steel using material type 24.

Density (Mg/mm ³)	7.86E-09
Young's Modulus (MPa)	200.E+03
Poisson's Ratio	0.33
Yield Stress (MPa)	464.0
Strain Rate Effects	none
Plastic Strain at Failure	0.295
Increments of Strain	0.0 0.02 0.03 0.07 0.12 0.16 0.295 1.0
Increments of Stress (MPa)	464 595 680 850 895 920 890 0

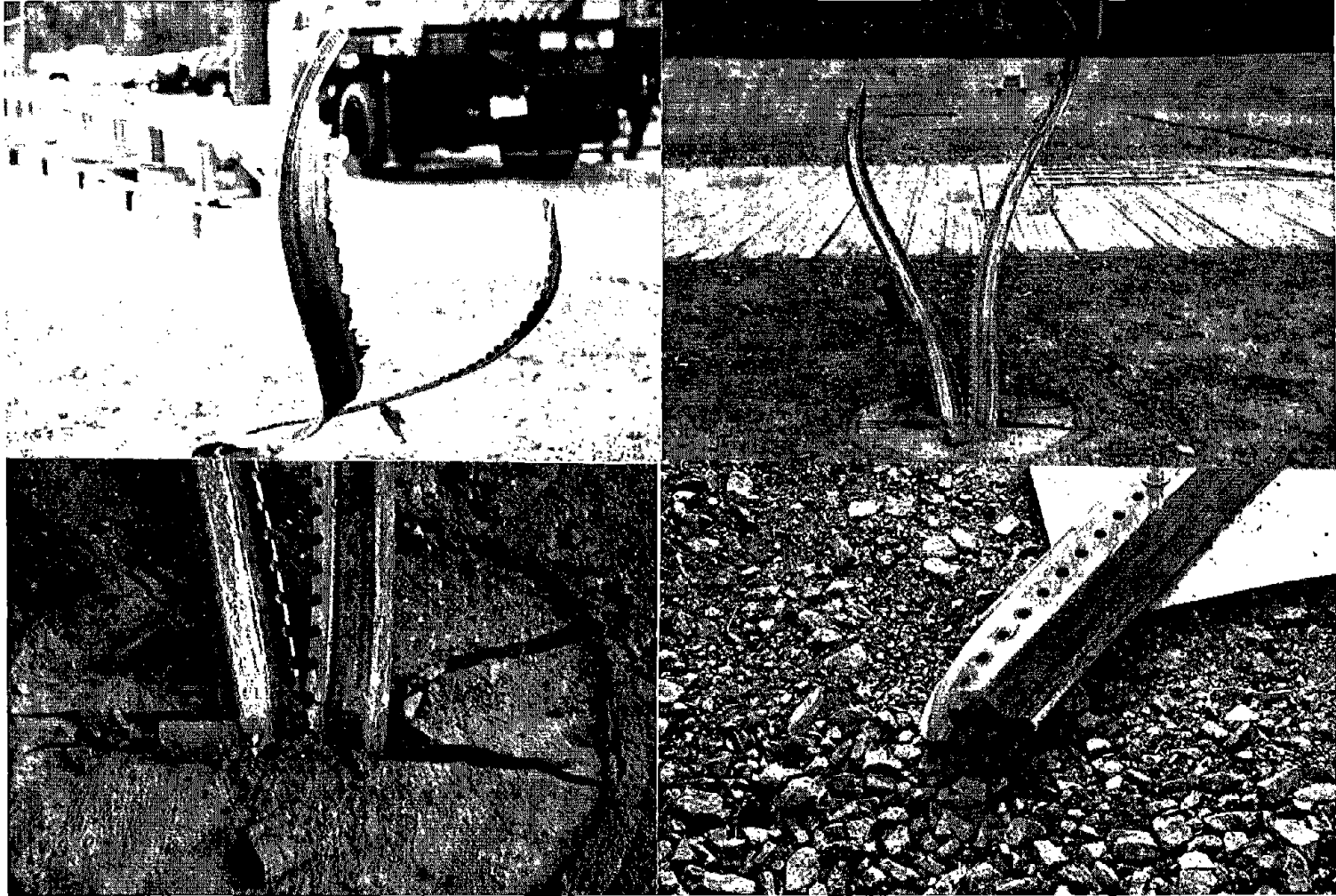


Figure 32 Photographs of flanged channel sign support failure modes.

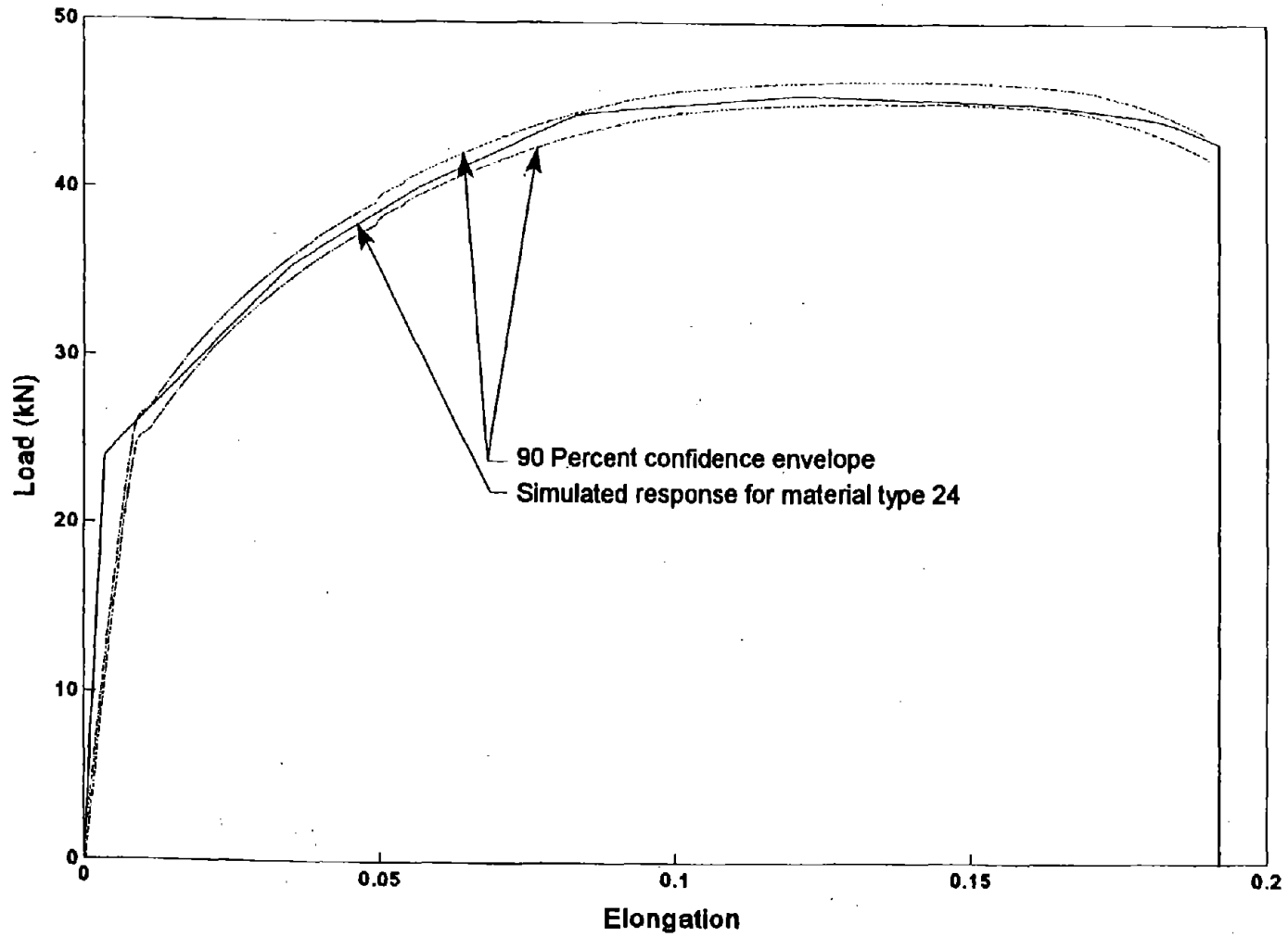


Figure 33 Load versus elongation curve of the simulated response of ASTM A-499 Grade 60 steel using material type 24.

CHAPTER 6. FORD FESTIVA FENDER

Particular types of cars are specified in NCHRP Report 350 for performing full-scale crash tests. The Ford Festiva, shown in figure 34, is a small car that meet the specifications for an NCHRP Report 350 820c vehicle.⁽¹⁹⁾ In 1994 the Federal Highway Administration developed the finite element model of a 1989 Ford Festiva shown in figure 35 in an effort to use finite element simulations to replicate crash tests.⁽²⁰⁾ Although the finite element model resembles a Festiva and it has been validated for frontal narrow object impact simulations, the model uses general material definitions based on literature sources.⁽²¹⁾ While steel properties are generally similar for Young's modulus and Poisson's ratio, steels vary in the amount of elongation, yield stresses, failure strains and failure stresses. There is a need to collect data for the various components of the Festiva that experience large deformations in a collision including the bumper, fenders and the frame. Manufacturers of vehicles do not normally disclose either the steel type used or its properties. Experimental tests are necessary to both identify the steel and to determine the material definitions required by LS-DYNA3D. Using the results of quasi-static tension tests, the material parameter definitions for LS-DYNA3D can be inferred. The material properties for the left fender of a 1990 Ford Festiva are found in this section.

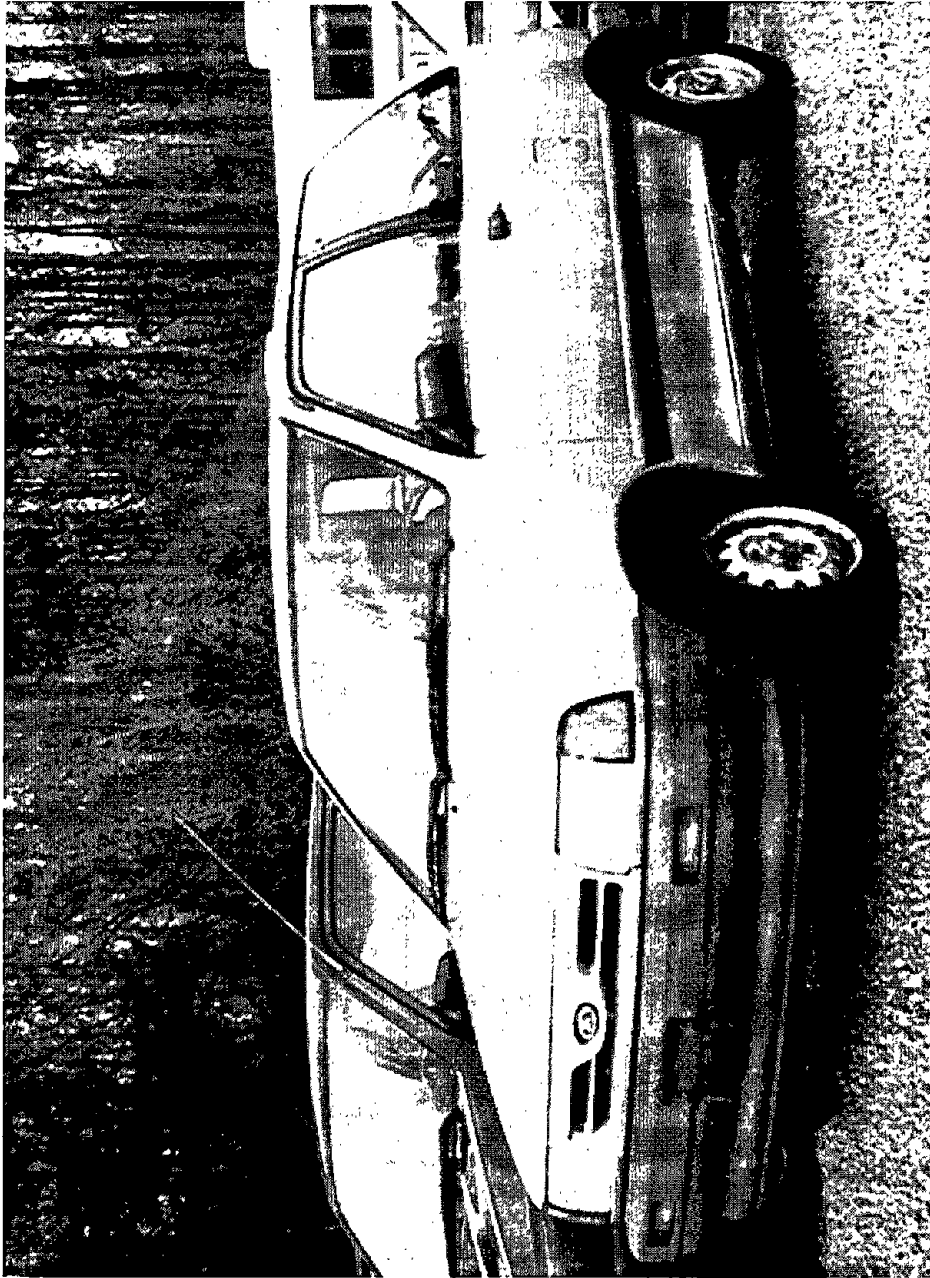


Figure 34 Photograph of a 1988 Ford Festiva.

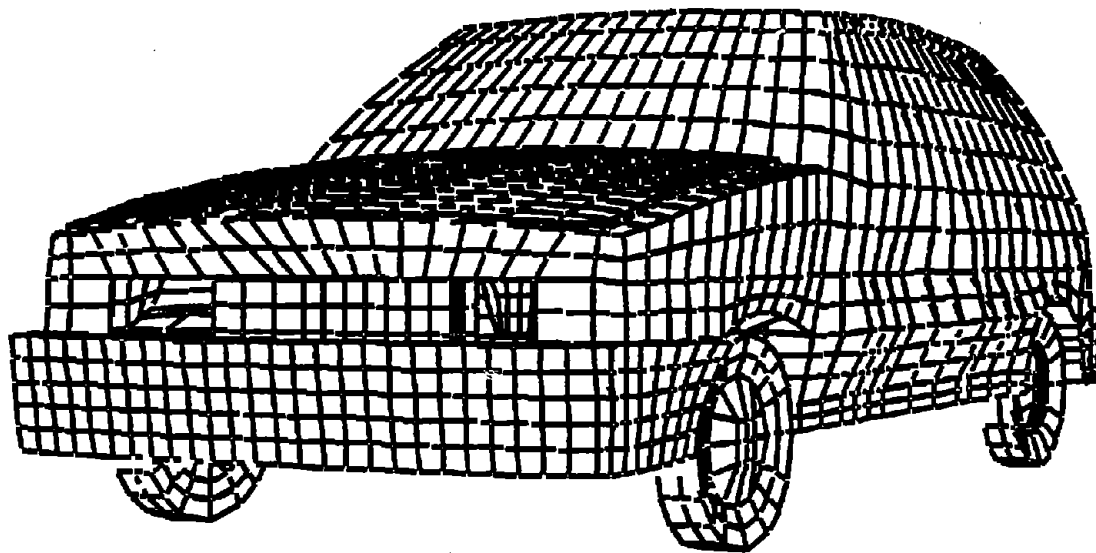


Figure 35 Finite element model of a 1989 Ford Festiva.

Experimental Results

Four samples of fender steel were cut, machined and tested according to AASHTO T-244. The specimens were cut from the flattest part of the fender. The thickness of the specimens varied from 0.749 mm to 0.775 mm. The load-versus-elongation curves for the three specimens are shown in figure 36 and the actual failed specimens are shown in figure 37.

Table 13 Longitudinal flat tension tests of a 1990 Ford Festiva fender.

	Tests	ASTM A611 Grade A
Number of tests	4	--
Min. Yield Strength (MPa)	282	170
Min. Tensile Strength (MPa)	303	290
Elongation in 50 mm (%)	31	26

Sources: Tests by Federal Highway Administration, Structures Division (HNR-10), September 8, 1995.

Table 13 summarizes mechanical properties of fender steel obtained from the longitudinal flat tension tests. The specific type of steel is unknown. Using the Automotive Steel Design Manual, the mechanical properties found for the fender do not meet the minimum requirements of any steel listed. One of the three minimum requirements for yield stress, tensile stress or percent elongation is too low for all the steels listed.⁽²²⁾ The fender's materials properties do match for ASTM A611 Grade A, in the Standard Specification for Steel, Sheet, Carbon, Cold-Rolled, Structural Quality. While the minimum requirements are just met, little else is known to match the steel.⁽²³⁾ In table 13 the properties for A611 are listed.

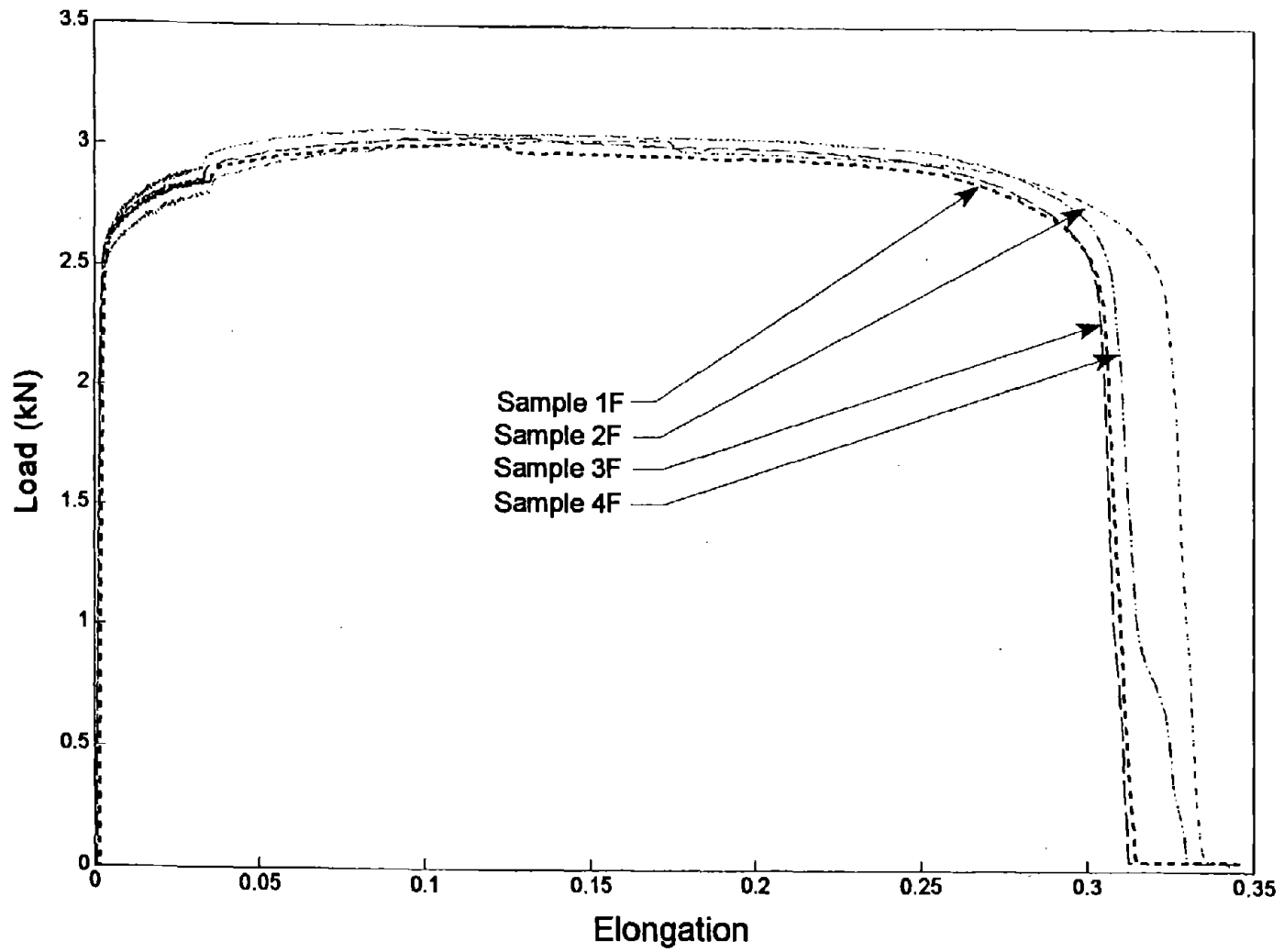


Figure 36 Load versus elongation curves for Festiva fender steel.

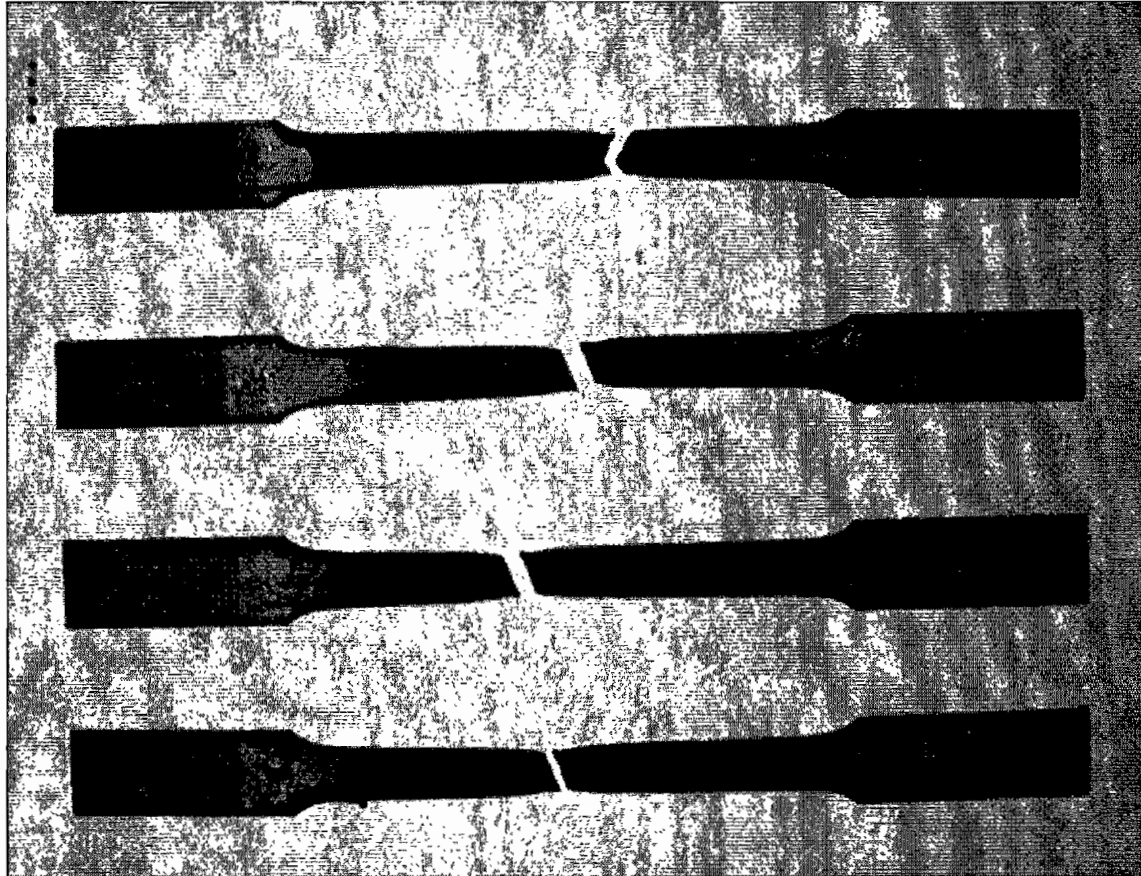


Figure 37 Post-test photograph of Festiva fender steel test specimens.

Finite Element Analysis Results

The parameters that would result in behavior similar to longitudinal flat tension tests were found conducting finite element analysis using LS-DYNA3D. The material was modeled using the Belytschko-Tsay shell formulation with five integration points through the thickness. This type of shell element is often used for modeling sheet steel in crashworthiness applications. Two LS-DYNA3D material types were investigated: the Kinematic/Isotropic Elastic-Plastic material model (type 3) and the Rate-Dependent Tabular Isotropic Elastic-Plastic material model (type 24). The 90th percentile envelope of the results of the tests was created to compare to the simulations as shown in figure 36.

Material Type 3

When a simple material model is desired, LS-DYNA3D material type 3 is a good choice for mild steels. Material type 3 is a bilinear model making it difficult to fit the response completely within the 90th percentile confidence envelope. Material type 3 parameters were found for two different types of material behavior: bilinear (elongations up to 11 percent) and elastic-perfectly plastic (elongations up to 25 percent). The parameters for these types of behavior are summarized in table 14 and the load-elongation plots for these simulations are shown with the test results in figure 38 and figure 39 respectively.

Table 14 LS-DYNA3D material parameters for modeling Festiva fender steel for material type 3.

Bilinear model (elongations less than 11 percent)	
Density (Mg/mm ³)	7.86E-09
Young's Modulus (MPa)	200.E+03
Poisson's Ratio	0.33
Yield Stress (MPa)	325.0
Tangent Modulus	600.0
Hardening Parameter	1.0
Perfectly plastic model (elongations up to and including failure)	
Density (Mg/mm ³)	7.86E-09
Young's Modulus (MPa)	200.E+03
Poisson's Ratio	0.33
Yield Stress (MPa)	352.0
Tangent Modulus	180.0
Hardening Parameter	1.0
Plastic Strain at Failure	0.59

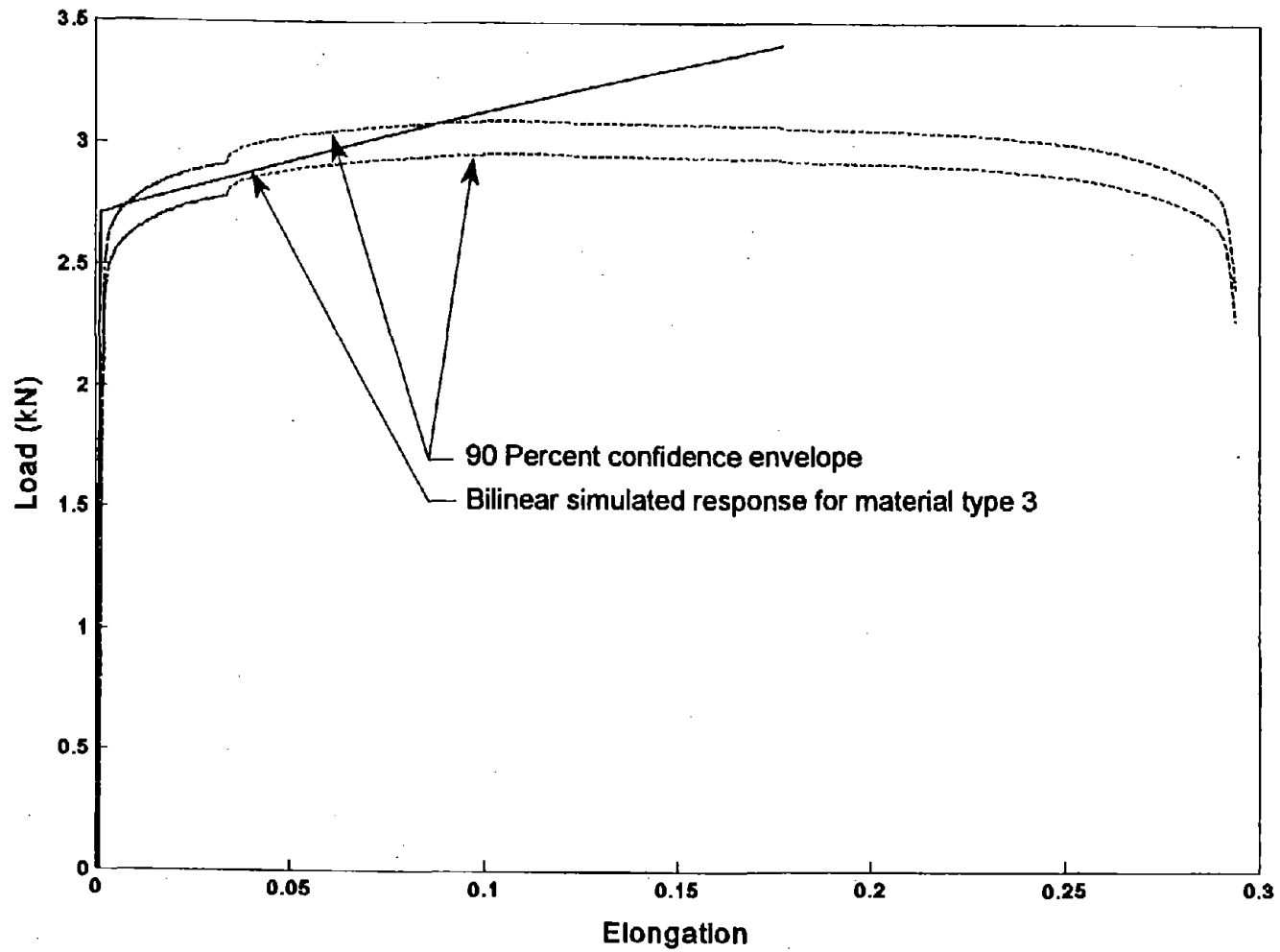


Figure 38 Load versus elongation curve of the bilinear simulated response of Festiva fender steel using material type 3.

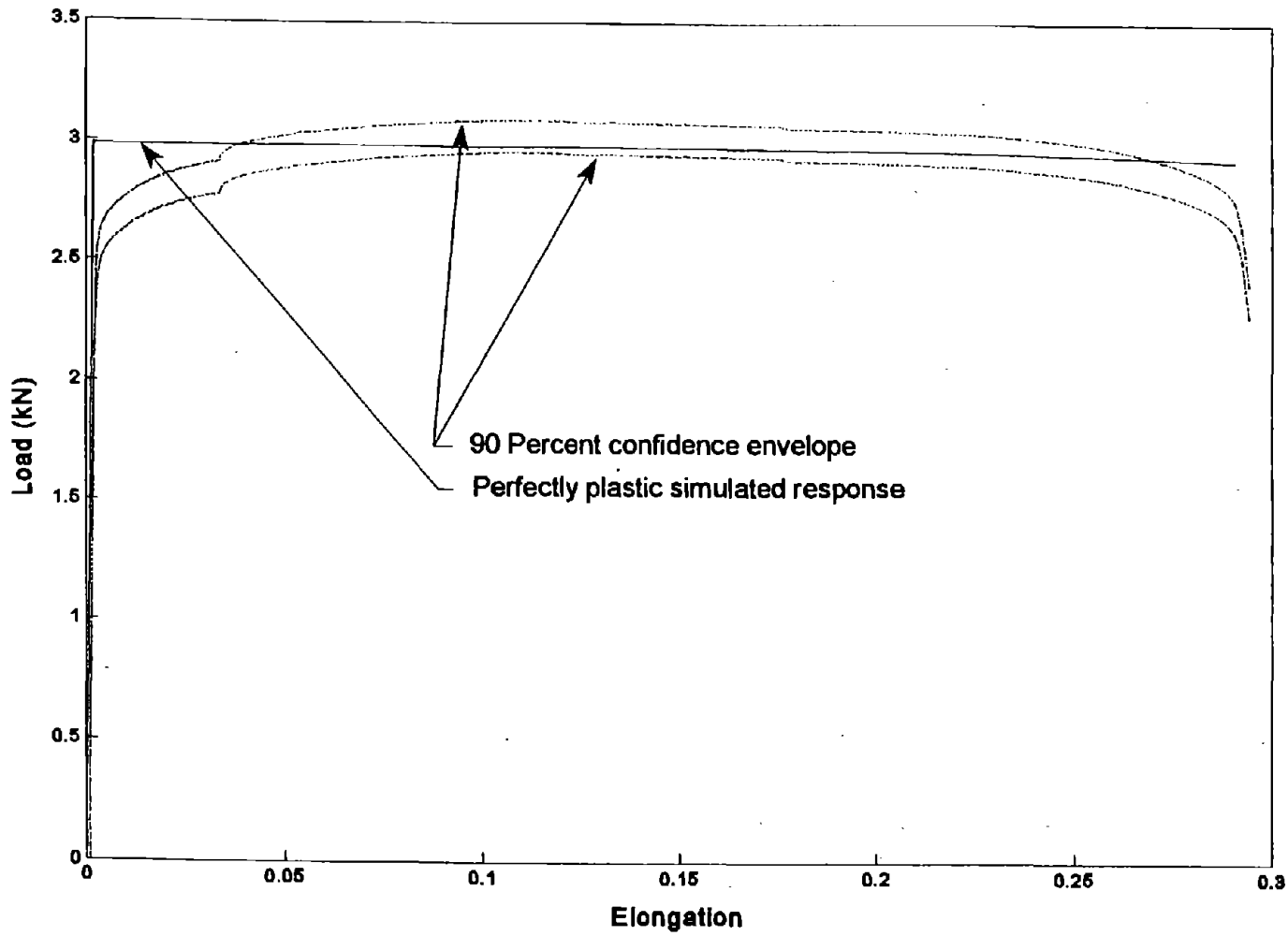


Figure 39 Load versus elongation curve of perfectly plastic simulated response for Festiva fender steel using material type 3.

When elongations are expected to be very large (e.g., up to 25 percent), a perfectly plastic material model is adequate. For this model, the yield stress is increased above the actual value and the true-stress true-strain tangent modulus is 180 MPa resulting in the perfectly plastic force-elongation response shown in figure 39. Since the yield stress is artificially high, this formulation requires 0.8 Joules more strain energy. The additional 0.8 Joules is only about 2 percent of the 45 Joules required to fail the specimen. The effect on the simulations is considered negligible.

Material Type 24

In an impact, fenders generally fail in buckling as shown in figure 40. Fenders should usually be modeled as shell elements since the thickness of the section is very small in comparison to its other dimensions. The rate-dependent tabular isotropic elastic-plastic material (type 24) is suitable for use with failing shell elements. Table 15 shows the parameters for LS-DYNA3D material 24 that provide good correlation with the force-elongation tests performed on Festiva fender steel, and figure 41 shows the result of the simulation.

Table 15 LS-DYNA3D material parameters for modeling Festiva fender steel using material type 24.

Density (Mg/mm ³)	7.86E-09
Young's Modulus (MPa)	200.E+03
Poisson's Ratio	0.33
Yield Stress (MPa)	315.0
Strain Rate Effects	none
Plastic Strain at Failure	0.64
Increments of Strain	0.0 0.0195 0.05 0.15 0.30 0.50 0.64 1.0
Increments of Stress (MPa)	315 340 358 390 400 400 365 0



Figure 40 Typical impact damage to the sheet-metal of a small car after a guardrail test.

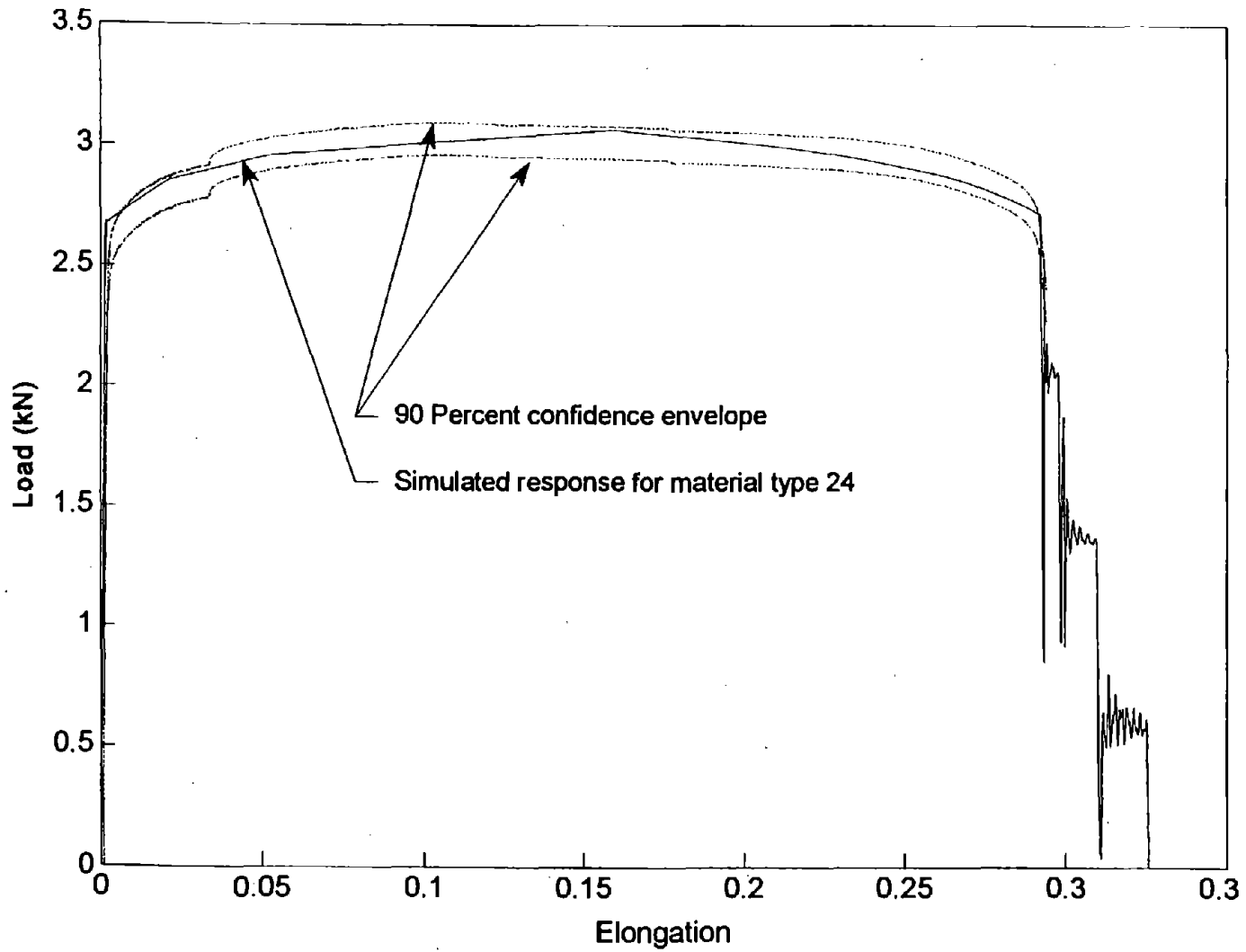


Figure 41 Load versus elongation curve of the simulated response of Festiva fender steel using material type 24.

CHAPTER 7. DYNAMIC TENSION COUPON TESTS

Full-scale crash testing involves a vehicle impacting a roadside hardware structure. The mechanical response of many materials under impact or dynamic loading differs from the mechanical response under quasi-static loading. The loading and deflection rates affect the mechanical response of the materials. The rate of deflection is also known as the strain rate which is defined as the change in strain over the change in time, $\Delta\varepsilon/\Delta t$. Because strain rate effects are significant for metals, an understanding of strain rate effects is necessary for the proper finite element modeling and design of roadside hardware.⁽⁵⁾

Strain rate significantly affects the mechanical response of mild steel. Lower yield stress steels are more strain-rate sensitive than higher yield-stress steels. The geometry of the material has no influence upon strain-rate sensitivity. Strain rate manifests itself by strengthening the material. In tensile loading, both the yield stress and ultimate stress are increased as the strain rate increases, the yield stress being influenced more.^(4, 24, 25) Unlike either the yield stress or the ultimate stress, the modulus of elasticity is not significantly influenced by strain rates according to experiments by

Soroushian and Choi.⁽²⁶⁾ The failure strain is strain-rate sensitive. The failure strain decreases as strain rate increases.

Additionally mild steel becomes more brittle as strain rate increases.^(27, 28) These findings are supported by Campbell and Cooper.⁽²⁹⁾

While temperature has been shown to greatly influence the effects of strain rate, these effects are not examined in this paper.^(30, 31)

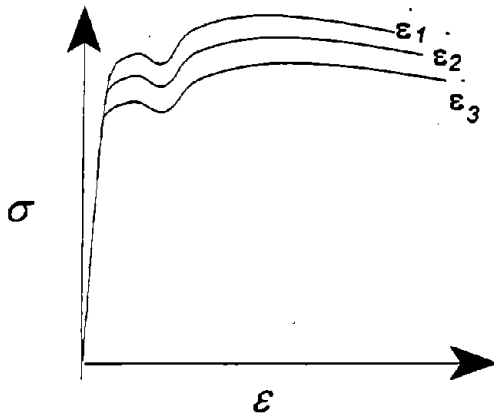


Figure 42 Stress versus strain curves with the typical strain rate effects for mild steel.

Many empirical models have been developed to model strain rate effects upon steel. The stress-versus-strain curves for steel usually shift upward as strain rates increase, as shown in figure 42. The Cowper-Symond empirical strain rate model is of particular interest. The model has been experimentally validated for many

steels. In addition to being very widely used, the model is incorporated into several LS-DYNA3D material models including material types 3 and 24. The empirical relationship developed by Cowper-Symonds is:

$$\frac{\sigma}{\sigma_0} = 1 + \left(\frac{\dot{\varepsilon}}{C}\right)^{1/p} \quad (4)$$

where σ_0 is the quasi-static stress, $\dot{\varepsilon}$ is the strain rate and σ is the resulting rate-affected dynamic stress. The constants, C and p , are material dependent with $C = 40.4 \text{ s}^{-1}$ and $p = 5$ being typical

values for mild steel.^(24, 7) The Cowper-Symonds equation is technically only a predictor of yield stress. It was not developed to predict the ultimate or the failure stress. Research by Jones found that when large strains are experienced, the Cowper-Symonds empirical equation over predicts the strengthening effect of strain rate.⁽³²⁾

Since roadside hardware fails under impact loadings, understanding the role of strain rates for common materials is important. The effect of strain rate is examined for AASHTO M-180 Class A Type II guardrail steel. Dynamic tensile tests were conducted at five different strain rates. The results of these tests are compared to LS-DYNA3D simulations of dynamic tensile tests. The material parameters for strain-rate sensitive simulations are presented.

Standard Laboratory Tests

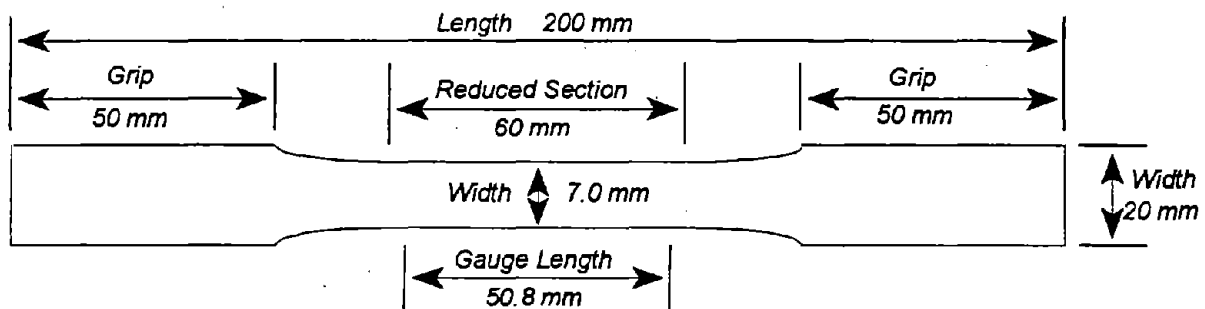


Figure 43 Dynamic tension specimen

Dynamic tensile tests were conducted at five strain rates: 1, 5, 10, 50, and 100 s^{-1} . The specimens were machined to AASHTO T-244 specifications, however, due to machine limitations the gauge section was milled to 7.0-mm width as shown in figure 43. The tensile tests were conducted on an MTS 312 servo hydraulic testing machine at Vanderbilt University. The constant strain rate was produced by linearly increasing the stroke. The results of the tensile tests conducted at a strain rate of 100 s^{-1} were not accepted as valid since both the load and the stroke were filtered differently than the tests at other strain rates.

The experimental results are summarized in table 16 through table 19. In these tables the yield stress, ultimate stress, percent elongation and the reduction in area are presented. The yield stress and ultimate stress increase as the strain rate does. The average percent elongation decreases with the increased strain rate when comparing these tests. There was no significant change in the reduction of area. The engineering stress versus strain curves for each strain rate are presented in figure 44 through figure 47.⁽³³⁾

Table 16 Tensile test results for strain rate 1 ($\dot{\epsilon}^p \approx 1 \text{ s}^{-1}$)

Specimen	Yield Stress	Ultimate Stress	%	%
ID	(MPa)	(MPa)	Elongation	Red. Area
1	573.80	707.92	29.7	61.18
2	606.60	744.40	33.95	65.87
3	547.50	718.71	30.2	63.96
Mean	575.97	723.67	31.28	63.67
Stand. Dev.	29.60	18.74	2.32	2.36

Table 17 Tensile test results for strain rate 2 ($\dot{\epsilon}^p \approx 5 \text{ s}^{-1}$)

Specimen	Yield Stress	Ultimate Stress	%	%
ID	(MPa)	(MPa)	Elongation	Red. Area
1	626.23	764.31	24.70	66.35
2	632.79	761.81	24.42	61.79
3	672.13	754.37	26.90	62.11
Mean	643.72	760.16	25.34	63.42
Stand. Dev.	24.82	5.17	1.36	2.55

Table 18 Tensile test results for strain rate 3 ($\dot{\epsilon}^p \approx 10 \text{ s}^{-1}$).

Specimen	Yield Stress	Ultimate Stress	%	%
ID	(MPa)	(MPa)	Elongation	Red. Area
1	665.57	772.59	22.96	60.52
2	652.46	754.35	24.81	60.97
3	718.03	770.10	24.22	65.19
Mean	678.69	765.68	23.90	62.23
Stand. Dev.	34.70	9.89	0.95	2.58

Table 19 Tensile test results for strain rate 4 ($\dot{\epsilon}^p \approx 50 \text{ s}^{-1}$).

Specimen	Yield Stress	Ultimate Stress	%	%
ID	(MPa)	(MPa)	Elongation	Red. Area
1	845.90	793.13	21.28	62.68
2	790.16	881.99	23.09	61.72
3	672.13	985.87	22.08	62.30
Mean	769.39	886.99	22.15	62.23
Stand. Dev.	88.72	96.46	0.91	0.48

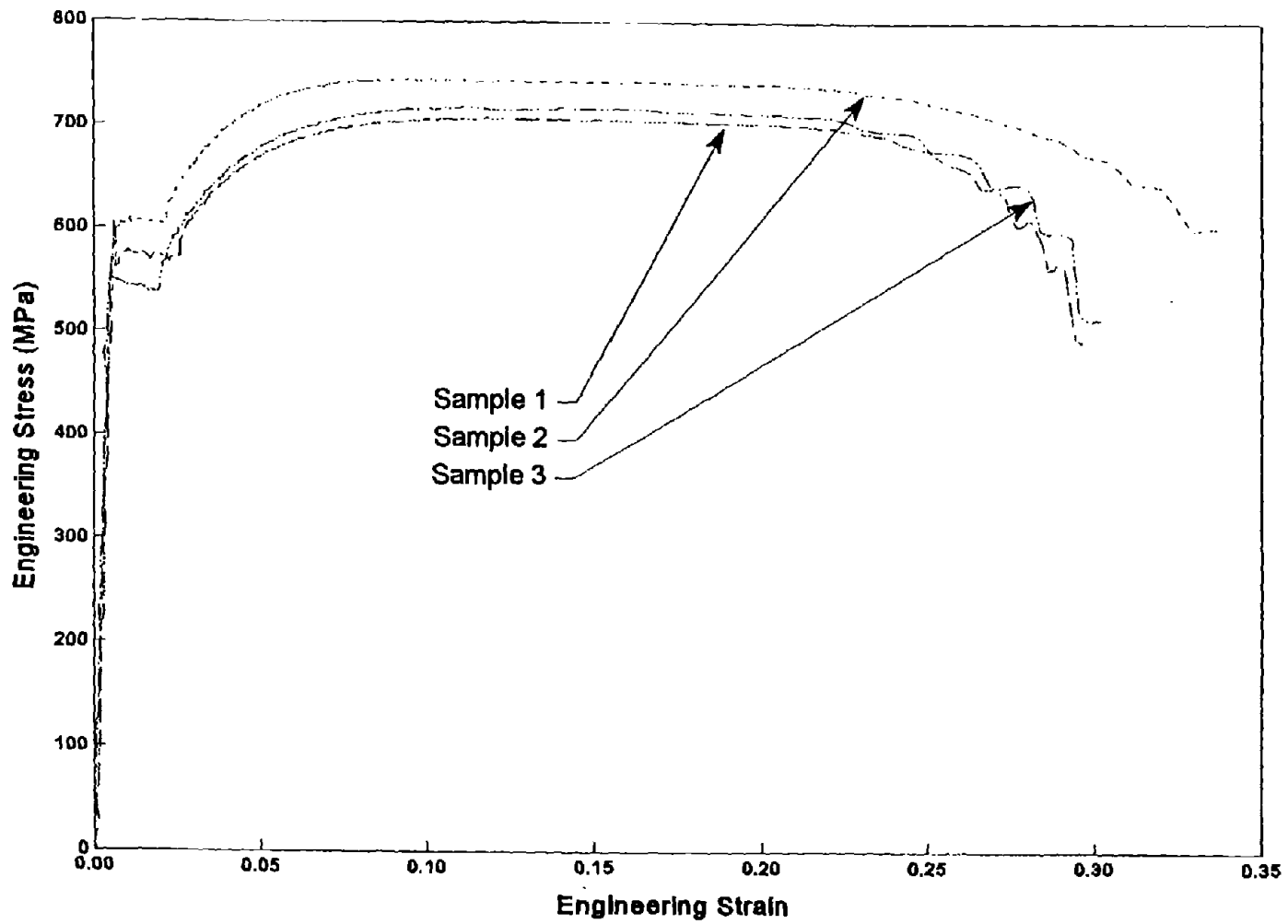


Figure 44 Engineering stress versus engineering strain for M-180 guardrail steel tested at a strain rate of 1 s^{-1} .

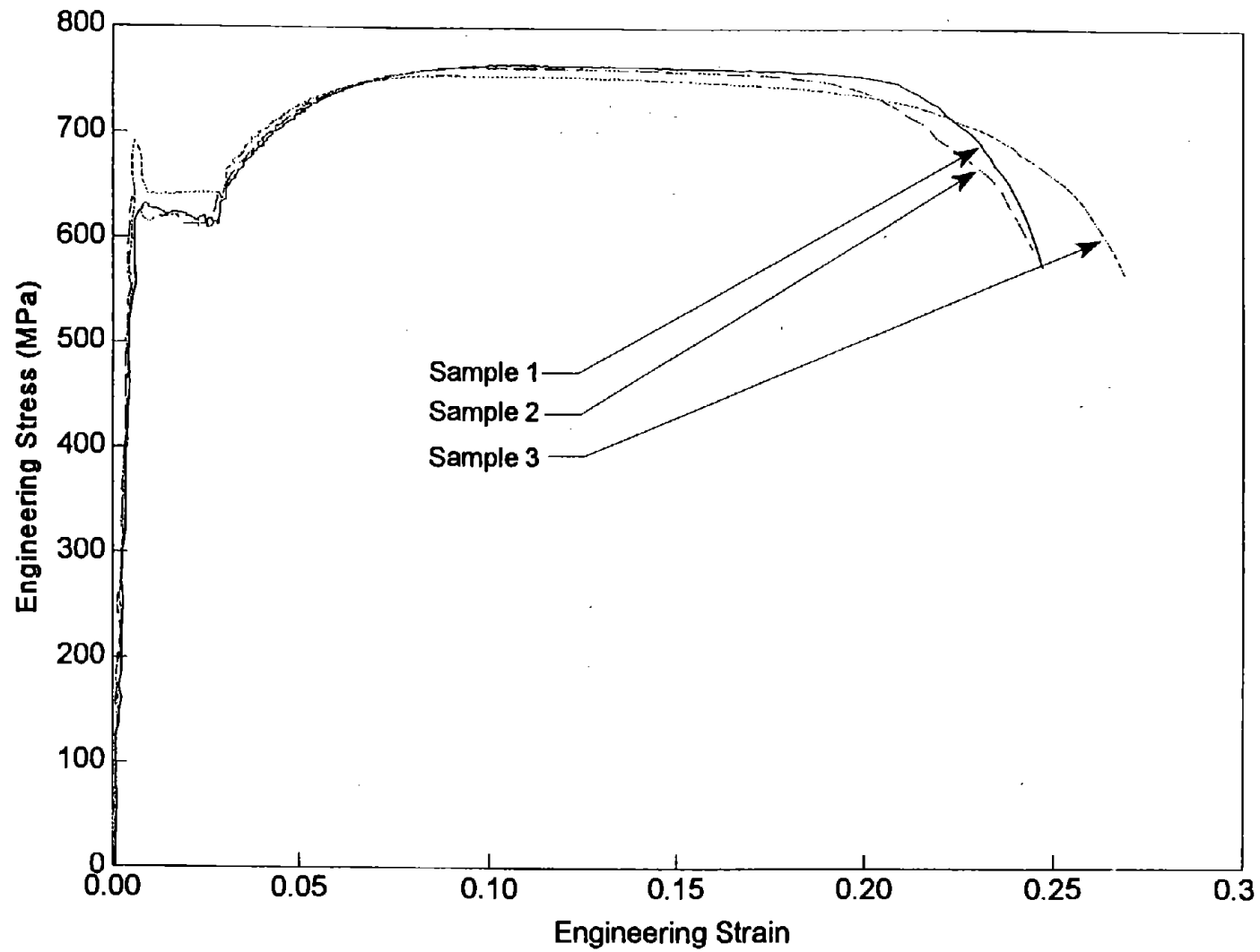


Figure 45 Engineering stress versus engineering strain for M-180 guardrail steel tested at a strain rate of 5 s^{-1} .

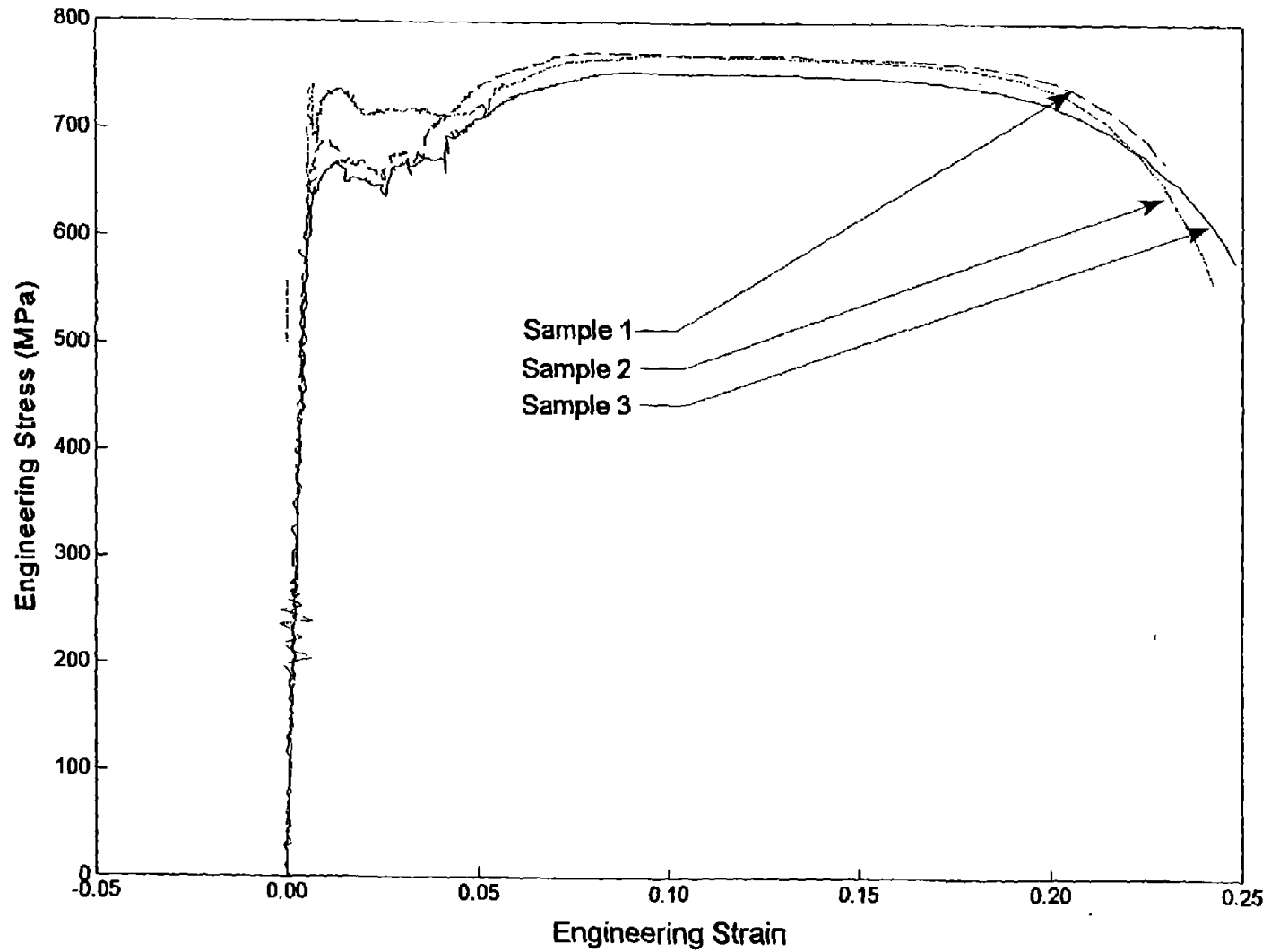


Figure 46 Engineering stress versus engineering strain for M-180 guardrail steel tested at a strain rate of 10 s^{-1} .

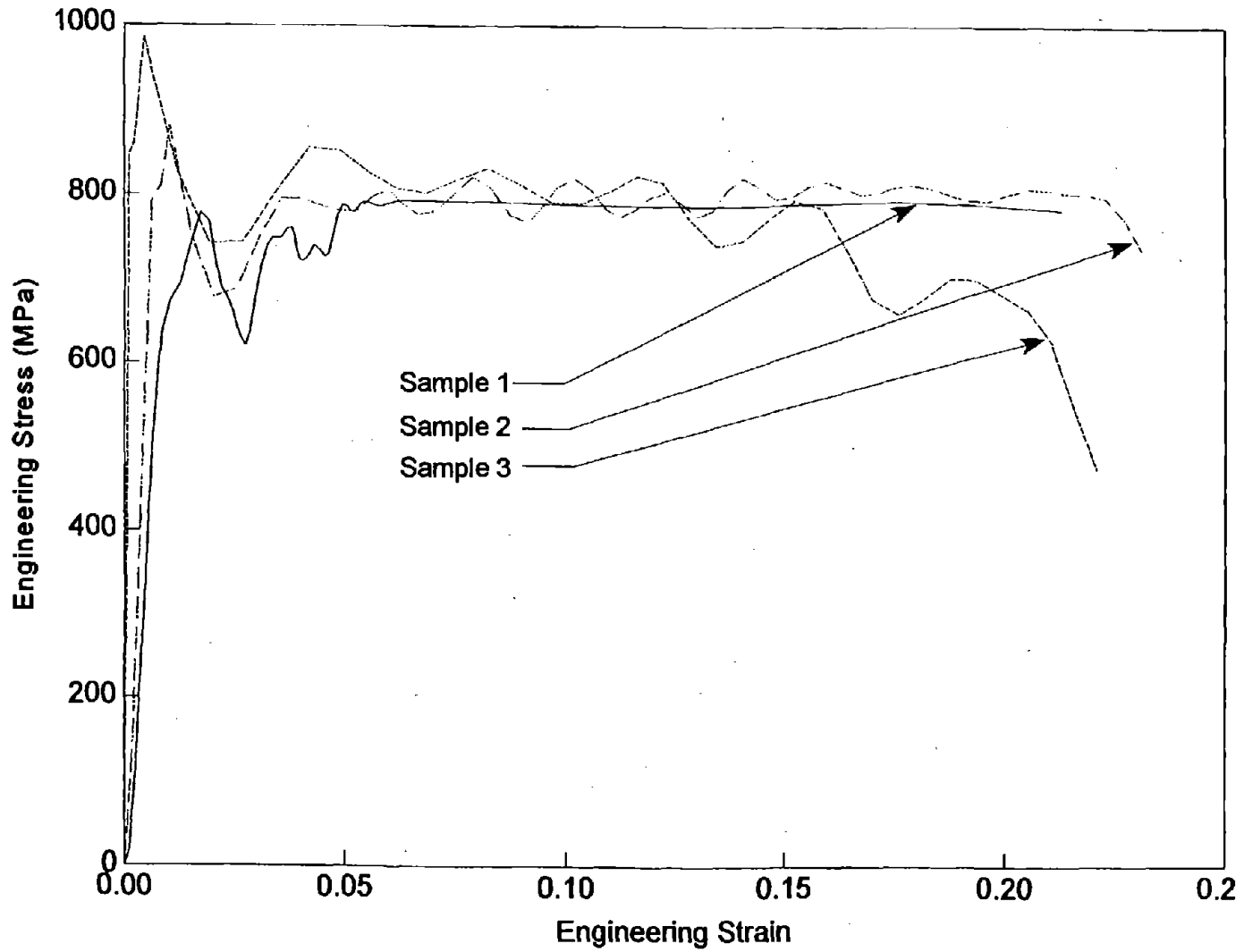


Figure 47 Engineering stress versus engineering strain for M-180 guardrail steel tested at a strain rate of 50 s^{-1} .

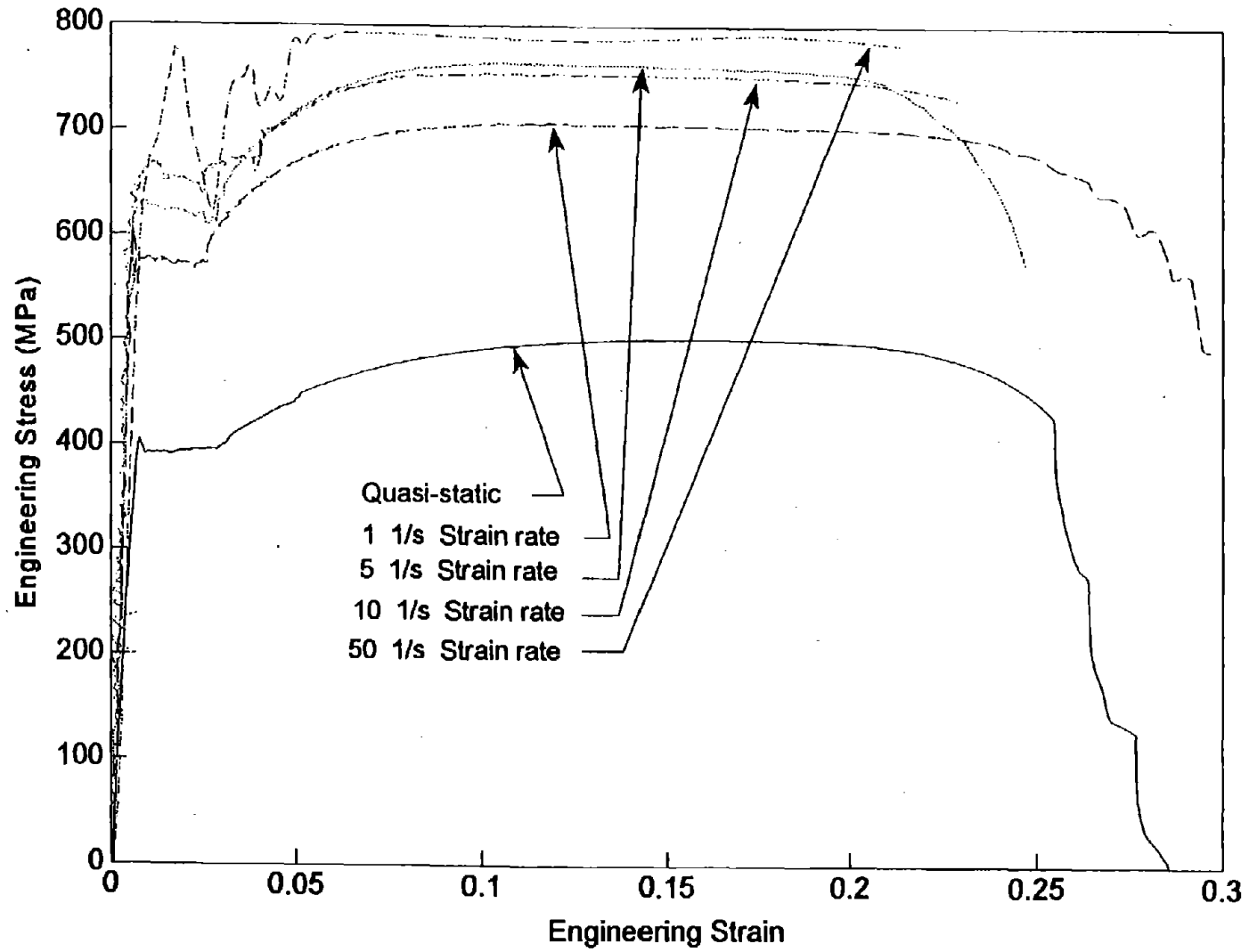


Figure 48 Engineering stress versus engineering strain for M-180 guardrail steel at various strain rates.

Figure 48 has stress versus strain curves of one specimen from each of the different strain rates and the average quasi-static response. The graph shows how the stress versus strain curves shift upward as the strain rate increases. The steel behaves similarly to other steels in that the failure strain tends to decrease as the strain rate increases. This behavior is demonstrated by the reduction in the percent elongation as the strain rate increases in the experimental tests. Figure 49 shows the percent elongation at failure versus the strain rate. The logarithmic regression results in an R-squared value of 0.81. The regression line is plotted on the graph indicating the relationship between the percent elongation and the strain rate. Figure 50 shows a similar, but not as strong of a relationship between strain energy and strain rate. The strain energy decreases as the strain rate increases. The logarithmic regression results in an R-squared value of 0.58. The regression line is plotted on the graph indicating this relationship.

Consistent with findings of other researchers who have investigated other mild steels, both the yield stress and the tensile stress increase as the strain rate increases for AASHTO M-180 steel. (See references 26, 24, 27, and 29) Figure 51 has the experimental yield stress versus the strain rate. The logarithmic regression line that is plotted has an R-squared value of 0.73. It demonstrates how the yield stress increases with the strain rate increase. Because the yield stress does behave like other steels, the Cowper-Symonds material dependent parameters were investigated for AASHTO M-180 steel. Values for C and p, the material dependent parameters, were calculated based on the experimental results. Values of $C=100.4 \text{ s}^{-1}$ and $p=4.9$ were found by a regression analysis to be good predictors. The Cowper-Symonds predicted yield stress values are plotted for the four experimental strain rate values shown in figure 51. While the material parameter values differ from the conventional values for mild steel, they are within the reasonable range for mild steels. The Cowper-Symonds' values have a large range for steels. Stainless steel has parameters of $C=100 \text{ s}^{-1}$ and $p=10$.⁽²⁴⁾ The parameter values found for AASHTO M-180 steel were used for simulations of dynamic tension tests.

In future strain-rate sensitivity testing of roadside safety hardware materials, it is recommended that more than three specimens be tested for each strain rate. In addition, any galvanizing or paint should be removed to reduce problems experienced during these tests. All results should be filtered and analyzed similarly for consistent results. Although the results of these strain rate tests were filtered with a Chebyshev, 2.0dB with an order of two, the band was Lowpass and the Nyquist frequency was 0.2, the filter was not adequate when higher strain rates were analyzed.⁽³³⁾

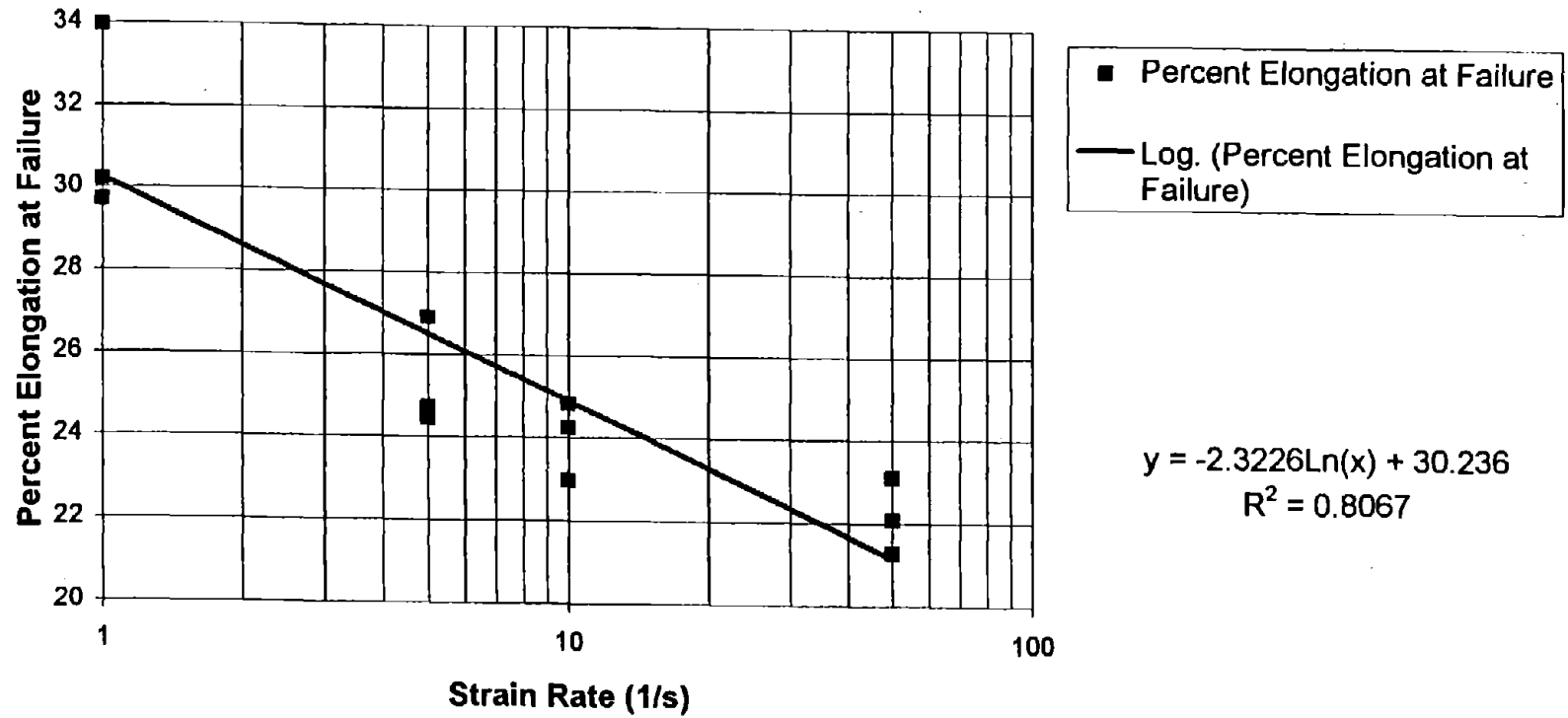


Figure 49 Percent elongation versus strain rate.

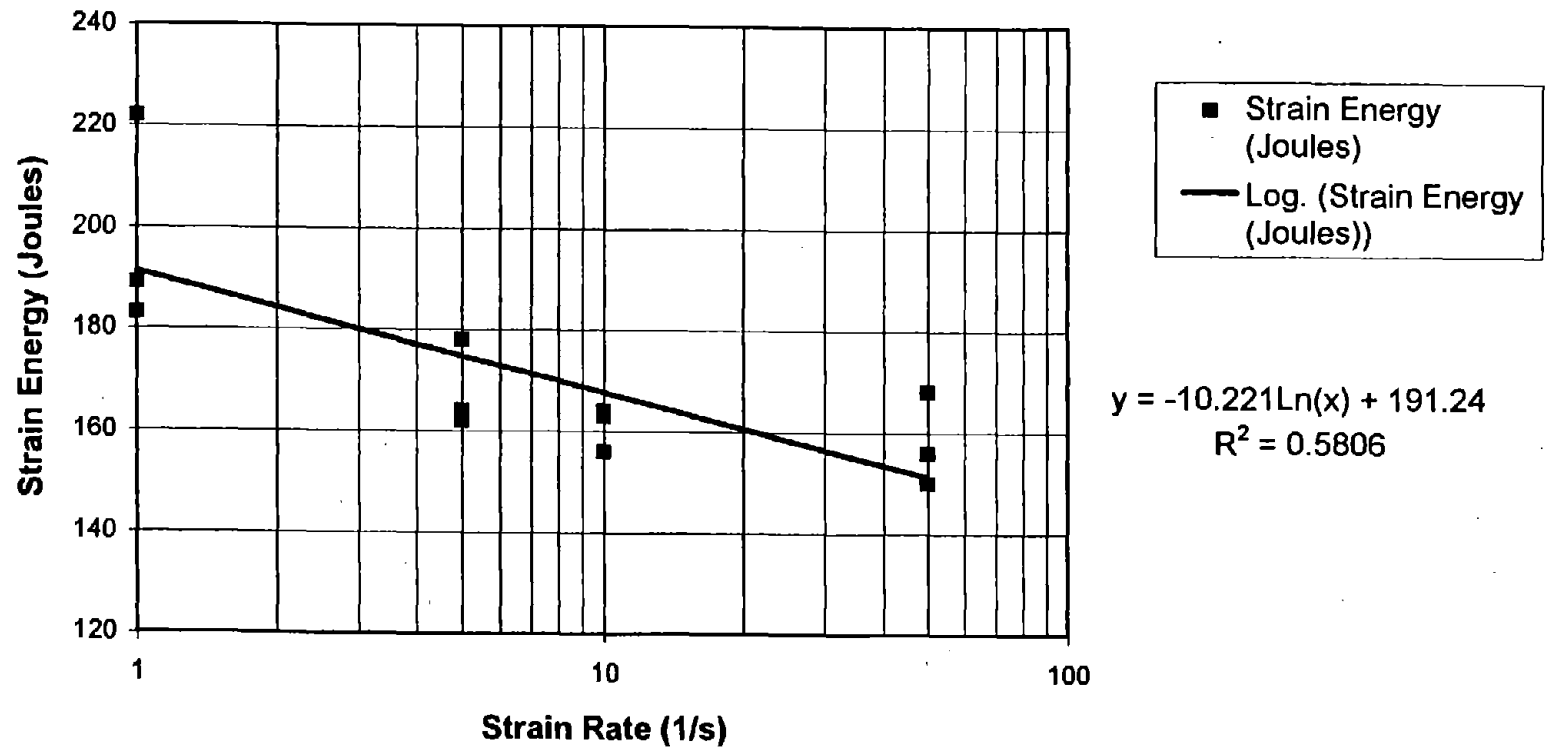


Figure 50 Strain energy versus strain rate.

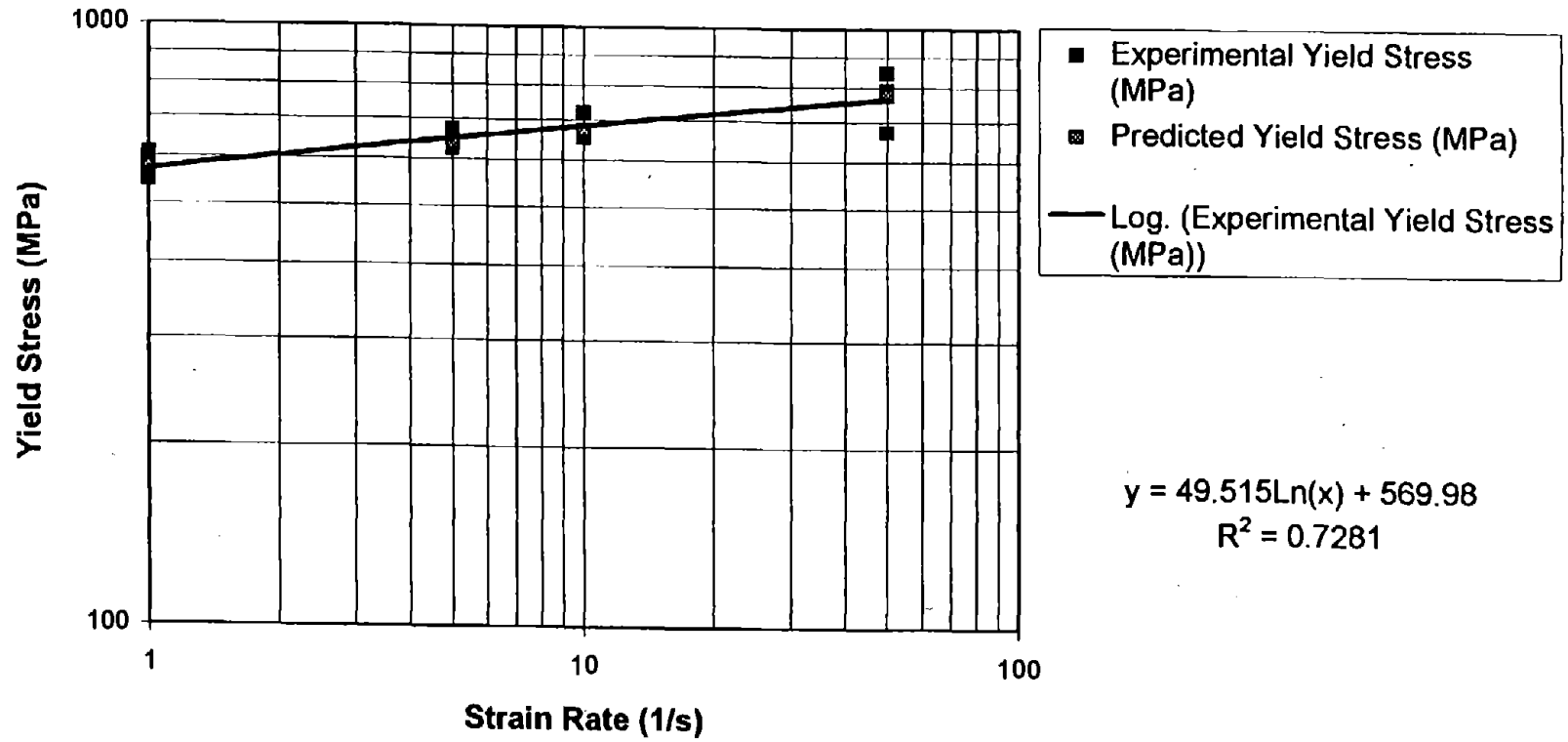


Figure 51 Yield stress versus strain rate with Cowper-Symonds predicted yield stress using the constants $C=100.4 \text{ s}^{-1}$ and $p=4.9$.

Finite Element Simulations

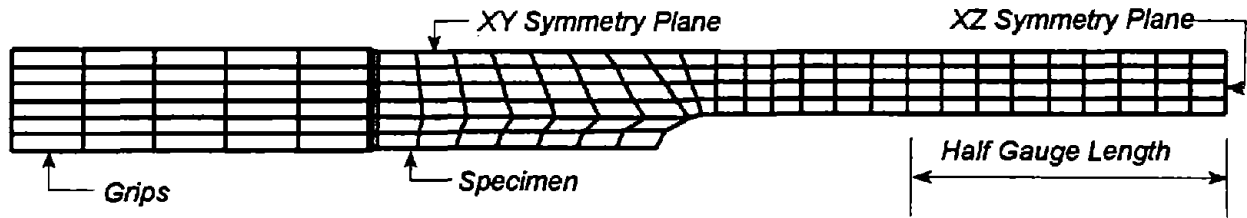


Figure 52 Quarter model of a longitudinal flat tension test.

The finite element mesh used to simulate the dynamic tension tests was similar to the mesh used for the quasi-static tests. The XY and XZ planes of symmetry were again used permitting the use of the quarter model in figure 52. The width of the model was not modified to match the new width of the specimens used in the experimental tests.

The dynamic tension tests are performed at a constant strain rate. Simulating a constant strain rate using LS-DYNA3D should be straight forward, but problems arise from the way LS-DYNA3D uses of the instantaneous strain rates. First, the simulation must be done such that a constant strain rate is applied to scale stresses so that the behavior of the material models may be compared to the experimental results. Second, strain rate effects must be permitted during the simulation so the mathematical material models selected must be strain-rate sensitive. The material model parameters must be verified to find the set which best duplicate the response of the tested materials.

A constant strain rate is accomplished using a constant loading rate in the finite element simulation. A constant loading rate over a fixed distance, the gauge length, gives a constant strain rate as shown by the following equation:⁽³⁴⁾

$$\dot{\epsilon} = \frac{\Delta \epsilon}{\Delta t} = \left(\frac{\Delta l}{l_o} \right) \left(\frac{v_o}{\Delta l} \right) = \frac{v_o}{l_o} \quad (5)$$

where ϵ is strain, l_o and Δl are the initial and incremental length, Δt is the time, increment, Δv is change in velocity, and v_o is the initial velocity. The loading rates for the proposed simulations were found using the same strain rates used in the experimental tests. The length of the specimen is 25.4 mm, the desired strain rates are 1, 5, 10 and 50 s^{-1} so the loading rates required to achieve these strain rates are 25.4, 127, 254 and 1270 mm/s respectively.

Material Models

LS-DYNA3D has several mathematical material models that are strain-rate sensitive: Material type 3 (Kinematic/Isotropic Elastic-Plastic), material type 19 (Strain Rate Dependent Isotropic Plasticity), and material type 24 (Piecewise Linear Isotropic Plasticity).

Material types 3 and 24 are very similar in their treatment of strain rates. Both materials use the Cowper-Symonds equation to directly model strain rate effects on the stress:

$$\sigma_y = [1 + (\frac{\dot{\epsilon}}{C})^{\frac{1}{p}}] (\sigma_0 + \beta E_p \epsilon_{eff}^p) \quad (6)$$

where σ_y is yield stress, ϵ is strain rate, C and p are Cowper-Symonds constants, σ_0 is stress, β is strain hardening, E_p is the tangent modulus, and ϵ_{eff}^p is the effective plastic strain. The Cowper-Symonds equation was developed as a multiplier for the yield stress only, but LS-DYNA3D multiplies all the stresses by this value. LS-DYNA3D appears to be scaling the hydrostatic stress by the multiplier too. The strains are then increased to compensate for the increase in hydrostatic stress. In order to have the correct deviatoric stress, the strains are increasing more in the simulation than they do in reality, thus, resulting in strains that appear to be scaled.⁽¹⁰⁾ Figure 53 shows how the load-elongation curve is shifted upward and to the right resulting a failure strain that is much too high. The failure strain should be approximately 0.24 mm/mm, but the simulation has it as 0.61 mm/mm. If the strain rate is known for material type 3 and material type 24, the effective plastic strain at failure could be input for the expected strain rate, however, this is not possible if the strain rate is unknown.

Material type 19 permits the user to specify load curves that model the effect of strain rate on the yield stress, Young's modulus, tangent modulus and the failure stress. When using sheet steel, this is useful for the yield and failure stresses. Young's modulus has been shown not to be greatly affected by strain rate effects.⁽²⁶⁾ In this model the yield stress is defined as:

$$\sigma_y = \sigma_0(\dot{\epsilon}) + E_h \bar{\epsilon}^p \quad (7)$$

Where σ_y is yield stress, σ_0 is stress, $\dot{\epsilon}$ is strain rate, E_h is hardening modulus, and $\bar{\epsilon}^p$ is the effective plastic strain.

Instantaneous Strain Rates

LS-DYNA3D uses the instantaneous strain rate to both calculate the Cowper-Symonds multiplier and to scale material type 19. The strain rate that the model experiences can be verified using LS-TAURUS checking the strain rate in the x, y and z-directions as well as the effective strain rate. The effective strain rate incorporates the strain rate from the three directions since it is the length of the strain rate vector. This is the strain rate that is used in LS-DYNA3D. For the axial tension

test, it is expected that the z-direction strain rate and the effective strain rate will be very similar since the constant loading is only in the z-direction. The effect of the strain rates in the y-direction due to necking should be negligible and through the thickness necking is not modeled. The results of the simulations are examined and verified.

Through the verification of the material models, it became clear that the use of the instantaneous strain rates is not desirable. The simulated yield stress of 875 MPa is much higher than the Cowper-Symonds predicted value of 718 MPa for a strain rate of 7.9 s^{-1} with $C= 40.4 \text{ s}^{-1}$ and $p= 5$ in figure 53. The high yield stress is due to the use of the instantaneous strain rate. In figure 54, the effective strain rate for material type 24 is shown. The effective strain rate is again too high and very noisy. The expected strain rate for the applied loading rate is around 7.8 s^{-1} , however, the resulting simulated strain rate oscillates around 60 s^{-1} . This could be due to the noisy strain rate. The coupon test is in the z-direction so the effective strain rate should be similar to the strain rate in the z-direction. Figure 54 shows that these two curves are very different. The z-direction strain rate is also very noisy. It is also both positive and negative indicating the passing of tensile and compressive strain waves although the coupon is under a constant tension loading. If the strain rate graph for a simulation with strain-rate sensitivity (figure 54) is compared to a simulation without strain-rate sensitivity (figure 55) it can be seen that they are quite different. The simulation without strain-rate sensitivity produces similar strain rates for the effective strain rate and for the z-direction strain rate. The instantaneous strain rate appears to be unstable perhaps because of numerical noise caused in calculating the strain rate. In addition by applying the new stress due to the strain rate the model changes too rapidly and the stress waves cause the model to ring. The coupon starts straining in the y-direction at an unstable strain rate, thus resulting in a higher than expected effective strain rate. While the instantaneous strain rate does not work well, the material model appears to be doing what it is supposed to do for a strain rate of 60 s^{-1} .

The problem with instantaneous strain rates may be due to numerical noise. When calculating a strain rate, the difference between two strains is taken and divided by the time interval. The calculation of the strains requires taking the difference in displacement between two time steps. The time steps for the simulation are on the order of 10^{-3} . The displacement during this time is very small. Thus, the strain rate is the difference of the difference of very small numbers which may result in a loss of significant figures. The fluctuation of the numbers does not matter for the strain, but once these numbers are used to scale the stresses, their fluctuation appears to have drastic effects. This does not appear to be a good method of applying strain rates sensitivity to mathematical material models.

The noisy high strain rate also occurs with material type 3 and material type 19. In the material type 3 stress-strain curve in figure 58, the yield stress multiplier is too high for the constant loading rate of 200 mm/s that is applied to the model. The resulting yield stress is 1000 MPa. The expected value is approximately 660 MPa when using the Cowper-Symonds equation to scale yield stress. The failure strain is also too high. The strain should be less than the quasi-static failure strain. The strain rate curve seen in figure 59 for the strain-rate sensitive simulation is noisy and resembles the results for material type 24. The effective strain rate curve is higher in magnitude than the z-direction strain rate curve. The strain rate curves without strain-rate sensitivity are nearly identical in figure 60. Material type 3 handles strain rates very similarly to

material type 24 resulting in similar results. Material type 3 does not provide a useful strain-rate sensitive mathematical material model.

The stress-strain curve for material type 19 shown in figure 61 is much too high at 798 MPa for a tension test with a strain rate of 10 s^{-1} . The yield stress should be around 680 MPa for this strain rate. The failure stress (920 MPa) is higher than the expected failure stress (750 MPa) found from the experimental results. The strain rate curves seen in figure 62 for the effective strain rate and the z-direction strain rate are similar to the curves for both material type 24 and material type 3. Material type 19 has essentially the same strain rate curves for the z-direction and the effective strain when strain-rate sensitivity is removed from the simulation as seen in figure 63. Material type 19 does not appear to provide a useful strain-rate sensitive mathematical material model.

All three material models are inadequate for modeling impact simulations for crashworthiness. The use of instantaneous strain rate causes the models to behave in a manner that is not desirable for roadside safety hardware development. Implementing strain-rate sensitivity would actually be harmful since the simulations give erroneous results.

Conclusions

Because strain rate effects are important when examining impacts, there is a need for the development of strain-rate sensitive mathematical material models that model sheet steel behavior in a more physically useful manner. The use of an average or filtered strain rate for scaling may be a better solution, however, new problems arise when using averages. While there would be time step effects due to averaging, the simulation would not be subject to the instability of the instantaneous strain rate. In addition to changing the strain rate application, there needs to be a modification to account for the change in effective plastic strain at failure as a function of strain rate in material type 3 and material type 24. Currently, the effective plastic strain at failure is scaled outward, but the experimental tests demonstrate that the failure strain is reduced as strain rate increases as shown in figure 48. Future research should examine the failure stress, failure strain and the strain energy to find a mechanism for predicting the failure of sheet steels. The failure mechanism could then be incorporated into the strain-rate sensitive material model.

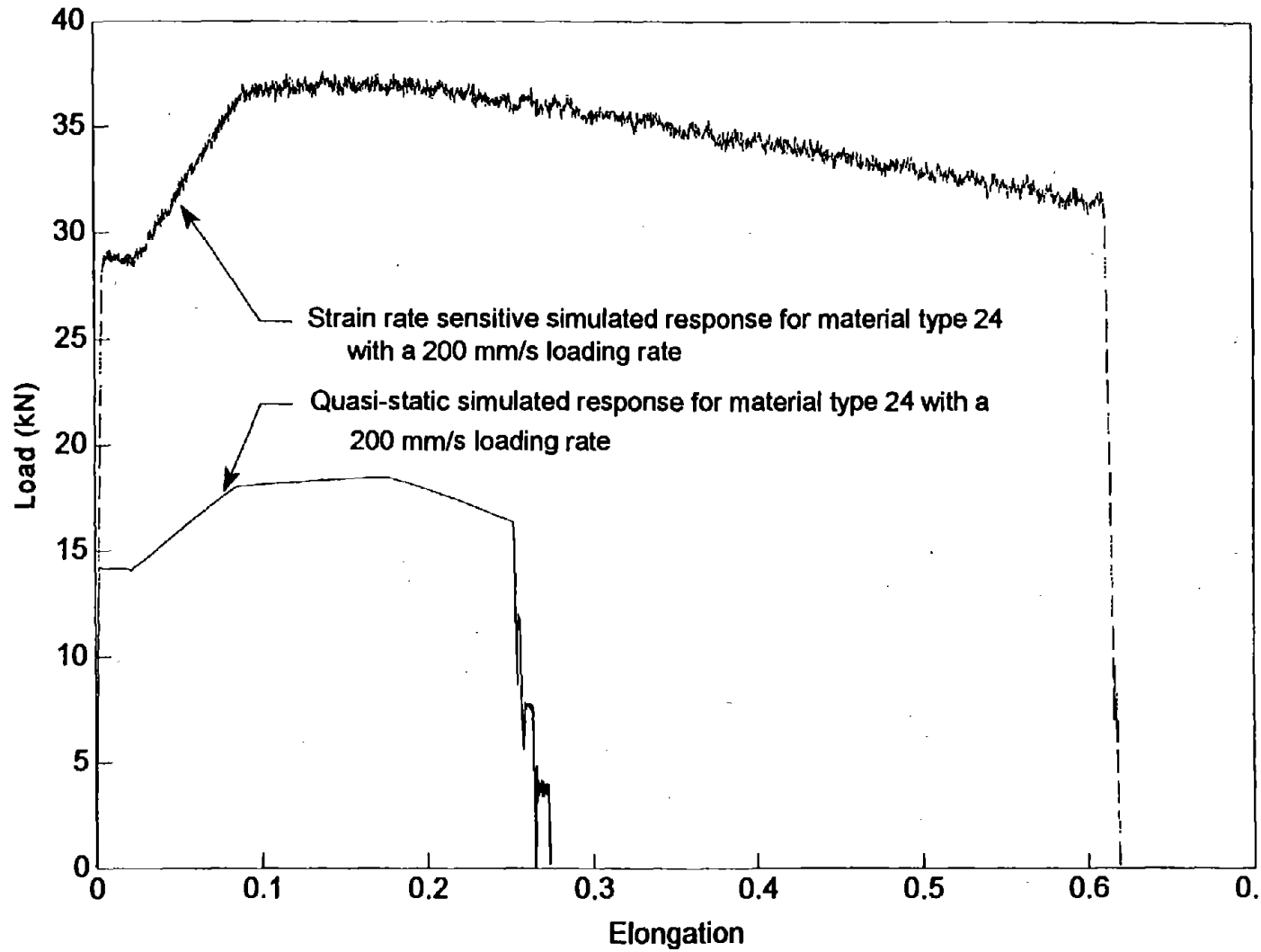


Figure 53 Material type 24 load versus elongation curve with and without strain rate sensitivity.

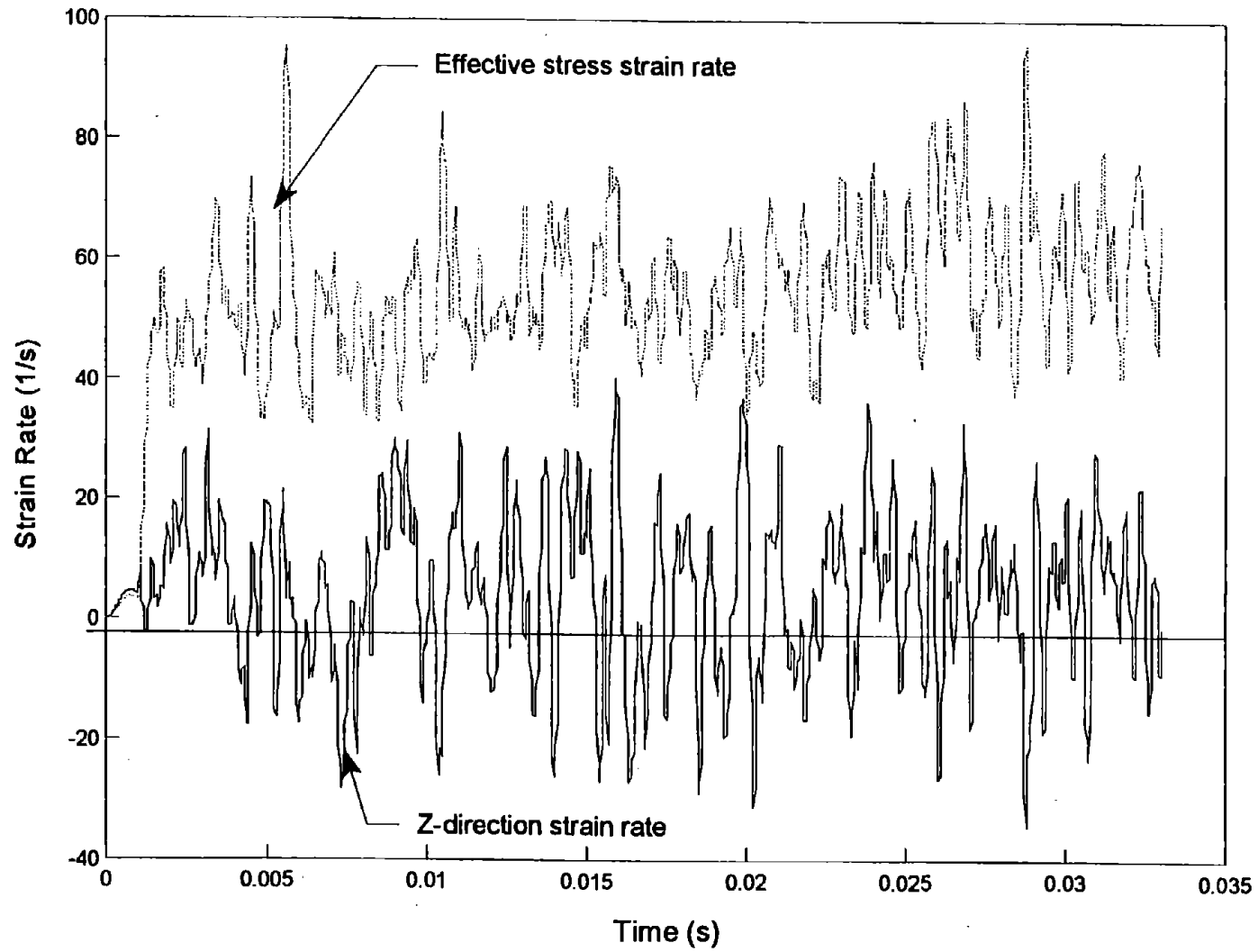


Figure 54 Effective stress strain rate and z-direction strain rate versus time for material type 24 with strain rate sensitivity.

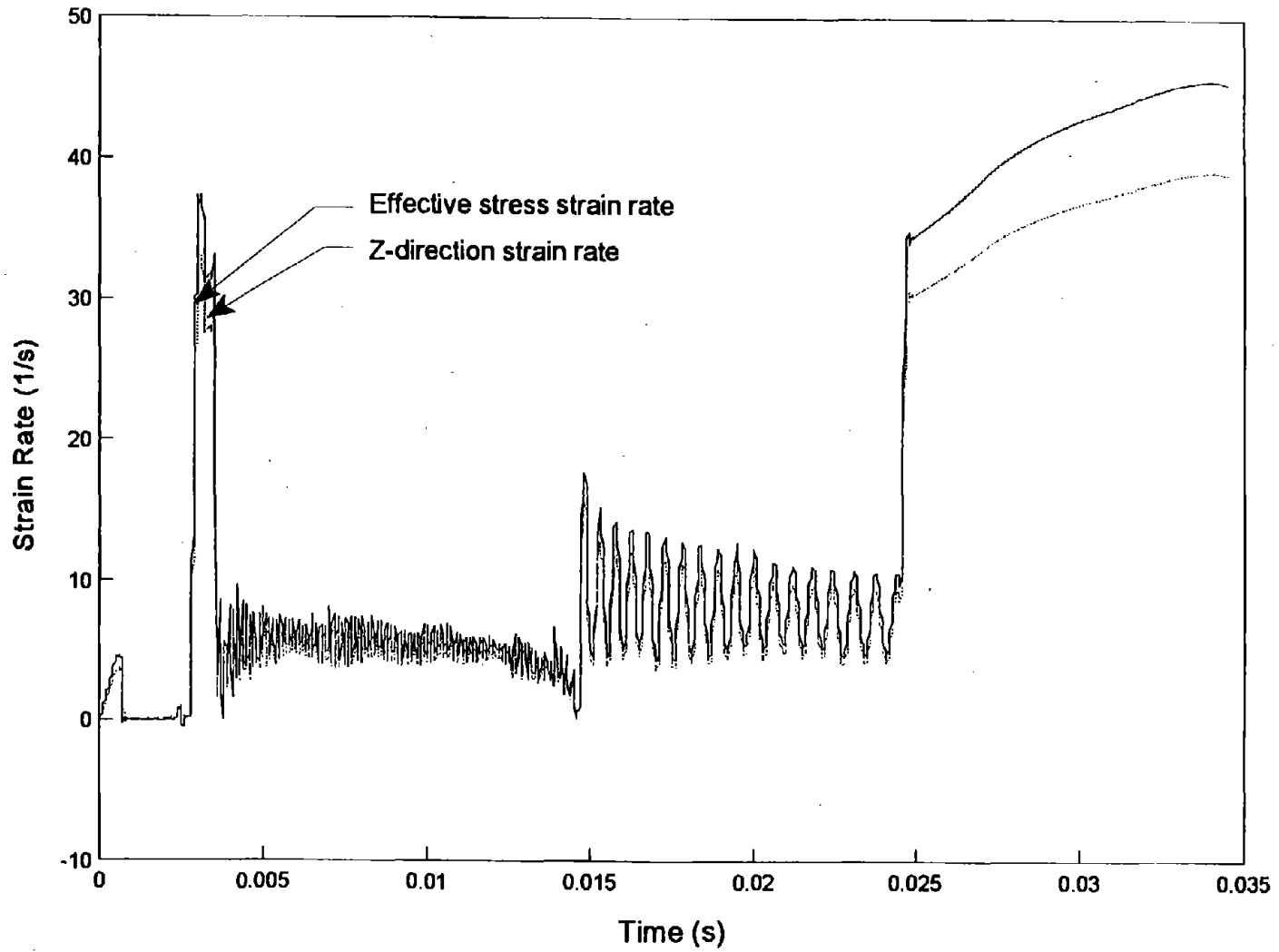


Figure 55 Effective stress strain rate and z-direction strain rate versus time for material type 24 without strain rate sensitivity.

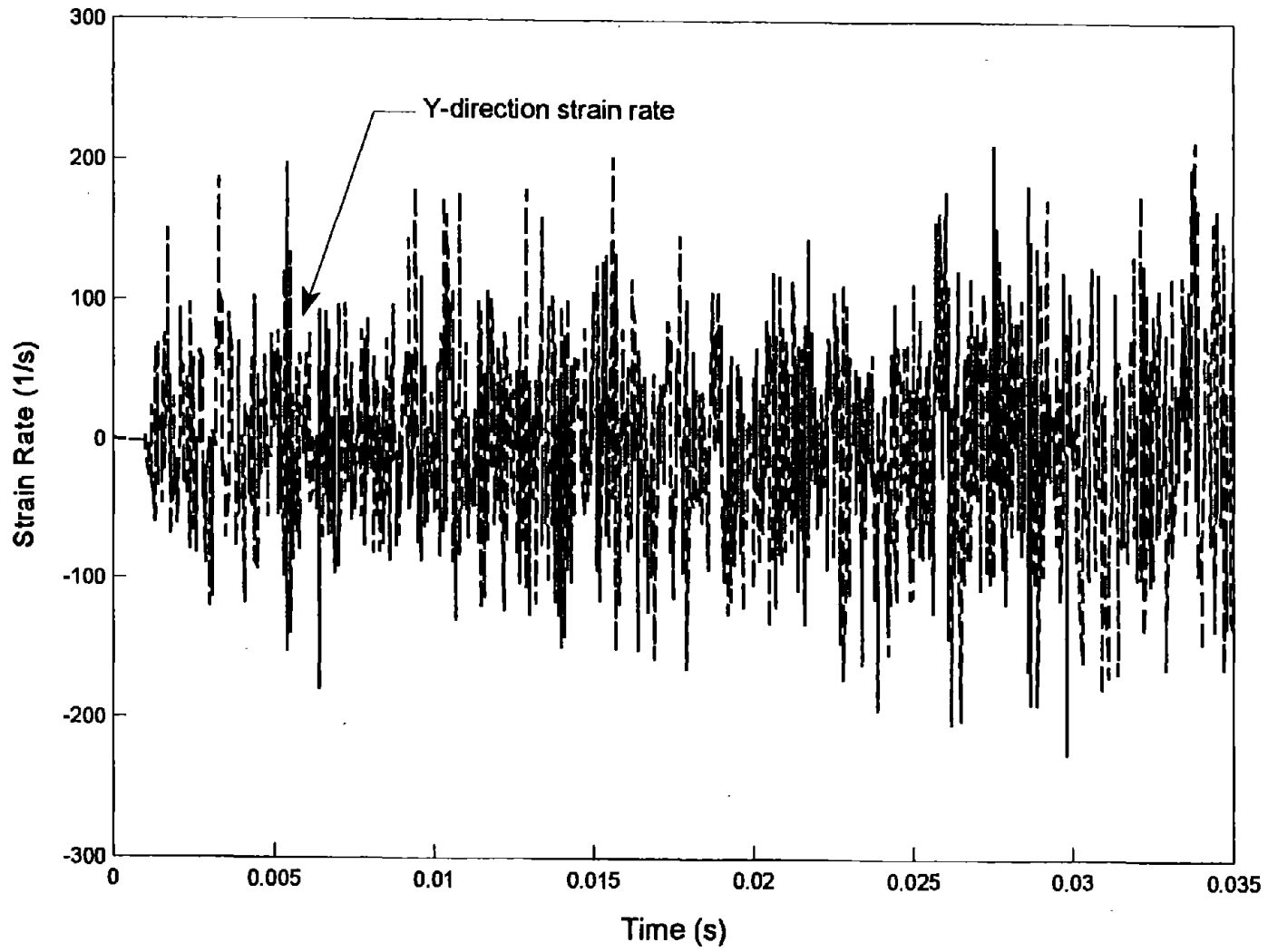


Figure 56 Y-direction strain rate versus time for material type 24 with strain rate sensitivity.

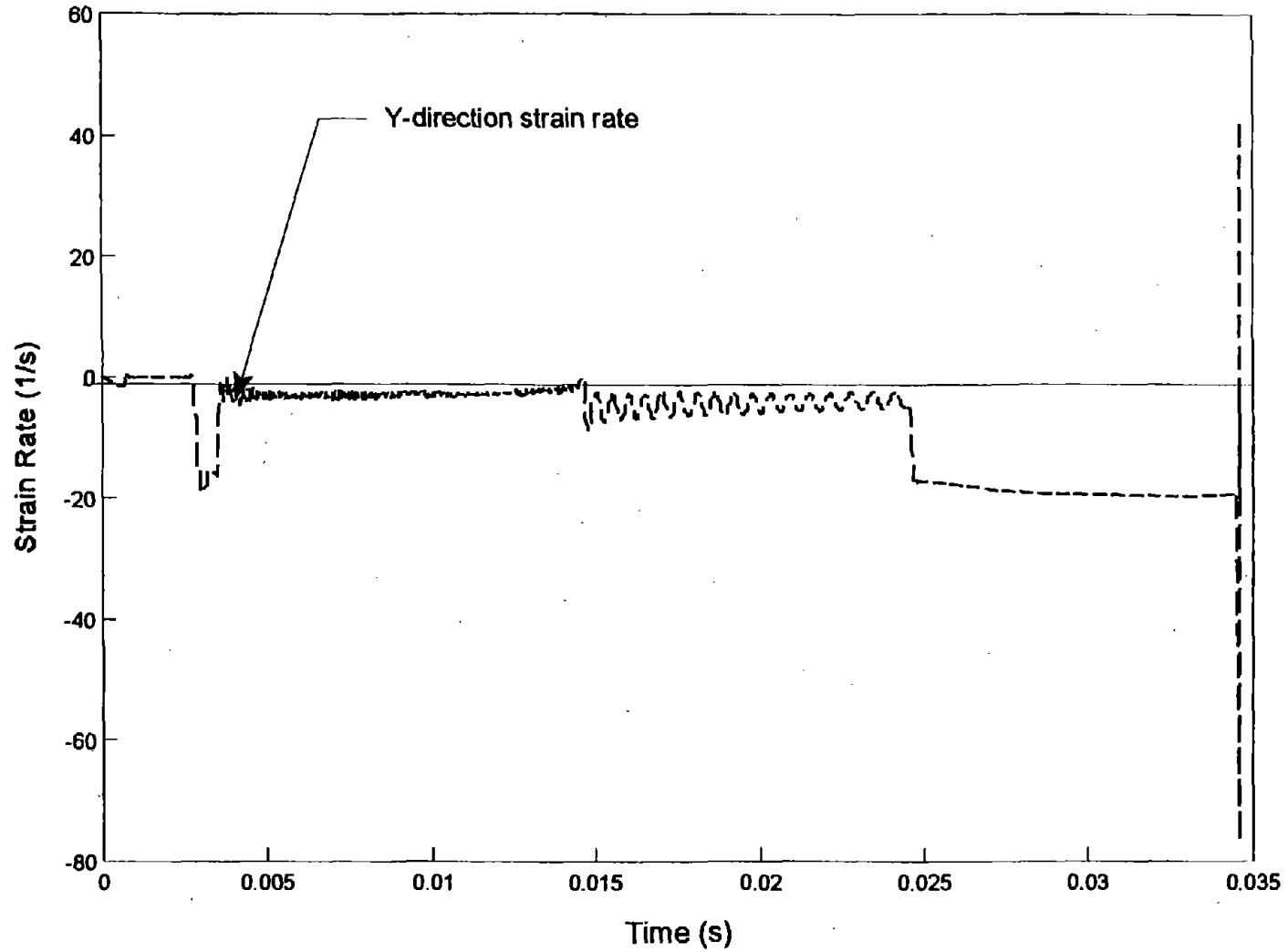


Figure 57 Y-direction strain rate versus time for material type 24 without strain rate sensitivity.

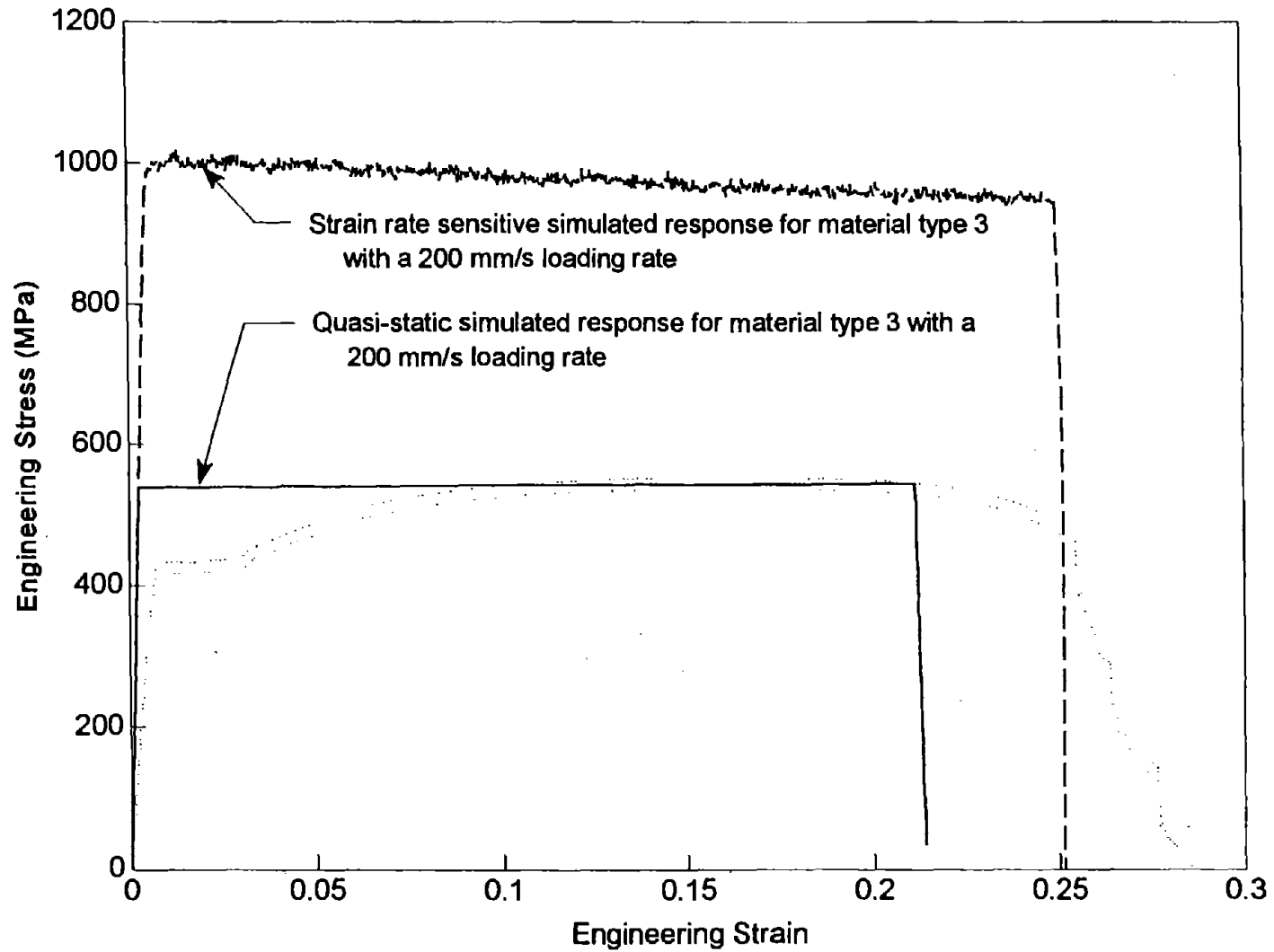


Figure 58 Engineering stress versus engineering strain for material type 3 with and without strain rate sensitivity.

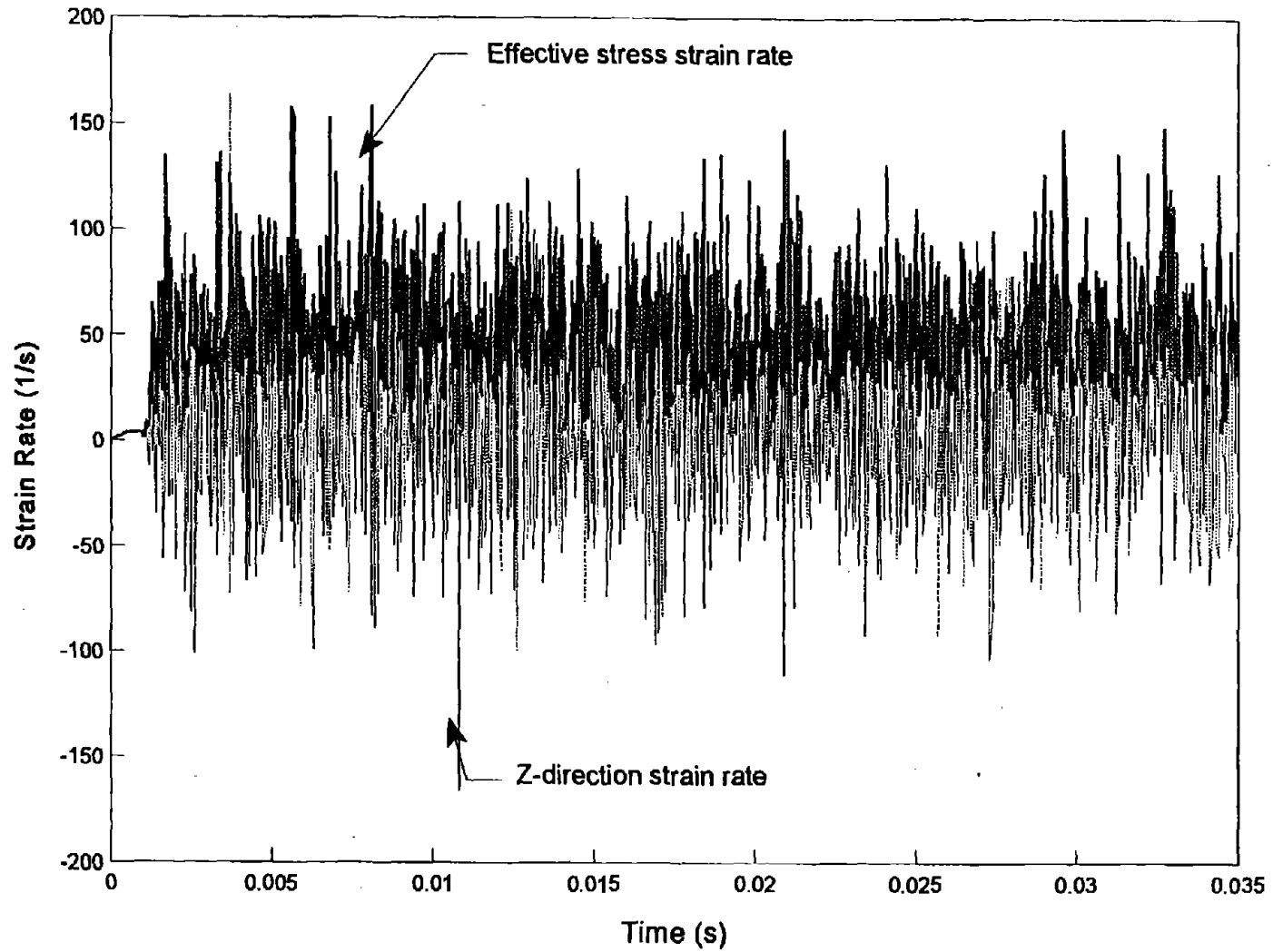


Figure 59 Effective stress strain rate and z-direction strain rate versus time for material type 3 with strain rate sensitivity.

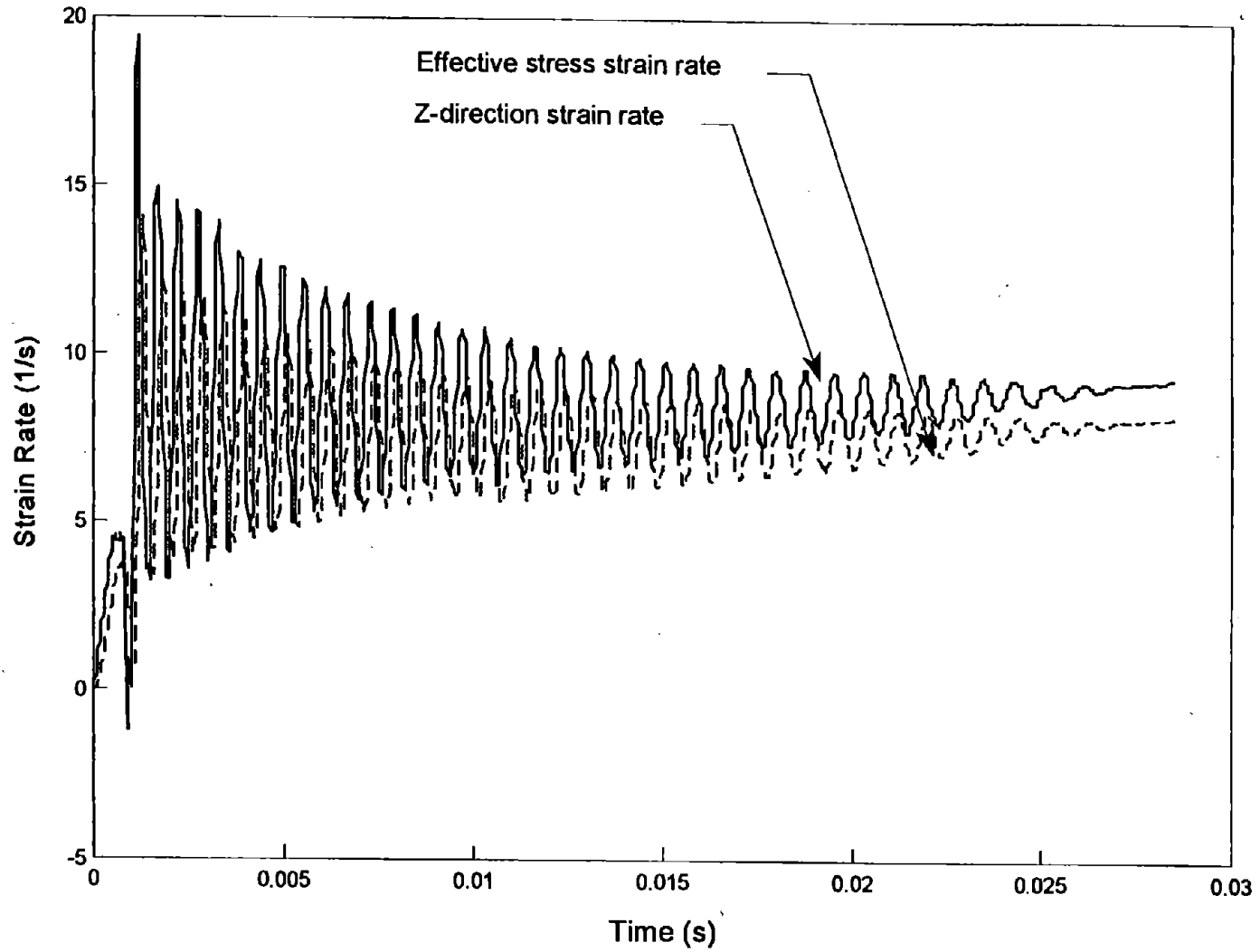


Figure 60 Effective stress strain rate and z-direction strain rate versus time for material type 3 without strain rate sensitivity.

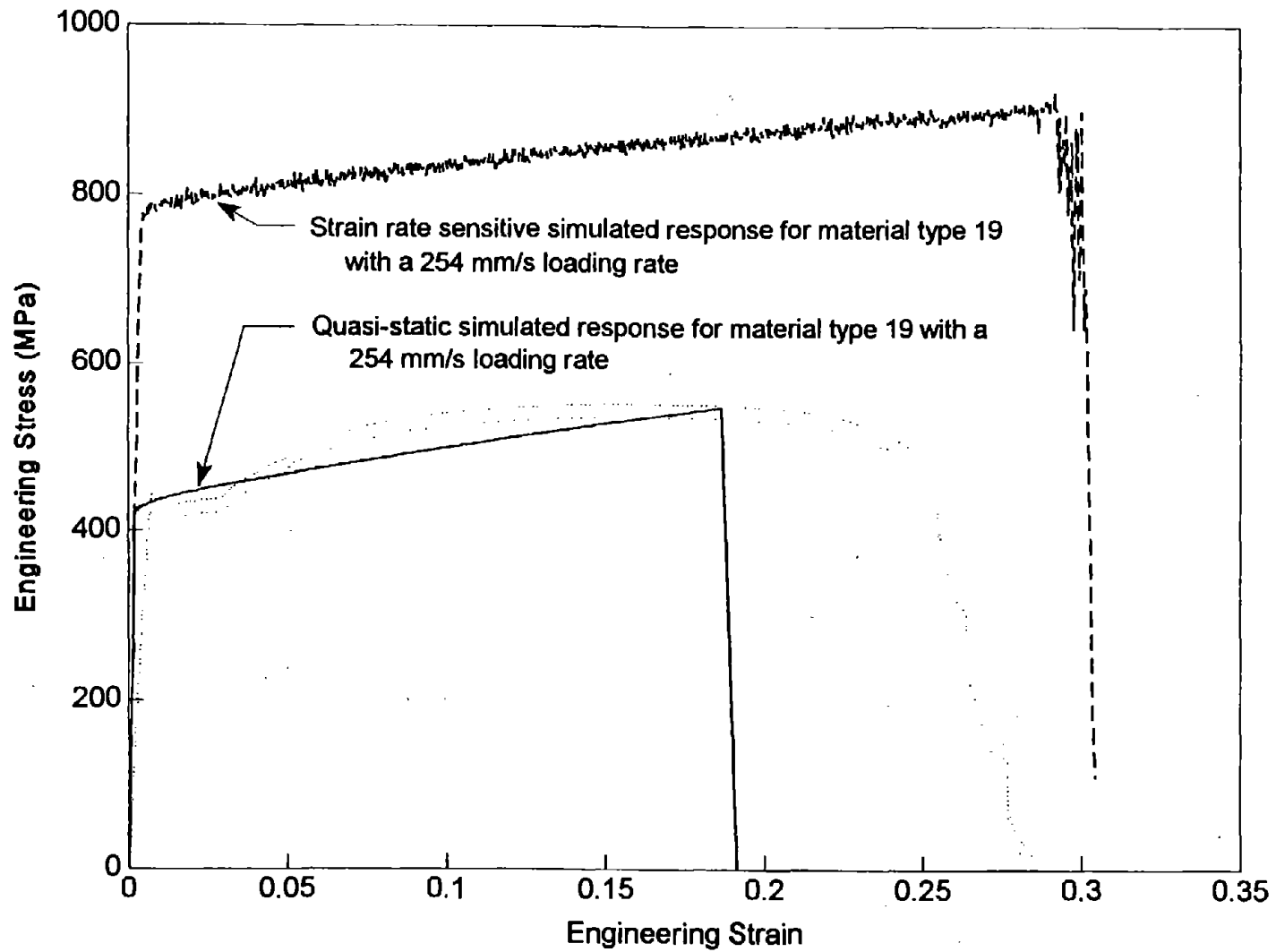


Figure 61 Engineering stress versus engineering strain for material type 19 with and without strain rate sensitivity.

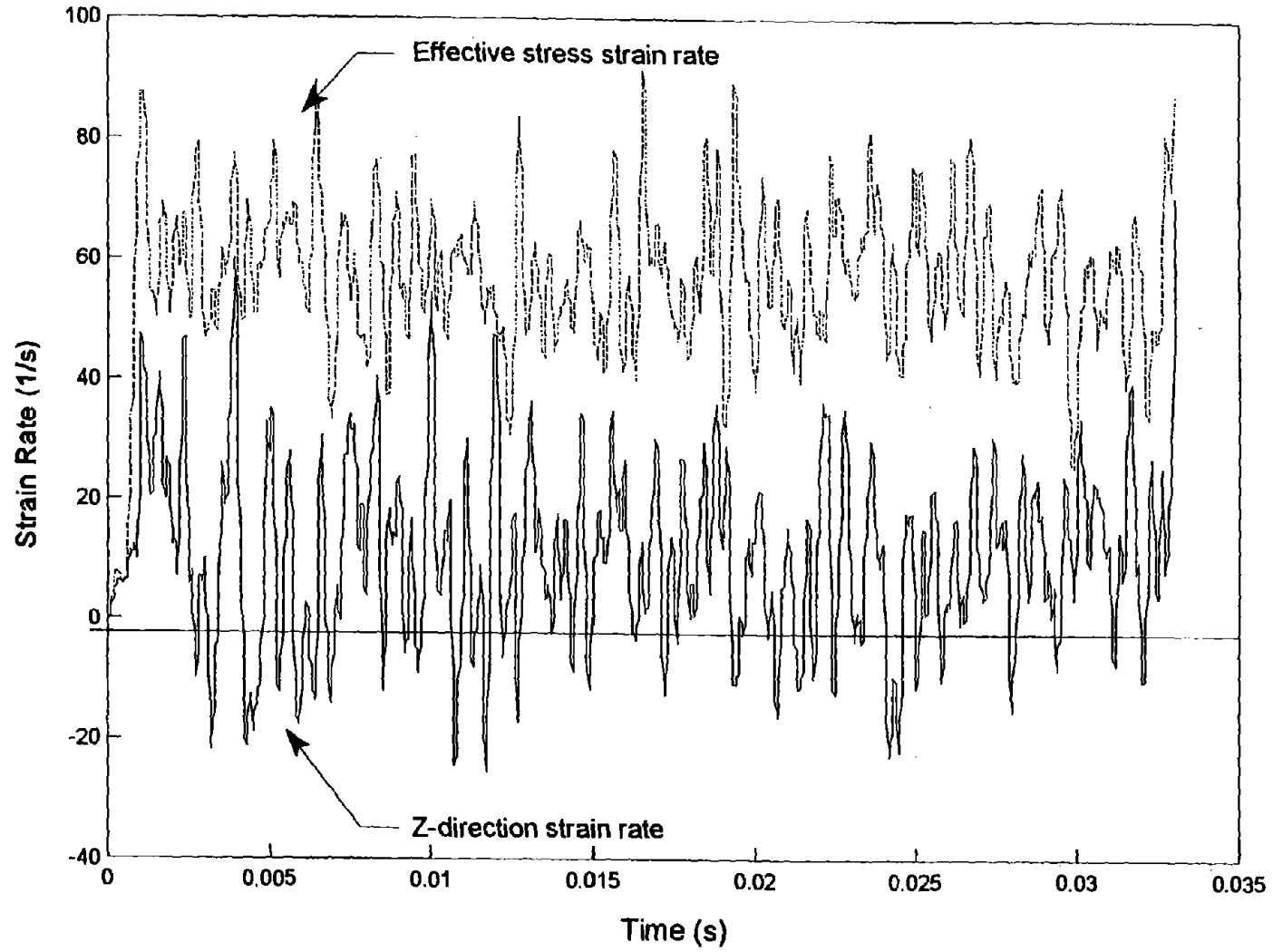


Figure 62 Effective stress strain rate and z-direction strain rate versus time for material type 19 with strain rate sensitivity.

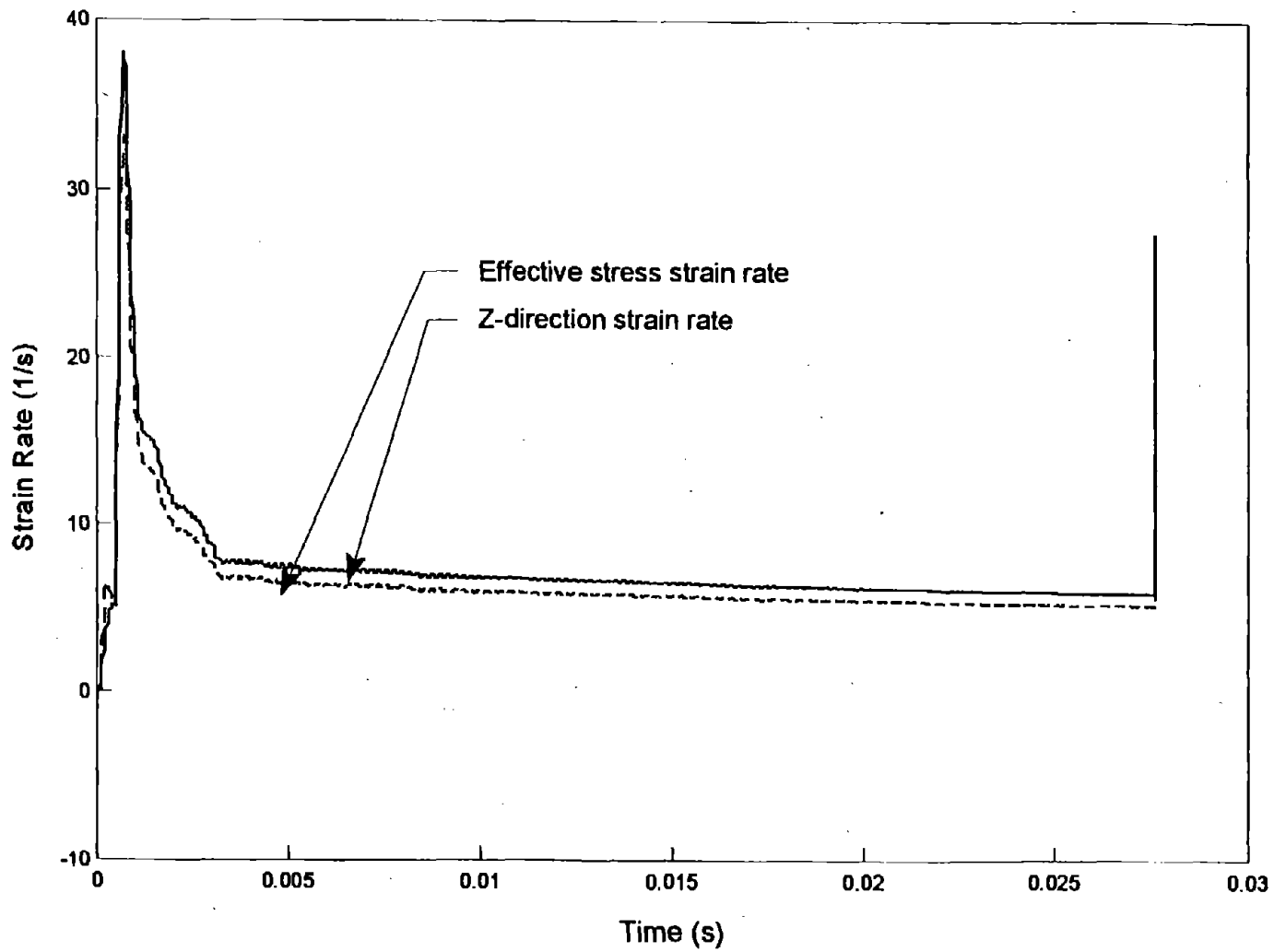


Figure 63 Effective stress strain rate and z-direction strain rate versus time for material type 19 without strain rate sensitivity.

CHAPTER 8. CONCLUSION

The parameters found for modeling roadside hardware materials using LS-DYNA3D are listed in this report. The parameters were found based upon the results of the quasi-static experimental tests. Three material models were presented, type 3, type 19 and type 24. In tables 20, 21, 22 and 24, the material parameters are summarized for material type 3, type 24 and type 19.

Choosing the best material model for a particular analysis is an important modeling decision that is based on (1) accuracy considerations, (2) computational cost, and (3) minimizing computational difficulties. Generally the simpler material type 3 is sufficient for good results, however, there may be times when a more complex material model is desired. The material type 24 model provides the most accurate model of the three since it remains wholly within the 90 percentile envelope. The other two models provide an accurate response as well provided they are not used outside the appropriate range of elongations. The chief advantage of material 24 is that it is accurate for the entire elongation response including failure.

While material type 24 is generally considered the more computationally demanding, the run time for the three material models was nearly identical (1.5 CPU hours) for these simulations. Material type 24, however, uses a more costly contact algorithm so in cases where the material is being contacted, the computation time may go up. In addition, numerical and contact problems can sometimes be avoided by using simpler material models.

The method used in LS-DYNA3D to model strain rates is currently no an effective way to incorporate strain rate effects in crashworthiness applications. The use of the instantaneous strain rate causes inappropriate scaling of the stresses. The instability escalates the strain rates to a higher magnitude causing the material to behave like it is having a much higher strain rate applied than actually is. Until the material models in LS-DYNA3D incorporate strain rates differently, the use of strain-rate sensitive material models is not recommended. Strain-rate sensitivity is an area requiring more research to develop material models that incorporate strain rates better as well as finding material parameters for strain-rate sensitive models.

Table 1 Summary of material type 3 bilinear model material parameters.

	AASHTO M-180	AASHTO M-183M	ASTM A-499	Festiva Fender
Density (Mg/mm³)	7.86E-09	7.86E-09	7.86E-09	7.86E-09
Young's Modulus (MPa)	200.E+03	200.E+03	200.E+03	200.E+03
Poisson's Ratio	0.33	0.33	0.33	0.33
Yield Stress (MPa)	400.0	315.0	464.0	325.0
Tangent Modulus (MPa)	1700.0	2000.0	6000.0	600.0
Hardening Parameter	1.0	1.0	1.0	1.0

Table 2 Summary of material type 3 perfectly plastic model material parameters.

	AASHTO M-180	AASHTO M-183M	ASTM A-499	Festiva Fender
Density (Mg/mm³)	7.86E-09	7.86E-09	7.86E-09	7.86E-09
Young's Modulus (MPa)	200.E+03	200.E+03	200.E+03	200.E+03
Poisson's Ratio	0.33	0.33	0.33	0.33
Yield Stress (MPa)	525.0	440.0	810.0	352.0
Tangent Modulus (MPa)	300.0	300.0	750.0	180.0
Hardening Parameter	1.0	1.0	1.0	1.0
Plastic Strain at Failure	0.24	0.235	0.155	0.59

Table 3 Summary of material type 24 material parameters.

	AASHTO M-180	AASHTO M-183M	ASTM A-499	Festiva Fender
Density (Mg/mm³)	7.86E-09	7.86E-09	7.86E-09	7.86E-09
Young's Modulus (MPa)	200.E+03	200.E+03	200.E+03	200.E+03
Poisson's Ratio	0.33	0.33	0.33	0.33
Yield Stress (MPa)	415.0	315.0	464.0	315.0
Plastic Strain at Failure	0.66	0.625	0.295	0.64
Increments of Strain	0.0 0.02 0.08 0.165 0.33 0.49 0.66 1.0	0.0 0.019 0.05 0.165 0.33 0.495 0.625 0.625 1.0	0.0 0.02 0.03 0.07 0.12 0.16 0.295 1.0	0.0 0.0195 0.05 0.15 0.3 0.5 0.64 1.0
Increments of Stress (MPa)	415 415 548 575 585 595 600 0.0	315 315 428 501 504 507 400 0.0	464 595 680 850 895 920 890 0.0	315 340 358 390 400 400 365 0.0

Table 23 Summary of material type 19 quasi-static material parameters.

	AASHTO M-180	
Density (Mg/mm³)	7.86E-09	
Young's Modulus (MPa)	200.E+03	
Poisson's Ratio	0.33	
Load Curves		
Strain Rate (s⁻¹)	0	1.0E+05
Yield Stress (MPa)	440.0	440.0
Young's Modulus (MPa)	2.0E+05	2.0E+05
Tangent Modulus (MPa)	970.0	970.0
Failure Stress (MPa)	640.0	640.0

APPENDIX A- TRUGRID INPUT FILE

```
title M-180 Cls A Type II -- 200 mm/s
c Malcolm H. Ray
c The University of Iowa
c March 1994
c modified by Amy Wright
cCarnegie Mellon University
c originally created for LLNL DYNA3D version 4.0.4 using the 88 large input format
$ 1. Change control card 9
$ 0 0 0 0 0 0 0 0 0 0 0.000E+00 0 0 0 0
c Read the trugrdo file with the above changes into ls-ingrid to create an
c LS-DYNA3D version 930 input format. Now add these lines to the ingrido file:
$ 2. Add these lines just before the load curve definition in the ingrido file
$ *
$ *-----Element time history blocks-----*
$ 137 137 138 138 139 139 140 140
$ *----- CROSS SECTIONS -----*
$ *
$ 7 0 6
$ 19 26 33 64 71 78 85
$ 13 14 49 50 51 52
$ 3. Change control card 20, parameter 1 to 2.500e-05, parameter 3 to 2.500e-5,
$ parameter 4 to 6, parameter 7 to 4
$ 4. Change control card 21, parameter 3 to 1
$ 5. Change control card 22, parameter 1 to 2.500E-5
$ 6. Change the number of integration pts through the thickness for the shell to 5
c this is located below the first material definition where the shell is named.
dyna3d
dynaopts term 0.05 prti 2.5E-5 plti 2.5E-3 ticsf 2.5E-5;
c parameters for scaling up or down the stress-strain relationship
para
yld 415 c yield stress
ult 600 c true ultimate stress
fail 0.66; c plastic strain at failure (about = to elongation at failure)

c curve for constant head loading rate,
c for a more stable response, the load is ramped up to the desired value(AEW 7-9-95)
lod 1 0. 0. 2.5e-5 200. 9. 200.;
c use symmetry to reduce problem size and take advantage of the two axes symm.
plane 1 0. 0. 0. 0. 1. 0. 0. 5 symm;
plane 2 0. 0. 0. 0. 0. 1. 0. 5 symm;

c (1) the COUPON part
block -1;1 3 7; 1 6 13 15 18 30;
0;
-10. -6.4262 0.;
-70. -50. -31.88 -30. -25. 0.;
dei ;1 2;3 6;
thic 2.67
mate 1
sfi ;1 2;-3;cy 0 -10. -30. 1 0 0 3.5738
sfi ;-2;3 4;cy 0 -10. -30. 1 0 0 3.5738
lini ;;-2;
lini ;-3;2 4;
```

npb 1 2 5 1 3 5

c The width of the gauge length narrowed to better match the specimens

c this is allowed in AASHTO T-244 specifications(AEW 6-1-95)

ma 1 2 6 y 0.127

endpart

c (2) the GRIPS

c Added the grips to get a non-reflecting boundary across top (MHR: 5-16-94)

block 1 3;1 7;1 6;

-5. 0.;

-10. 0.;

-70. -50.;

nr 1 1 1 2 2 1

c give the grips a constant velocity

fvi ;;; 1 1. 0. 0. -1.

mate 2

endpart

c FAILING GUARDRAIL MATERIAL

c properties based on HNR-10 coupon tests.

c belytchko-lin-tsay shell with 5 through the thickness integration pts.

dynamats 1 24 shell

rho 7.86e-9 e 200.E3 pr 0.33 sigy %yld lc 0 efp 0.66 tsti 5

eps 0. 0.02 0.08 0.165 0.33 0.495 0.66 1.;

es %yld %yld 548 585 591 595 600 0.;;

c dummy steel for the tester grips

dynamats 2 1

rho 7.86e-9 e 200.E3 pr 0.33;

merge

stp 0.25

REFERENCES

1. R. G. Whirley and B. E. Engleman. *DYNA3D: A Nonlinear, Explicit, Three-Dimensional Finite Element Code for Solid and Structural Mechanics—User's Manual*. Livermore, CA: Lawrence Livermore National Laboratory, Report UCRL-MA-107254 revision 1, November 1993.
2. J. O. Hallquist, D. W. Stillman, and T. L. Lin. *LS-DYNA3D User's Manual: Nonlinear Dynamic Analysis of Structures in Three Dimensions*. Livermore CA: Livermore Software Technology Corporation, April 1994.
3. AASHTO. "Mechanical testing of steel products (T-244)." *Standard Specifications for Transportation Materials and Methods of Sampling and Testing: Sixteenth Edition 1993 Part II Tests*. (with interim specifications through 1991) American Association of State Highway and Transportation Officials, Washington DC: 1993.
4. J. Harding. "Chapter 4: The effect of high strain rate on material properties." *Materials at High Strain Rates*. Essex: Elsevier Applied Science Publishers Ltd., 1987.
5. Dean Sicking. "Applications of simulation in design and analysis of roadside safety features." *Transportation Research Circular: Roadside Safety Issues*. Washington DC: Transportation Research Board, No. 435, January 1995.
6. William Johnson. *Impact Strength of Materials*. London: Edward Arnold Publishers, 1972.
7. John O. Hallquist. *LS-DYNA3D Theoretical Manual*. Livermore, CA: Livermore Software Technology Corporation, LSTC Report No. 1018 Rev. 3, April 1994.
8. Livermore Software Technology Corporation. "LS-DYNA3D Advanced Course Notes 1995." Livermore Ca: Livermore Software Technology Corporation, LSTC Report 1044, 1995.
9. P.A. DuBois. "Crashworthiness Engineering with LS-DYNA3D Course Notes," H.E.N.V., November 1994.
10. Livermore Software Technology Corporation. *LS-DYNA3D User's Manual: (Nonlinear Dynamic Analysis of Structures in Three Dimensions) version LS-DYNA3D 932*. Livermore CA: Livermore Software Technology Corporation, LSTC Report No. 1007 Rev. 3, May 1995.
11. Malcolm H. Ray. "Repeatability of full-scale crash tests and a criteria for validating simulated results." *Transportation Research Record*, Washington DC: Transportation Research Board, Paper No.961295, 1996.
12. Jay L. Devore. *Probability and Statistics for Engineering and Sciences*. Pacific Grove, CA: Brooks/Cole Publishing Company, 1991.

13. AASHTO. "Corrugated sheet steel beams for highway guardrail (M-180)." *Standard Specifications for Transportation Materials and Methods of Sampling and Testing Sixteenth Edition 1993: Part I Specifications*. Washington, DC: American Association of State Highway and Transportation Officials, 1990.
14. AASHTO-AGC-ARTBA Joint Committee. "RWMO2a W-beam rail." *Task Force 13 Report: A Guide to Standardized Highway Hardware*. Washington DC: American Association of State Highway and Transportation Officials, May 1995.
15. AASHTO-AGC-ARTBA Joint Committee. *Task Force 13 Report: A Guide to Standardized Highway Barrier Hardware*. Washington DC: American Association of State Highway and Transportation Officials, May 1995.
16. AASHTO. "Structural Steel (M-183M-93)." *Standard Specifications for Transportation Materials and Methods of Sampling and Testing: Part I Materials*. Washington DC: American Association of State Highway and Transportation Officials, 1990.
17. AASHTO-AGC-ARTBA Joint Committee. "PFE01 Flanged-channel post." *Task Force 13 Report: A Guide to Standardized Highway Barrier Hardware*. Washington DC: American Association of State Highway and Transportation Officials, May 1995.
18. ASTM. "Standard specifications for steel bars and shapes, carbon rolled "T" rails (A 499-81)." *1995 ASTM Annual Book of ASTM Standards: Section 1 Iron and Steel Products*. Philadelphia, PA: American Society for Testing and Materials, Volume 01.05, 1995.
19. National Cooperative Highway Research Program. *NCHRP Report 350: Recommended Procedures for the Safety Performance Evaluation of Highway Features*. Washington DC: National Academy Press, 1993.
20. J. W. Wekezer. *Finite Element Modeling of Motor Vehicles. Protocol for Developing INGRID Data Input Decks for DYNA3D Computer Code*. McLean, VA: Federal Highway Administration, Publication No. FHWA-RD-94-153, February 1995.
21. Emmanuel Cofie. *Finite Element Model of a Small Automobile Impacting a Rigid Pole*. McLean, VA: Federal Highway Administration, Publication No. FHWA-RD-94-151, June 1995.
22. American Iron and Steel Institute. *Automotive Steel Design Manual*. Southfield, MI: American Iron and Steel Institute, Revision 4, February 1993.
23. ASTM. "Standard Specifications for steel, sheet, carbon, cold-rolled, structural quality (A611-94)." *1995 ASTM Annual Book of ASTM Standards: Section 1 Iron and Steel Products*. Philadelphia, PA: American Society for Testing and Materials, Volume 01.03, 1995.
24. Norman Jones. *Structural Impact*. Cambridge: Cambridge University Press, 1989.

25. S. Timoshenko. *Strength of Materials: Part II Advanced Theory and Problems*. Princeton NJ: D. Van Nostrand Company, Inc., third edition, 1956.
26. P. Soroushian and K. Choi. "Steel mechanical properties at different strain rates." *Journal of Structural Engineering*. New York, NY: American Society of Civil Engineers, Vol. 113, No. 4, April 1987.
27. M. Kassar and W. W. Yu. "Effects of strain rate on material properties of sheet steels." *Journal of Structural Engineering*. New York: American Society of Civil Engineers, Volume 118, Number 11, November 1992.
28. A. P. Boresi, R. J. Schmidt, and O. M. Sidebottom. *Advanced Mechanics of Materials*. New York NY: John Wiley and Sons, Inc., fifth edition, 1993.
29. J.D. Campbell and R. H. Cooper. "Yield and the flow of low-carbon steel at medium strain rates." *Proceedings of the Conference on the Physical Basis of Yield and Fracture, Oxford 1966*. Oxford: Institute of Physics and the Physical Society, September 1966.
30. J.D. Campbell and W.G. Ferguson. "The temperature and strain-rate dependence of the shear strength of mild steel." *A Philosophical Magazine: Physics of Condensed Matter, Defects and Mechanical Properties*. London: Taylor and Francis, Vol. 21, 1978.
31. Lothar W. Meyer. "Dynamic tension studies of strength and formability characteristics of high alloyed steel with respect to thermal activation." *Mechanical Properties at High Rates of Strain: Proceedings of the Conference on Mechanical Properties of Materials at High Rates of Strain held in Oxford, 9-12 April 1984*. London: The Institute of Physics, Conference series No. 70, 1984.
32. Norman Jones. "Scaling of inelastic structures loaded dynamically." *Structural Impact and Crashworthiness: Volume 1 Keynote Speakers*. New York NY: Elsevier Applied Sciences, 1984.
33. P. C. Bastias. "Report on the Mechanical Properties of Guardrail Steel." Prepared for the Federal Highway Administration. Unpublished, August 1995.
34. Marc A. Meyers. *Dynamic Behavior of Materials*. New York, NY: John Wiley and Sons, Inc., 1994.



BIBLIOGRAPHY

ASTM. "Standard practice for conducting constant amplitude axial fatigue tests of metallic materials (E466-82)." *The Annual Book of ASTM Standards*. Section 3, Vol. 03.01, 1995.

Chatfield, D. A. and Rote, R. R. "Strain rate effects on the properties of high strength, low alloy steels." *SAE Technical Paper Series 740177*. Warrendale PA: Society of Automotive Engineers, 1974.

Collins, J. A. *Failure of Materials in Mechanics and Design: Analysis, Prediction, Prevention*. New York, NY: Wiley-Interscience Publications, 1981.

Department of Defense. Military Handbook: Metallic Materials and Elements for Aerospace Vehicle Structures. MIL-HDBK-5E, Vol 1, November 1, 1990.

Hauser, Frank E. "Techniques for measuring stress-strain relations at high strain rates." *Experimental Mechanics*. CT: Society for Experimental Stress Analysis, Vol 6, 1966.

Holzer, A. J. "A tabular summary of some experiments in dynamic plasticity." *Journal of Engineering Materials and Technology*. American Society of Mechanical Engineers, Vol. 101, July 1979.

Lindholm, U. S. "Review of dynamic testing techniques and material behavior." *Mechanical Properties at High Rates of Strain: Proceedings of the Conference on Mechanical Properties of Materials at High Rates of Strain held in Oxford, 2-4 April 1974*. London: The Institute of Physics, Conference series No. 21, 1974.

Nicholas, Theodore. "Tensile testing of materials at high rates of strain." *Experimental Mechanics*. CT: Society of Experimental Stress Analysis, Vol 21, 1981.

